ABSTRACT

LYE, JASON. Semi-Empirical MO-Methods in Dye Chemistry: Studies Involving Disperse and Metal Complex Dyes. (Under the direction of HAROLD STANLEY FREEMAN).

This dissertation pertains to the applications and limitations of modern molecular modeling tools for predicting structural, physical, and chemical properties of synthetic organic dyes. Data generated by MOPAC, ZINDO, molecular mechanics, and PPP based modeling packages were assessed by comparison with experimental results.

Studies aimed at determining the most useful semi-empirical method for generating accurate conformations, bond lengths, and bond angles by comparing the results of semi-empirical modeling studies to experimental x-ray data, were undertaken. The accuracy of CI Disperse Yellow 86 and CI Disperse Red 167 models was assessed in terms of bond length and molecular conformation prediction. The models were produced using a combination of manual adjustments and molecular mechanics to obtain crude starting structures, followed by AM1 or PM3 semi-empirical geometry optimizations to refine the structures. This procedure proved to be the best way to reproduce experimental x-ray data for these structures. Earlier semi-empirical methods such as MINDO/3 and MNDO tended to compromise the planarity of both chromogens, and often omitted intramolecular hydrogen bonds that are essential to technical properties such as photostability.

It would appear that none of the most recent semi-empirical methods are suitable for modeling anthraquinone dyes, as all of the methods tended to distort the structure into a butterfly shape. Other limitations include the tendency of AM1 to predict the *cis* isomer of azobenzene derivatives to be more stable than the *trans*, and the tendency of PM3 to distort the planarity of conjugated aromatic amines. Also, AM1 appears to be the inferior to PM3 in its ability to reproduce intramolecular hydrogen bonds.

Optimization studies have led to the development of a set of protocols that may be used for manually refining the input geometry for quantum mechanical based optimizations. When implemented, the protocols generate starting structures that give lower energy and less distorted geometries after optimization. The protocols are designed to be applied to azo dyes, structures containing hydrogen bonds, and metal complex dyes. Such modifications to starting structures help circumvent the problems of input geometry dependence and local minima generation by geometry optimizers.

No single method was generally useful in all modeling situations -- each method had strengths and weaknesses. For instance, in studies involving the prediction of the position and intensity of the longest wavelength absorption band of disperse dyes, the PPP SCF MO method was found to be clearly superior to the INDO/S method. Similarly, the AM1 method was useful for prediction of the octanol-water partition coefficients of azo dyes; however, the PM3 method was superior to AM1 for predicting hydrogen bonding in hydroxybenzotriazoles.

By comparing experimental x-ray crystal and equilibrium stability data of a 1:2 Cr (III) complex dye with the modeled structure, it became clear that the INDO/2 UHF SCF method was an appropriate tool for geometry optimizations of metal complex dye structures. Although the accuracy of this method is somewhat less than that of PM3 and AM1 in terms of calculating bond lengths, the INDO/2 method was able to predict the occurrence of long versus short metal-ligand bonds in Cr (III) complex dye structures, as well as the strengths of bonds between ligands and the central metal atom. For instance, the INDO/2 method predicted Cr (III) complex dyes to contain stronger bonds to the central metal atom than those in Fe (III) complex dyes. In the case of Fe (III) azo dyes, there was little difference between metal-ligand bonding in the high and low spin configurations, however in the case of the formazan dye modeled, the low-spin configuration was predicted to be more strongly bond than the high-spin configuration.

Magnetic susceptibility measurements showed the Fe (III) complexed azo dyes used in this study to be high-spin complexes, whereas the formazan dyes employed were low-spin complexes. These results helped explain why the latter are brightly colored red-violet and faster to light and laundering compared to their brown-black azo counterparts. The INDO/2 method can be used to predict which ligands will give rise to low-spin Fe (III) complexes, and which would give rise to high-spin Fe (III) complexes. An acceptor type ligand is one which contains a double bond at the atom directly attached to the central metal atom;- the π and π^* orbitals of such ligands interact with and reduce the energy of t_{2g} d-orbitals of the metal atom. In this regard, it was determined that at least two of the three chelating atoms of the dye ligand should be of acceptor type in order for the resultant Fe (III) complex to be low spin. If the calculated bond order of pertinent bonds in the ligand tend to equalize after complexation with the metal atom, the chelating atoms in that section of the ligand may be thought of as of acceptor-type. It would appear that the INDO/2 method can be used to design custom ligands for Fe (III) that give low-spin, colorful, stable dyes.

SEMI-EMPIRICAL MO-METHODS IN DYE CHEMISTRY: STUDIES INVOLVING DISPERSE AND METAL COMPLEX DYES

By

JASON LYE

A thesis submitted to the Graduate
Faculty of North Carolina State University
in partial fulfillment of the requirements for the
Degree of Doctor of Philosophy

FIBER AND POLYMER SCIENCE

RALEIGH, NC
1998

APPROVED BY:

_____
HAROLD S. FREEMAN
CHAIRMAN, ADVISORY COMMITTEE

_____ _____
KEITH R. BECK RALPH MCGREGOR

_____ _____
CARL L. BUMGARDNER MYUNG H. WHANGBO

BIOGRAPHY

By Dawn E. Fraser

On the morning of October 29th, 1970, chilly winds heralded the arrival of Jason Lye to his parents Roger and Jenny, who named their son after watching the movie “Jason and the Argonaughts”. He was born in the seaside town of Gt. Yarmouth, in England and in the years to follow, Jason and his sister Julie were joined by two other siblings, Christopher and Jessica, also born in the same area of the UK.

Jason finished his primary education at Palgrave VCP, Norfolk, England. He attended Hartismere High School, (Eye, Suffolk) excelling in many of his subjects, and leaving with five GCE O-Levels and two CSEs. His attention to detail and preoccupation with the sciences made his decision to follow a scientific career an obvious choice. Following his completion of three GCE A-levels and one Special Level course at Diss VI Form Centre (Diss, Norfolk, UK), Jason moved to the Roman town of Colchester, where he worked for Imperial Chemical Industries (ICI Imagedata) on D2T2 electronic photography for a year.

In fall 1990, Jason left his rural roots and headed for the big city of Leeds to pursue a bachelors degree in Colour Chemistry. Jason graduated with a First Class Honors degree, as well as a diploma in Dyeing in 1993. In addition, Jason was awarded the Crabtree prize, a Society of Dyers and Colourists scholarship, and a Sponsorship by Courtaulds Research during his studies at Leeds. He also gained a good grounding in the practical aspects of colouration during his vacations, which were spent working for ICI on electronic photography, and Courtaulds Research on a new fiber known as Tencel.

Through his work at Courtaulds, Jason discovered the nuances of Derby - the town of lights, music, fun, and coal! Jason found the fun side of Derby that the tourist guides missed when they described the beautiful landscapes of the area. He left there with very fond memories before returning to Leeds to finish his degree.

After graduation, Jason decided to take it easy for a while and re-coup some of the finances he had squandered during his wild party days at Leeds. While his application at NC State was being processed, Jason turned his hand to electronics assembly, working on the night shift production line. The routine work was a nice rest for his brain which still ached after finishing his degree.

Six months later, passport, air-line ticket, and acceptance letter in hand, Jason set off for America. On arriving at NC State, Jason initiated his Ph.D. studies, working in the field of organic dye chemistry under the direction of Harold S. Freeman. While at NC State, his hobbies have been varied, and have included photography, fixing old American cars, as well as extensive socializing with his friends.

ACKNOWLEDGMENTS

First, I would like to thank Dr. Harold S. Freeman, the chair of my committee for his calm guidance, patience, and for being a constant source of stability throughout my graduate school career. Through his example, he has tempered my mood and helped me to find new peace of mind.

I would also like to thank my parents, grandparents, and siblings for their love and support during the times that I could not see the light at the end of the four and a half year long tunnel. Also, thanks for the love and support of my roommates, Dawn Fraser (who also wrote my biography), Alison Lamp, Richardo Coelho, Brian George, Jenny Lobdell, and Mickey the cat, as well as my neighbors and dear friends, Micheal Ausbon and Anthony Lindsey.

I appreciate the support and attendance of my advisory committee, Drs. Keith R. Beck, Ralph McGregor, Carl L. Bumgardner, and Myung H. Whangbo, as well as other professors who have given their time for helpful discussions, including Drs. Anton Schreiner, Dave Schultz, Chris Gorman, Warren Jasper, Sam Hudson, Mohan Srinivasarao, and Rudolf Naef. Also, thanks to Dave Hinks, David Jenkins, Robert Kyles, Norman Aminudin, Darrin Guthrie, Jolanta Sokolowska-Gajda, and Russ Cox for beneficial chemistry/computer chats.

I would like to thank the remaining students in the College of Textiles for their friendship and camaraderie. In particular special thanks is extended to other members of Dr. Freeman's group and my office mates, viz., Natacha Berthelon, Julie Clemmons, Heather Bardole, Sachin Nayar, Laura Edwards, Jin-Seok Bae, Monthon Nakpathom, and Vikki Martin, who have helped make this Ph.D. journey a fun learning experience.

This research was funded by a grant from the US Dept. of Commerce through the National Textile Center grant number 99-27-07400.

CONTENTS

LIST OF TABLES

LIST OF FIGURES

1. INTRODUCTION

1.1 DISPERSE AND METAL COMPLEX DYES

Disperse Dyes may be used for the coloration of hydrophobic synthetic fibers such as polyester (polyethylene terephthalate, PET), cellulose acetate, and nylon. Devoid of water solubilizing groups, such dyes are sparingly soluble in water and so may be applied to the fiber either as an aqueous dispersion at high temperature and pressure, or by means of a pad-dry-thermosol or sublimation transfer process. This particular class of dyes is structurally diverse; however, the azo chromophore dominates, followed by anthraquinone and nitrodiphenylamine moieties. CI Disperse Yellow 86, CI Disperse Red 167, and CI Disperse Blue 56 are examples of nitrodiphenylamine, azo, and anthraquinone dyes, respectively, which may be used in situations requiring high lightfastness.

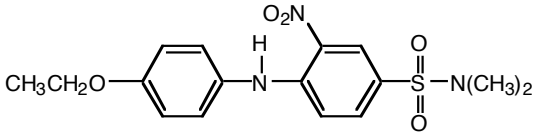

CI Disperse Yellow 86

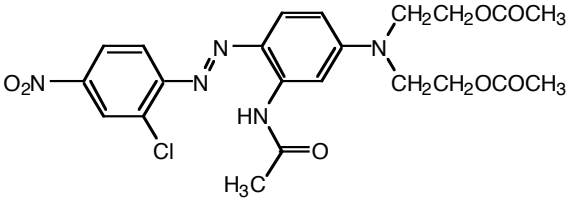

CI Disperse Red 167

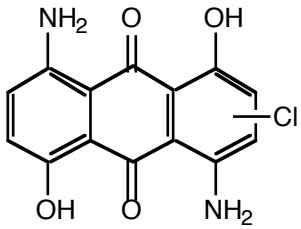

CI Disperse Blue 56

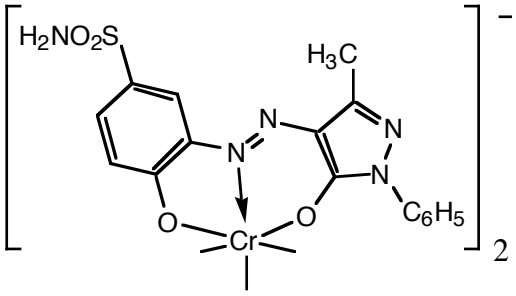

CI Acid Orange 60

Another class of dyes for hydrophobic fibers is 1:2 metallized acid dyes for wool and nylon, of which CI Acid Orange 60 is an example. Although not

always true of metal complex dyes, CI Acid Orange 60 is an example of a metallized acid dye which contains no ionizable ring substituents. However in this case, sulfonamide groups assist water solubility and transport of the dye from the bath to the fiber.

1.2 THE FATE OF EXCITED MOLECULES

Light absorption is prerequisite for color. However, dye molecules must necessarily be resistant to chemical attack arising as a result of the absorption of light, either by the dye molecule itself, or by neighboring species. Before we discuss known light fading reactions of dyes in their end-use environments, it is worthwhile to recount some basic photochemical principles.

The photochemist is principally concerned with the fate of excited molecules. The most commonly observed photochemical processes can be summarized on a Jablonski state diagram such as Figure 1.1, in which bold horizontal lines represent electronic states, and the finer horizontal lines represent vibrational sub-states. The vertical axis gives the energy of a state, while the position of the state along the horizontal axis gives an indication of the degree of bonding associated with a state.

Absorption of light (process a) results in the promotion of the molecule to an *excited state*. The *Franck-Condon principle* states that the atomic centers do not move during an electronic transition, and so a low energy conformation in the ground state will often be a more energetic situation in the excited state. *Vibrational relaxation* (process b) rapidly (within 10^{-13}s) delivers the molecule into the lowest vibrational level of the first singlet excited state. If light absorption promoted the molecule to a much higher state, for instance S_2 (via process a'), then *internal conversion* (process c) delivers the molecule into the S_1 state within 10^{-11}s. Thus, within 10^{-11}s after the absorption of light, the molecule is delivered into the lowest vibrational level of the first excited state. Almost without exception, all photochemistry occurs from this state because internal conversion from this state (process d) is much slower (typically 10^{-8}s),

presenting the opportunity for chemical reactions to occur. In rigid molecular systems with poor internal conversion, *fluorescence* (process e) may successfully compete with internal conversion, dissipating the excited state energy as light. The difference between the absorption wavelength and the emission wavelength is know as the *Stoke's shift*. *Intersystem crossing* events (process f) occur if an electron spin is reversed, usually on a timescale of 10^{-2} to 10^{-5}s. The probability of this process is increased when the triplet-singlet state splitting energy (ΔE_{ST}) is small and other factors are present, such as poor internal conversion (rigid systems), or the presence of heavy atoms.

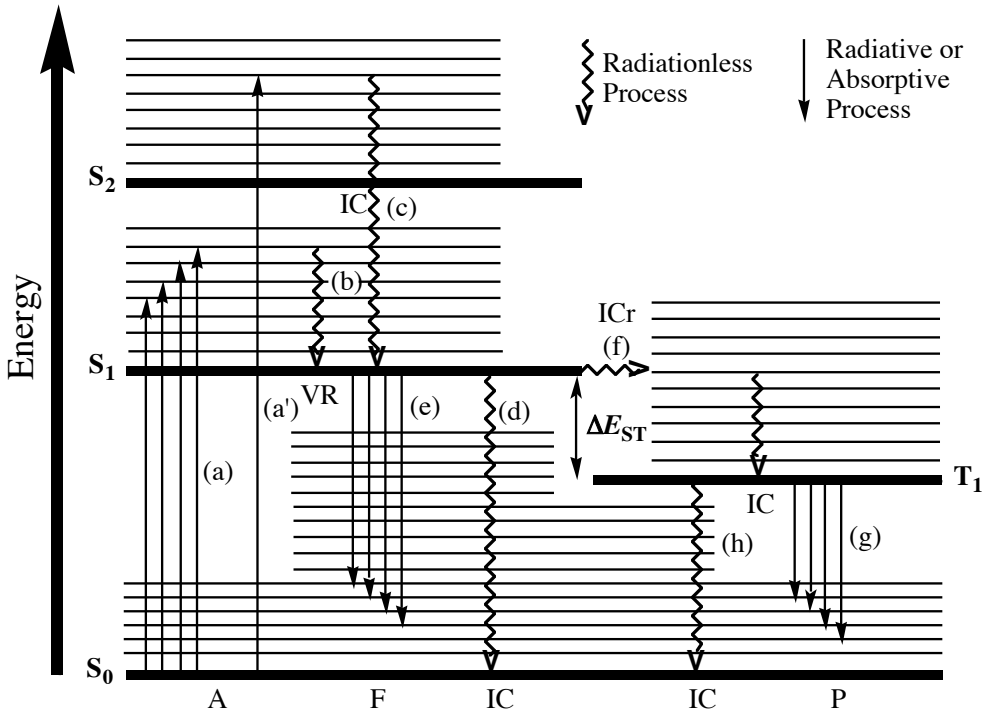

Figure 1.1 *Generalized Jablonski diagram showing major photochemical processes.*

Unless an efficient internal conversion mechanism (process h) is available to deliver the molecule back to the ground S_0 state, *phosphorescence* (process g) will occur with the emission of light. As triplet-singlet transitions are

spectroscopically forbidden, phosphorescence is a characteristically slow process, and may have a lifetime of several seconds. The extremely long lifetimes of these states (0.1 - 1 s) compared to others makes triplet states significant in terms of photoreactivity.

In order to be useful as a dye, the quantum efficiency of fading should remain well below 10^{-4} [1]. This suggests that when chemical photodegradation does take place, it may involve quantum mechanically forbidden pathways which may prove difficult to anticipate [2].

1.3 NON-STRUCTURAL PHOTOFADING CONSIDERATIONS

An extensive review of the non-structural factors which affect photofading would be somewhat redundant, given the preponderance of good reviews published on this subject matter [3, 4, 5]. Bancroft [6] seems to have been the first to report that light induced fading of dyed textiles could proceed via oxidative or reductive pathways, and in the intervening 180 years, a number of studies and reviews have been published which have established the contribution of the state of the dye in the fiber, the nature of the polymer, and also the physical and atmospheric conditions to the fading of dyed polymers [4, 5]. Humidity, temperature, wavelength of the incident radiation, dye aggregation, concentration and distribution of dye in the fiber, substrate characteristics such as diffusion characteristics, dye purity, and functionality are all known to play roles in azo dye photofading [7, 8, 9, 10, 11, 12, 13, 14, 15]. Several workers have taken a less holistic approach to the problem of lightfastness and focused their attention on the dye structures [16].

1.4 PHOTODEGRADATION OF AZO DYES

1.4.1 GENERAL OBSERVATIONS

Azo dyes degrade by undergoing a variety of photochemical reactions, including photocyclization, photoreduction, photooxidation, and photorearrangements. It is difficult to generalize the photodegredation reactions of azo dyes, however free-energy relationships have been identified for series of closely related structures [17, 18, 19, 20, 21, 22, 23, 24]. Griffiths [1] has pointed out that free energy relationships attributed to photoreduction are also consistent with free radical addition reactions at the azo group.

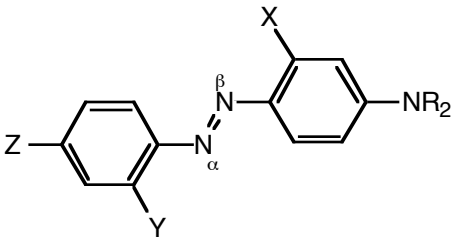

1

Interestingly, Bridgeman and Peters [25] showed that within a series of aminoazo dyes, the photofading rate was inversely proportional to the pK_a of the α azo nitrogen of **1**. Kitao *et al.* [26] also found that photofading generally proceeded faster for less basic dyes when Z or Y = NO_2. Shibusawa and coworkers [27] showed that the pK_a of the α azo nitrogen depended mostly upon the aniline coupler used, and was only mildly affected by the Hammett σ-constant of the substituent Z.

Variations in the assignment of the azo nitrogens as α and β were found in the literature [25, 27, 28, 29]. However, the present review uses only one convention for the sake of clarity.

The lone pair electrons on the terminal amino group have also been implicated in photodegradation [1, 30, 31, 32, 33]. It appears that dealkylation of the amino group of **1** is retarded if electron-withdrawing groups are incorporated into the alkyl chains (R) [1, 31].

1.4.1.1 ORTHO-NITRO SUBSTITUTED AZO DYES

Generally, it had been observed that increasing the electron-withdrawing capability of the acceptor moiety in aminoazo dyes leads to an improvement in lightfastness and a bathochromic shift [18, 19, 21, 22, 23, 25, 28, 30, 34]. An exception is the case in which a nitro group occupies an *ortho* position in the acceptor benzene ring. Such an arrangement always leads to lower than expected lightfastness, despite the electronegativity of the nitro group [26, 28, 39, 34, 35, 36, 37, 38]. This stands in contrast to results obtained from the introduction of a nitro group into the *para* position where good lightfastness on non-amide fibers was obtained. Kitao and coworkers showed that the photofading of 4-nitro substituted aminoazobenzene disperse dyes on polyamide was accelerated by the presence of oxygen, whereas the 2-nitro substituted analogs faded quickly in the presence or absence of oxygen. These results were consistent with intermolecular oxidation in the former case, and intramolecular oxidation in the later. A metastable azoxy compound was proposed as the initial product of intramolecular oxidation (Figure 1.2).

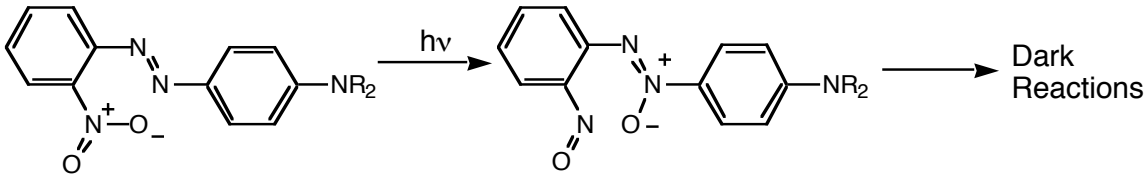

2 **3**

Figure 1.2 *Speculated initial photodegradation steps for ortho-nitro substituted azo dyes.*

This scheme was proposed as an attractive explanation for the deleterious effect of placing a nitro group *ortho* to an azo group in aminoazo dyes [26, 39]. Such dyes fade equally fast in the presence or absence of oxygen [26]. Attempts to isolate and characterize azoxy compound **3** were

unsuccessful [39]. Interestingly, in the same year that Kitao *et al*. proposed the same type of intramolecular reaction shown in Figure 1.2.

Bridgeman and Peters [25] showed that the fading rates of aminoazo dyes of general structure **1** were proportional to the reciprocal of the pK_a of the α-azo nitrogen atom. Attempting to explain the anomalous behaviour of the 2-nitro substituted dyes, Mehta and Peters [28] proposed that the proximity of the negatively charged oxygen to the β-azo nitrogen inhibited delocalization of electrons from the amino group into the azo group.

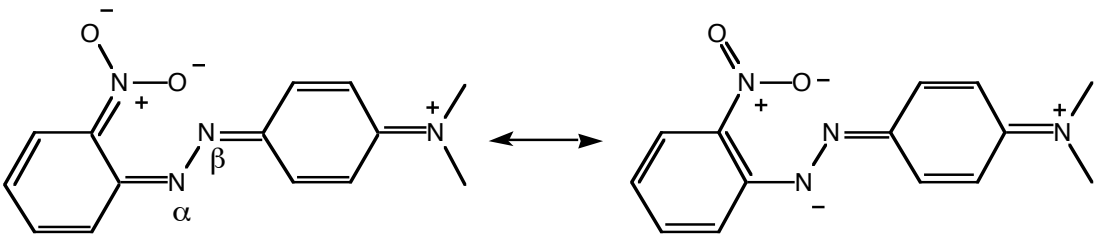

Figure 1.3 *Proposed canonical representation of an excited state of **2**.*

Thus, in 2-nitro substituted azobenzenes, the higher energy resonance form (b) would contribute more to the excited state. Furthermore, increased charge localization on the α-azo nitrogen would increase the pK_b of this atom in the excited state, and according to previous work by the same group [25], this would produce poor photostability [28].

If the proximity of the nitro group oxygen atom did in fact inhibit delocalization of electrons, then it follows that bond lengths about the azo group would be affected in such compounds. However, Freeman *et al.* [39] showed that this was not the case by solving the x-ray crystal structure of related *ortho*-substituted aminoazobenzenes [39, 40]. They found that substitution of the azobenzene skeleton with dialkylamino groups in the 4'- position [40] and also with electron-withdrawing groups, including a nitro group in the 2- position [39] had little effect on bond orders in the region of the azo group, suggesting that the proximity of the oxygen atom did not inhibit electron delocalization.

The x-ray studies of the Freeman group revealed the *ortho*-cyano substituted aminoazobenzene to be planar but the *ortho*-nitro substituted analog was not [39, 40]. The authors proposed that an unfavorable steric interaction between the nitro oxygens and the lone pair electrons on the azo α-nitrogen caused distortions in the molecule. Furthermore, this steric interaction was postulated to explain why *trans*→*cis* photoisomerism was not observed in the case of the *ortho*-nitro substituted azo dye [35] and it was also proposed that the lack of observed photochromism and the low lightfastness are closely related. However, highly sterically congested *cis*-azobenzenes have been prepared by photochemical means and isolated in the past, suggesting that steric interactions alone cannot account for the lack of observed photochromism in *ortho*-nitro substituted azobenzenes [41].

Freeman *et al*. [39] suggested that the proximity of the nitro oxygen to the α-azo nitrogen atom could feasibly lead to the formation of an unstable azoxy compound. An inability to form the *cis* isomer might facilitate azoxy formation and other destructive reactions, due to the loss of a potential non-destructive internal conversion mechanism.

1.4.1.2 PHOTOREDUCTION REACTIONS

It has been shown that reductive dye photofading takes place on synthetic and protein fibers, and also in certain synthetic fibers [15, 42, 43, 44].

Direct Photoreduction involves abstraction of hydrogen atoms from the solvent or polymer by the excited state of the azo compound. Interestingly, Formosinho [45] has shown that the (π, π^*) triplet state of azobenzene is likely to be weakly hydrogen-abstracting in nature. Aliphatic azo compounds do not exhibit direct photoreduction, and it is debatable whether the reduction of the azo group is a true photochemical reaction of the azo group itself [1]. It seems more likely that azo compounds undergo indirect photoreduction [1], whereby the ground state azo compound is reduced by a photochemically generated reducing species. For example, photoexcited ketones can abstract hydrogen

from solvents to give ketyl radicals, which will then readily reduce diaryl azo compounds [46]. Similarly, organic carboxylic acids may undergo light-induced cleavage generating carboxylic acid radicals (·COOH) which are strongly reducing [1].

1.4.1.2.1 PHOTOREDUCTION OF THE AZO GROUP

Reports of direct photoreduction of the azo group in which indirect pathways cannot be precluded are scarce. In 1949, Blaisdell [47] reported the reduction of 4-amino-4'-nitroazobenzene (**4**) in 2-propanol to give *para*-nitroaniline (**5**) and 4-amino-4'-nitrohydrazobenzene (**6**).

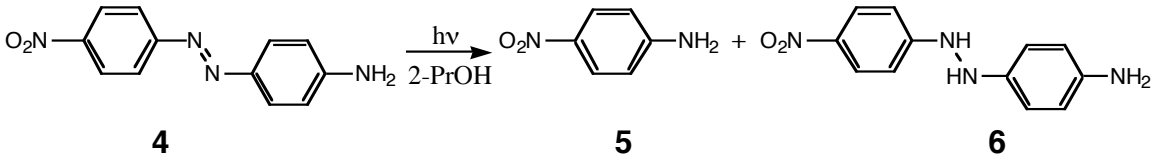

4 **5** **6**

Figure 1.4 *Reduction of aminoazo dyes in an alcoholic environment.*

Hashimoto and Kana [48] showed that (n, π^*) excitations of azobenzene lead only to photoisomerism and that (π, π^*) excitations not only induced *trans* ⇔ *cis* photoisomerism but also photoreduction in 2-propanol. On the basis of this study and quenching / sensitization experiments, the authors proposed that the 2nd triplet $^3(\pi, \pi^*)$ state abstracted a hydrogen atom from the solvent. In this case, hydrazobenzene was formed along with diphenylamine, benzidine, and aniline.

Although both Blaisdell [47] and Hashimoto *et al.* [48] took great care to provide anaerobic conditions for their studies, traces of ketonic impurities (such as acetone from the oxidation of isopropanol) could account for the results

obtained in both cases. This means that the possibility of indirect reduction from the $^3(n, \pi^*)$ state of acetone cannot be ignored [1].

Irick and coworkers [13, 49, 50] investigated the irradiation of 4-(N,N-diethyl)amino-4'-nitroazobenzene (**7**) in various solvents. Reduction was facilitated by protic solvents, such as 2-propanol with a quantum efficiency of 4.8×10^{-4} [50]. Aromatic sensitizers had no effect on the quantum efficiency of reduction, which suggested that the T_1 state of the dye was not involved in the reaction [50]. However, it is known that acetone and benzophenone had significant sensitizing effects on the reaction [13].

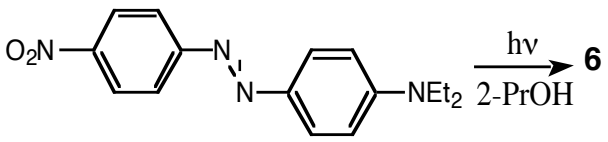

7

Later, Albini *et al.* examined the fading behavior of **7** in alcohol [14]. They showed that the rate of fading depended upon the hydrogen donating power of the solvent. In the most acidic solvent used, methanol, the reduction of **7** proceeded beyond the hydrazo compound **6,** to give *p*-nitroaniline (**5**) and *N,N*-diethyl-1,4-phenylenediamine (**8**).

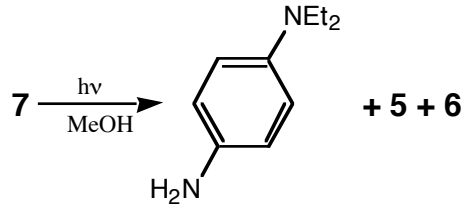

8

Figure 1.5 *Reductive cleavage of the azo group.*

The authors also found a wavelength dependence for the quantum efficiencey of fading in that the rate of fading increased as the wavelength of the incident light was reduced [14]. In agreement with earlier studies, the authors concluded that fading was not occurring from an (n, π^*) state, but more likely from a high-lying $^3(\pi, \pi^*)$ state. The results from this study have since been confirmed by other workers [15].

Griffiths [1] has pointed out that observing a positive correlation between reaction rate and substituent Hammett value is also consistent with a free radical reaction mechanism. Indeed, direct evidence supporting a radical

mechanism for azo dye photoreduction has been provided by other workers [51]. Sirbiladze *et al.* studied the kinetics of the photodegradation of reactive dyes on cotton and in solution. Direct evidence of free radical formation was provided by ESR experiments, and the involvement of free radicals in a photoreductive process was established after the authors observed that the presence of oxygen or free radical quenching entities caused induction times before the onset of photodegradation [51]. In addition, Heijkoop and VanBeek [52] detected hydrazyl and aminonaphthoxy radicals by ESR when they irradiated dye solutions in the presence of a sensitizer, under reductive conditions.

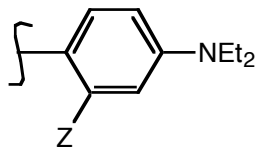

9

Arcoria *et al.* [53] found that variations in the functionality of the coupler affected photodegradation kinetics. *N,N*-Diethylaniline (**9**, Z=H) based dyes exhibited zeroth order kinetics, suggesting that photoreduction was proceeded by excitation of the polymer rather than the dye. In the case of the amido derivatives, Z = $NHCOCH_2CN$ and Z=$NHCOCH_3$, first order kinetics were observed, suggesting excitation of the dye was the initial step in these cases.

Freeman and Hsu studied the photofading of CI Disperse Red 1 (**10**) and CI Disperse Red 17 (**11**) on nylon and PET and showed that these dyes underwent reductive photodegradation, including reduction of the nitro groups and loss of the β-hydroxyethyl groups [42]:

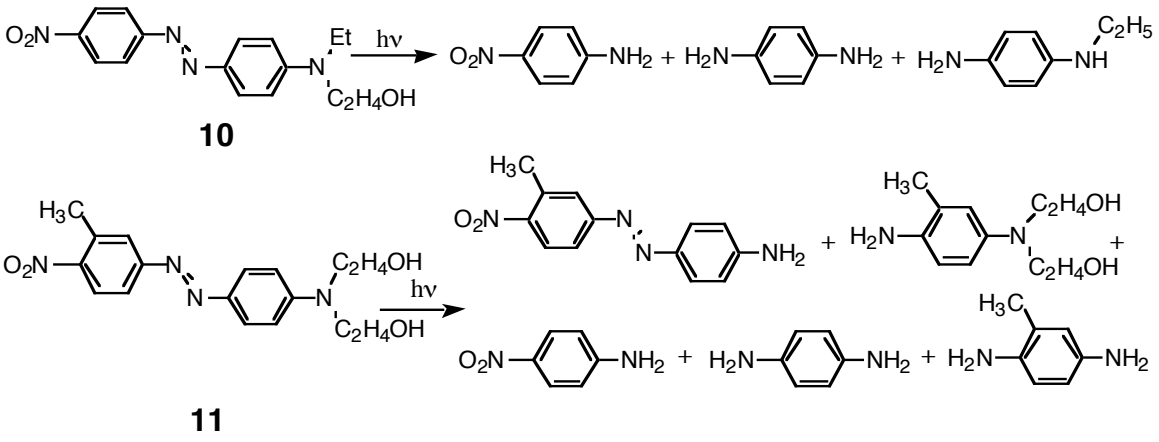

Figure 1.6 *Photodegradation products of CI Disperse Red 1 (**10**) and Red 17 (**11**) in PET and nylon.*

A mechanism was proposed to account for the loss of the β-hydroxyethyl groups during photodegradation [42]. Interestingly, acetaldehyde was formed during the proposed reaction, which could feasibly sensitize further reduction by dint of the hydrogen abstracting properties of photoexcited (triplet) aldehydes.

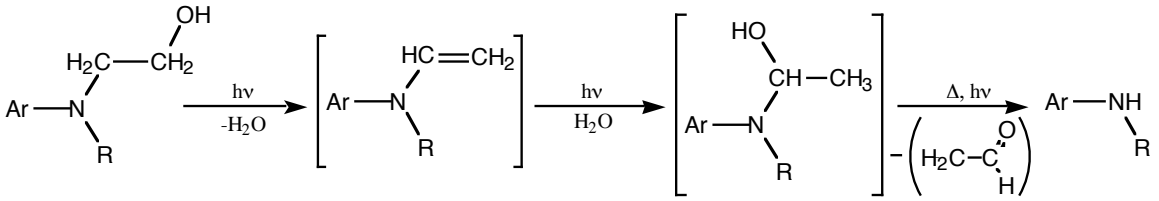

Figure 1.7 *Proposed mechanism for loss of β-hydroxyethyl groups from **10** and **11**.*

A similar photohydrolytic scheme has been proposed to account for the loss of β-hydroxyethyl groups from N-substituted azo-pyridone dyes (actually hydrazones) [54].

Photodegradation studies have been conducted by the Freeman group on the automotive dye, CI Disperse Red 167 (**12**) on PET [43] and also 4-[N,N-di(β-hydroxyethyl)]aminoazo-benzene (**13**) on cellulose acetate [55].

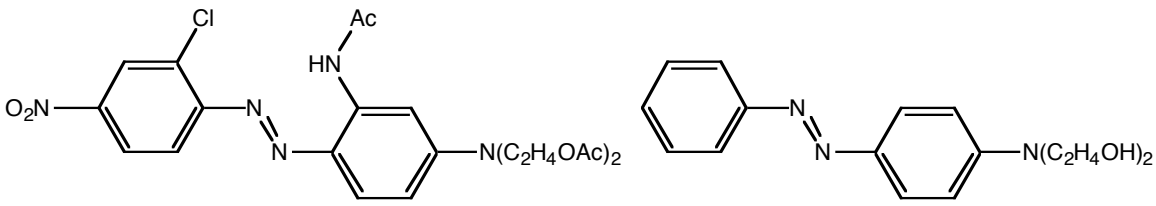

The products of photodegradation consisted of partially or completely reduced dye fragments. Loss of the *N*-alkyl groups was evident in both cases.

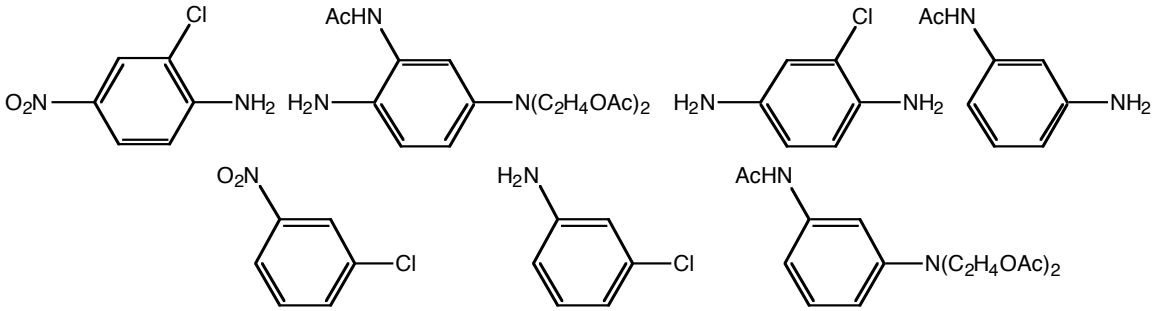

Figure 1.8 *Photodegradation products of CI Disperse Red 167 (**12**) on PET.*

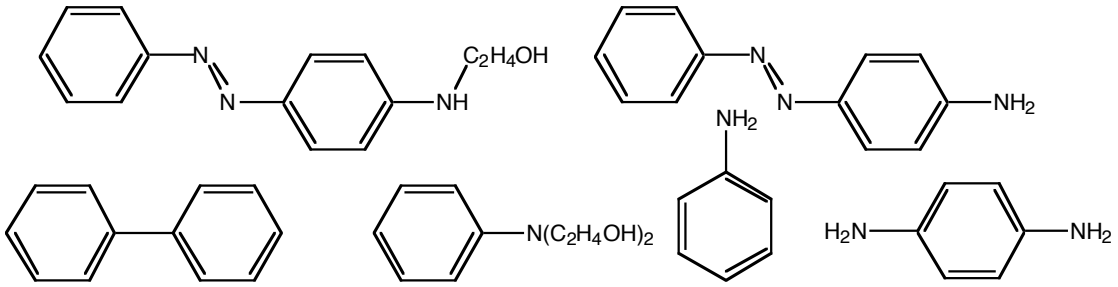

Figure 1.9 *Photodegradation products of **13** on cellulose triacetate.*

1.5 HEXACOORDINATE MEDIALLY METALLIZED AZO DYES

Although considered priority pollutants by the US Environmental Protection Agency, chromium, cobalt, and copper continue to enjoy use in metal complex dyes for wool and nylon in situations requiring high light and washfastness [lvi]. Commonly used for metallization, chromium is a known human carcinogen associated with *bronchogenic carcinoma*, a form of lung cancer [lvii], and concerns that chromium could enter the food chain and water supply have lead to restrictions which limit total chromium concentration in effluent to 1 mg. L^{-1} in the UK [lviii].

So far, metal complex dyes based upon nongenotoxic iron (III) have found limited use for the coloration of textiles, possibly due to a general belief that iron complexed dyes are inferior in fastness to Cr and Co complexed dyes, and that their color gamut is restricted to brown shades. Recent studies have identified black Fe complexes with high lightfastness on wool and suggested that such compound could serve as possible nongenotoxic replacements for Cr complexed black monoazo dyes [lix, lx]. In addition, black iron complex formazan dyes suitable for applications requiring high lightfastness on polyamide and protein fibers have been synthesized [lxi, lxii]. Strikingly, the formazan system also afforded red, violet, to blue shades on wool and nylon. Although perhaps not generally true of azo vs. formazan dyes, Freeman *et al.* found that the lightfastness of Fe-formazan black dyes was better than previously synthesized black Fe-azo dyes [lxi].

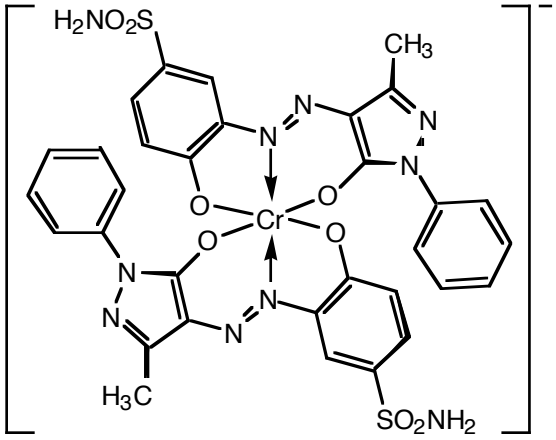

14

Figure 1.10 *CI Acid Orange 60*

Complexation of an azo chromophore with a metal ion (e.g.: Cu^{2+}, Cr^{3+}, Ni^{2+}, $Fe^{2+/3+}$, Co^{3+}) brings about a bathochromic shift, which has been attributed to a shifting of the $^1(\pi, \pi^*)$ state of the parent dye. In this case, the metal ion may be considered a perturbation on the chromogen. n-Orbital splitting is lost by donation to the central metal ion, and the maximum wavelength absorption band becomes purely (π, π^*) in character, as opposed to a crystal field transition associated with the metal [1, lxiii, lxiv].

The presence of the metal ion in the structure of a typical metal complex dye, such as **14** has a two fold bathochromic effect compared to the parent dye. Reaction of the metal salt with the hydroxy group produces a bond of appreciable ionic character; electron release from this oxygen atom to the π-system is easier. In addition, the electronegativity of the azo nitrogen will be increased, as electrons are donated from it to the central metal atom [lxiii].

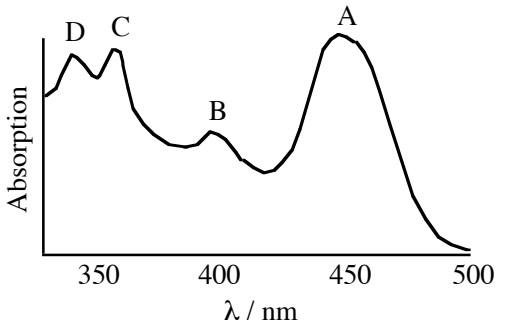

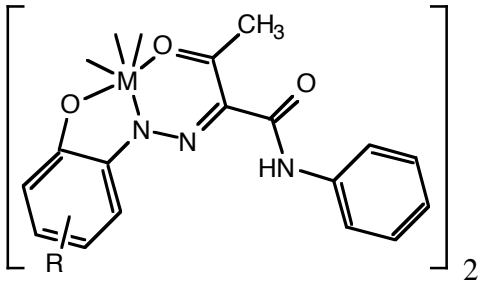

$M = Fe^{3+}, Cr^{3+}, Co^{3+}, Al^{3+}$

Figure 1.11 *Electronic spectrum and structure of **15***

Yagi [lxiv] has studied and assigned the four bands in the electronic spectrum of **15** to transitions localized on the ligand. Yagi was able to make the following conclusions after studying the spectra of the series of metal complexes (**15**) in which M = Fe^{3+}, Cr^{3+}, Co^{3+}, and Al^{3+}. As the metal — oxygen bond became more ionic in character, band A (Figure 1.11) became sharper and more intense, and band C was red-shifted [lxiv]. If an electronegative substituent R was placed *para* to the phenolic oxygen atom, the M—O bond became more polar. Yagi concluded that bonds to Co^{3+} were the most covalent out of the four metals studied; the bonds to Cr^{3+} were essentially ionic and the bonds to the Fe^{3+} atom were a mixture of non-equivalent bonds.

In the case of iron (III), there are two possible stable electronic configurations which would give rise to octahedral complexes. The low spin situation is referred to as a *penetration complex*, and is characterized by a doublet multiplicity. The $d\pi$—$p\pi$ interaction is small for the ligand bonds in the case of the penetration complex. Hexacyanoferrate (III) is an example of a low-spin iron complex. The high-spin (sextet multiplicity) configuration b) is usually formed when iron (III) is complexed with for instance fluoride ions. In this case, bonding electrons are biased in the direction of the ligand, and so the CMA—ligand bond length increases, as does the ionic character of the bond [lxiv].

1.5.1 MO CONSIDERATIONS OF METAL COMPLEX DYES

A molecular orbital diagram of an octahedral first row transition metal complex may be built up by initially considering the lone pairs of the ligand atom in orbitals of σ-symmetry. In an octahedral configuration, linear combination of the atomic orbitals gives six new orbitals; one a_{1g} MO (zero nodes), a triply degenerate set of t_{1u} orbitals (one node), and doubly degenerate e_g orbitals (two nodes) (cf. right hand side of Figure 1.12) [lxv]. The ligand orbitals interact with valence orbitals of the central metal atom of the same symmetry group to produce a new set of orbitals. As the lone pairs of the incoming ligands are

directed down the coordinate axis, the lobes of the t_{2g} orbitals of the central metal atom avoid interaction, and so the energy remains unchanged by the incoming σ-orbitals.

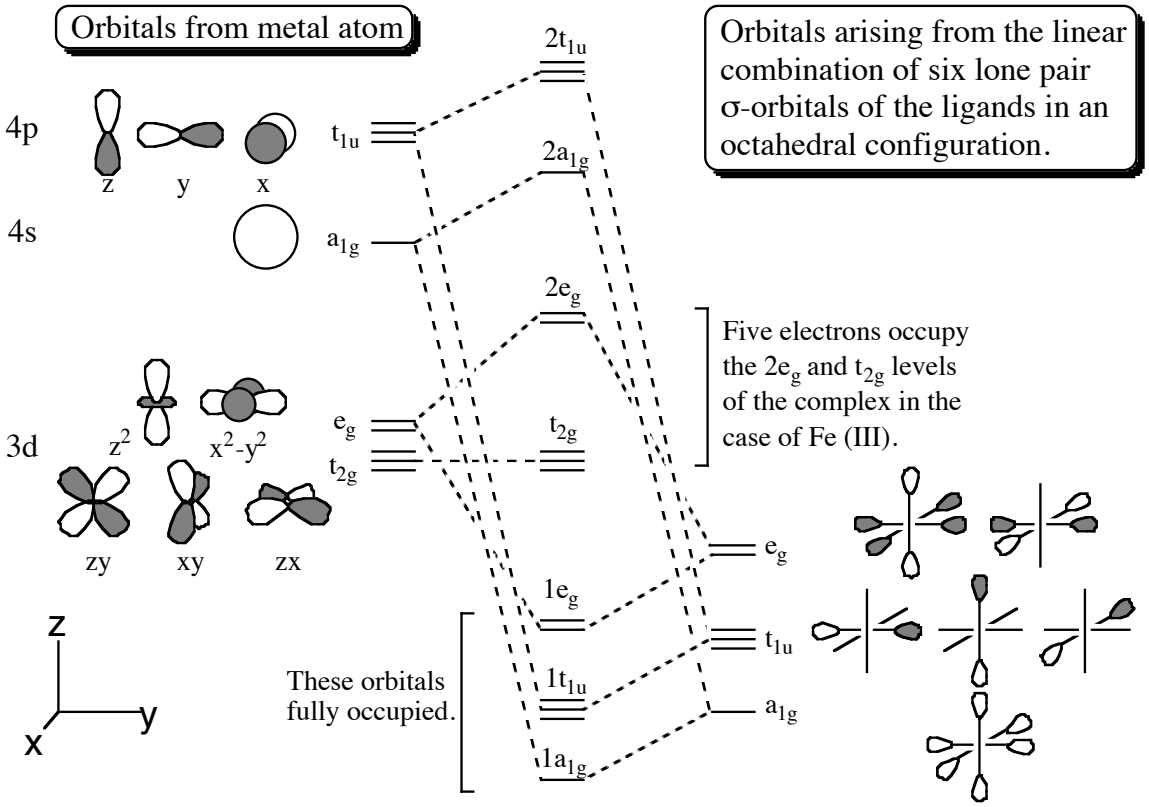

Figure 1.12 *Molecular orbital diagram showing the result of interactions between metal atomic orbitals and six ligand σ-orbitals arranged in an octahedron configuration.*

The first six MOs are filled by the incoming ligand lone pairs; in the case of Fe(III) complexes, five electrons now fill the remaining orbitals. If the t_{2g} and $2e_g$ orbitals are close in energy, then the remaining electrons remain uncoupled, distributing evenly between these orbitals to give a high spin complex. If the gap between the t_{2g} and $2e_g$ orbitals is appreciable, the five remaining electrons will occupy the three t_{2g} orbitals, all but one coupling giving rise to a low-spin complex. In the case of Cr (III) and Co (III), the t_{2g} - $2e_g$ splitting energy is not critical as the former has only three electrons to use to make a stable half-filled

t_{2g} level, and the later may use six electrons to fully occupy the t_{2g} level, stabilizing the low spin complex. Hence, Cr (III) always has an S=3/2 ground state and Co (III) complexes are usually low-spin. The t_{2g} orbitals lay close to the zero-energy (non-bonding) level; the $2e_g$ orbitals are anti-bonding in character, and so filling these orbitals leads to longer and weaker metal-ligand bonds. For this reason, high-spin iron (III) complexes generally contain longer iron-ligand bonds.

Although the t_{2g} orbitals do not interact with the σ-orbitals of the ligands, they are of the correct symmetry to interact with orbitals of π-type symmetry associated with the ligands (cf. Figure 1.13) [lxv]. Whether the t_{2g} orbitals are stabilized or destabilized by this interaction depends upon whether the ligand orbital is a p-atomic (non-bonding) orbital or a π-molecular orbital. Thus, we may define two types of ligands: donor ligands, such as water, OH^-, F^-, which contain a lone pair in a non-bonding p-orbital, and acceptor ligands, which contain π-bonding and antibonding orbitals, such as CN^- and CO.

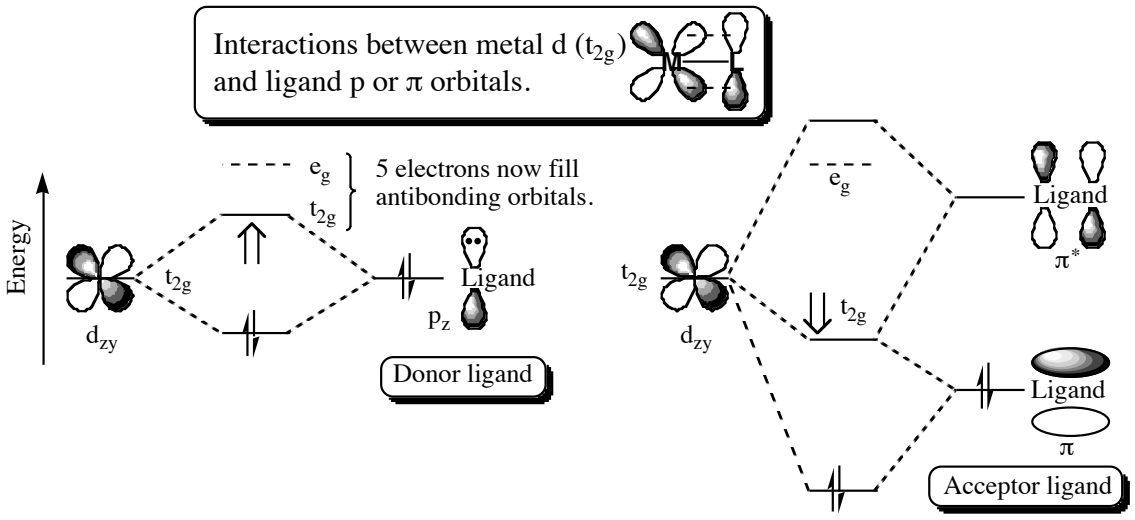

Figure 1.13 *Diagram showing destabilization of the t_{2g} metal d-orbitals by donor ligands (e.g. fluoride) and stabilization of the t_{2g} orbitals by the π-orbitals of acceptor ligands*

Donor ligands with lone pairs in non-bonding orbitals reduce the energy difference between the e_g and t_{2g} orbitals, whereas acceptor ligands containing π-orbitals tend to increase the difference. It stands to reason that acceptor ligands tend to give rise to low-spin complexes whereas donor ligands tend to produce complexes of high spin.

1.5.2 PHOTOCHEMICAL BEHAVIOR

Despite the significance of metal-complex dyes, precious little research into the photochemistry of these compounds has been reported. It is known, however, that metal complex dyes are resistant to oxidation by singlet oxygen [1]. Indeed, Chang and Miller [15] showed that the presence of oxygen inhibited the fading of certain metal complex dyes they examined.

Graves *et al.* [lxvi] studied the effect of metallization on the efficiency of singlet oxygen production by azo dyes. They found that complexation with $Cr^{3+}$and Fe^{3+} increased the quantum yield of singlet oxygen generation; however, they also showed that in cases such as Cu^{2+}, Ni^{2+}, and Co^{3+}, complexation quenched singlet oxygen production. The authors speculated that triplet energy was being transferred from a triplet state predominantly associated with the dye to one predominantly associated with the central metal atom, and indeed, Graves *et al.* showed that Cu^{2+}, Ni^{2+},and $Co^{2+/3+}$ ions posses an energy level below the triplet level of the complexed dye. Therefore, the metal ion is able to absorb the triplet energy [lxvi]. Heavy atom effects must have also played a role in shortening the lifetime of the triplet state in these dyes. In agreement with the results of Graves *et al.,* Sokolowska-Gajda [lxvii] concluded that a range of formazan dyes tested faded via a hydrogen abstraction mechanism, and went on to show that unlike Fe (III) formazan dyes, Co (III) formazan dyes were efficient singlet oxygen quenchers.

Freeman and Sokolowska-Gajda [lxviii] studied the photodegradation of CI Acid Orange 60 (**14**) in dimethylformamide and on nylon 6 6, and also observed reductive degradation. The photodegradation products were identified

as 3-amino-4-hydroxy-benzenesulfonamide (**16**), together with a small amount of **17**, believed to originate from the unstable amine **18**. The 1:1 metal complex was also found, but investigations showed this to be a thermolytic rather than a photolytic degradation product.

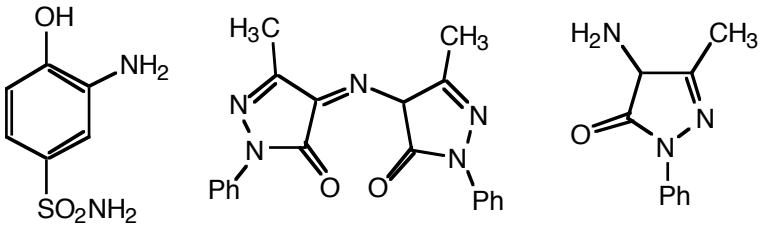

16 **17** **18**

Interestingly, excitation energy transfer from the ligand to the metal atom has been implicated in the photochemical displacement of fluorescent arene ligands in Fe, Ru, and Os complexes. Mann *et al*. [lxix] showed that if the d-d state localized on the CMA is lower in energy than the emissive state energy of the ligand, then excitation energy was transferred to the CMA d-d state and the arene was ejected. Conversely, if the d-d state was higher in energy, the arene would fluoresce with lasing action.

1.5.3 X-RAY CRYSTALLOGRAPHY

The crystal structures of isomeric Cr complex azo dyes **19** and **20** have recently been solved [lxx]. Lehmann and Rihs used a combination of preparative HPLC and x-ray crystallography to establish that at 100°C and pH 9, equilibrium favored the Nα, Nα' over the Nβ, Nβ' isomer [lxx]. The presence of the Nα, Nβ' isomer was also detected in the mixture.

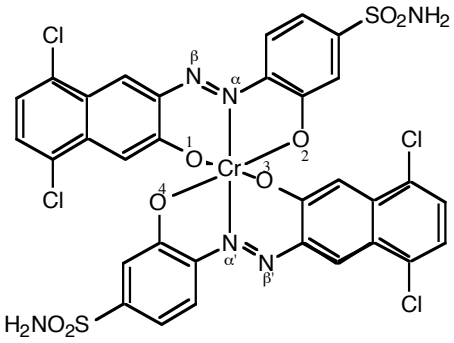
Cl
SO2NH2
β
N
α
N
1
O
Cr
3
O
2
O
Cl
4
O
N
α'
N
β'
Cl
H2NO2S
Cl

19

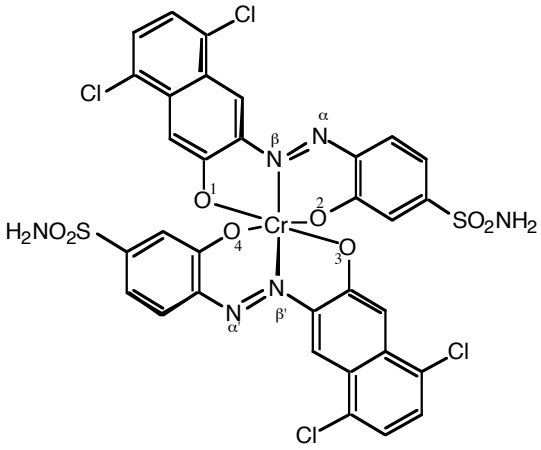
Cl
Cl
β
N
α
N
1
O
2
O
SO2NH2
H2NO2S
O
4
Cr
O
3
N
α'
β'
N
Cl
Cl

20

1.6 PHOTOCHEMISTRY OF NITRODIPHENYLAMINE DYES

1.6.1 GENERAL CONSIDERATIONS

Factors such as high lightfastness and low manufacturing cost have helped maintain the commercial significance of this dye class, despite characteristically low tinctorial strength [lxxi]. All of the commercially important nitrodiphenylamines contain an intramolecular hydrogen bond [43, lxiii, lxxi, lxxii]. Two important examples are CI Disperse Yellow 86 (**21**) and CI Disperse Yellow 42 (**22**).

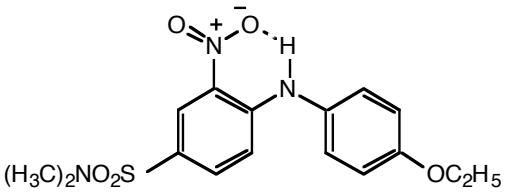

21

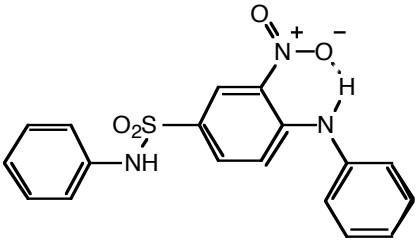

22

N-Methylation of nitrodiphenylamines has little effect on color, suggesting that the hydrogen bond has little bearing on color [lxiii]. However, the hydrogen bond is believed to augment the lightfastness of certain members of this dye class [lxiii, lxxi, lxxii, lxxiii, lxxiv, lxxv, lxxvi, lxxvii, lxxviii]. Generally, dyes in which hydrogen bonding between the nitro group and the amino hydrogen is possible tend to be faster to light than those which do not contain this interaction.

1.6.2 LIGHT ABSORPTION AND INTERNAL CONVERSION

Nitrodiphenylamine dyes fall into the donor-acceptor (simple acceptor) chromogen classification of Griffiths [lxiii], as light-induced charge migration is limited to a few atoms, and involves a movement of charge from the amine to

the nitro chromophore upon excitation. A quinonoid type excited state resonance structure has been proposed [lxxiv, lxxv, lxxvi], and internal conversion from this state is believed to be facilitated by efficient excited state intramolecular proton transfer (ESIPT, Figure 1.14) in the case of 2-nitro substituted dyes [lxxv].

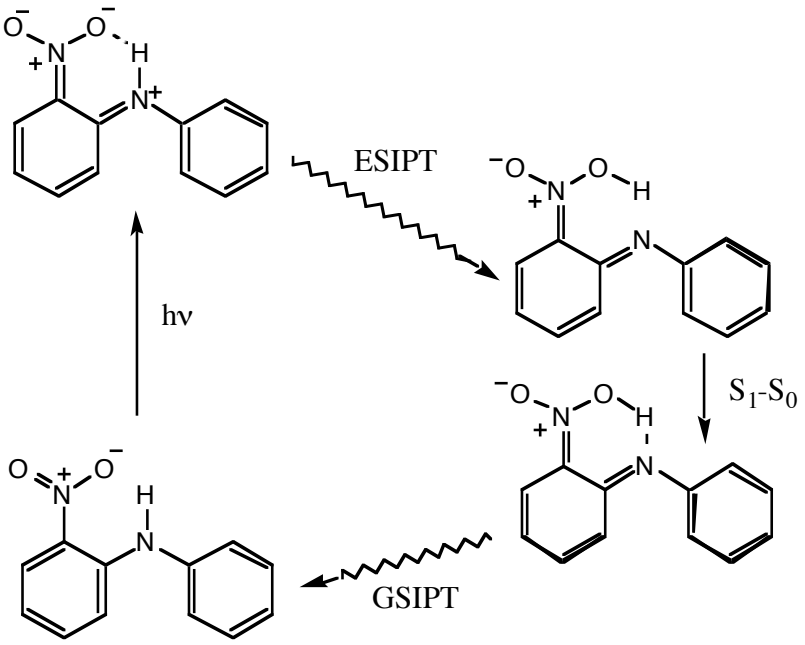

Figure 1.14 *Internal conversion via excited and ground state intramolecular proton transfer (ESIPT and GSIPT).*

Dyes which lack a nitro group at position 2 typically exhibit poor lightfastness [lxxi, lxxv, lxxvi]. Excited state proton transfer from nitrogen to oxygen via a proton tunneling mechanism has been observed spectroscopically in the case of 1-amido anthraquinone [lxxix]; however, these authors suggested that the efficiency of this internal conversion mode depended upon the pK_a of the proton donating nitrogen. In the case of 1-aminoanthraquinone, the pK_a of the donating nitrogen is approximately 25, and so excited state intramolecular proton transfer (ESIPT) is negligible [lxxix]. A search of the literature did not reveal any spectroscopic studies which could confirm that an ESIPT mechanism operates, although it is generally accepted that this process takes place. If the principal internal conversion mechanism of nitrodiphenylamines is indeed via ESIPT, then the increased electron density at the nitro group oxygen atoms compared to the anthraquinone oxygen atoms must facilitate the transfer process in excited nitrodiphenylamine dyes.

In situations where ESIPT is clearly unavailable as an internal conversion pathway, then low lightfastness may be anticipated. Interestingly, Szadowski and Przybylski [lxxii] showed that adding a second chromophore to a nitrodiphenylamine (in this case, an azo group) enhanced the lightfastness of *N*-alkylated nitro dyes such as **23**, compared to monochromophoric *N*-alkylated nitrodiphenylamines. Presumably, internal conversion of energy absorbed by the dye was assisted by the azo group [lxxii].

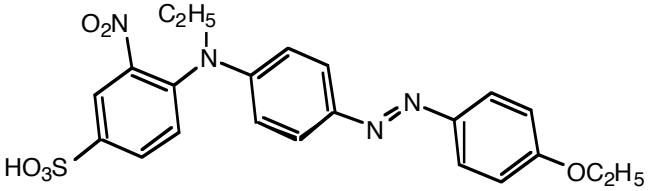

23

Two research theses from the Freeman group report the photoreductive degradation of CI Disperse Yellow 42 (**22**) in ethyl acetate [lxxx] and PET [43] under xenon arc and natural (Florida) sunlight. The breakdown products were identified by DCI mass spectrometry and TLC, which showed that the two chemical environments gave rise to similar photodegradation products. In addition to the compounds shown in Figure 1.15, an unidentified polymeric crystalline material was also isolated from the exposed ethyl acetate solution. The degradation products produced were found to be sensitive to both the chemical nature of the substrate and the spectral distribution of the incident radiation.

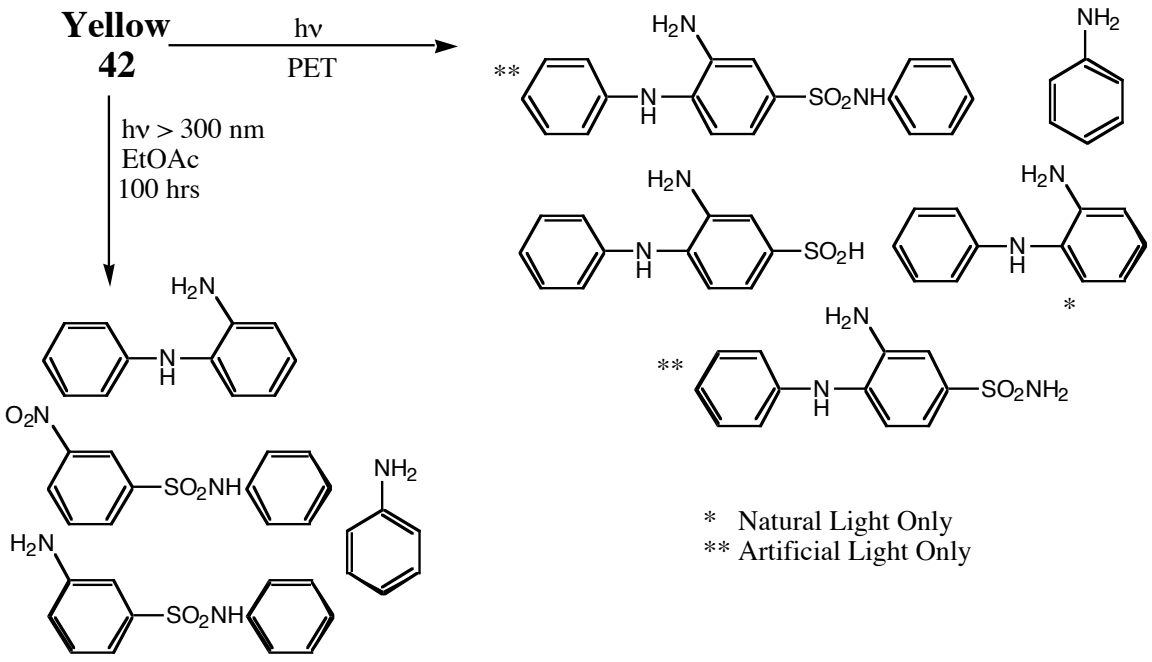

Figure 1.15 *Photoreductive products of CI Disperse Yellow 42.*

1.7 UV ABSORBING PHOTOSTABILIZERS

UV absorbers stabilize neighboring molecules (whether polymers or dyes) by absorbing and efficiently dissipating ionizing UV radiation before it causes damage. A cursory structural examination of the numerous commercial UV absorbers shows that all contain intramolecular hydrogen bonds in which hydrogen is attached to an sp^2 nitrogen or oxygen atom [lxxx].

1.7.1 HYDROXYBENZOPHENONES

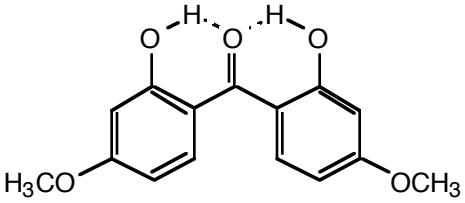

24

One of the first types of UV absorbers developed was hydroxybenzophenones, such as Ultrafast 830 (**24**) manufactured by BASF [lxxxi, lxxxii]. It is generally accepted that this class of compounds owes its light stability to facile intramolecular proton transfer in the excited state (ESIPT) [lxxxiii]. Indeed, transient absorption spectroscopic studies have shown that 2-hydroxybenzophenone undergoes photo-induced tautomerism as depicted in Figure 1.16 [lxxxiv]. In the ground state the phenolic tautomer is thermodynamically favored, but in the first excited state, the keto tautomer is favored; thus rapid ESIPT takes place within 10 picoseconds (in methylene chloride) [lxxxiv]. The corollary is that the ground state and excited state potential surfaces come into close proximity at the keto tautomer structure. As previously discussed (page 22), a similar ESIPT mechanism has been invoked to account for the high lightfastness of 2-nitrodiphenylamine dyes.

The parent compound, benzophenone, being devoid of protic groups undergoes *intermolecular* photoreduction from the long-lived $^3(n, \pi*)$ state to give the pinacol product. *Para* substitution by an electron-donating group such

OMe causes a redistribution of the energy levels such that the first triplet state is delocalized to form a $^3(\pi, \pi^*)$ state [46]. Delocalization of the state reduces the hydrogen-abstracting ability of the carbonyl oxygen. It is likely that the methoxy groups of the Ultrafast stabilizers increase the effectiveness of these products, not only by adjusting the absorption spectra [lxxxv] but also by reducing the reactivity of the triplet excited state.

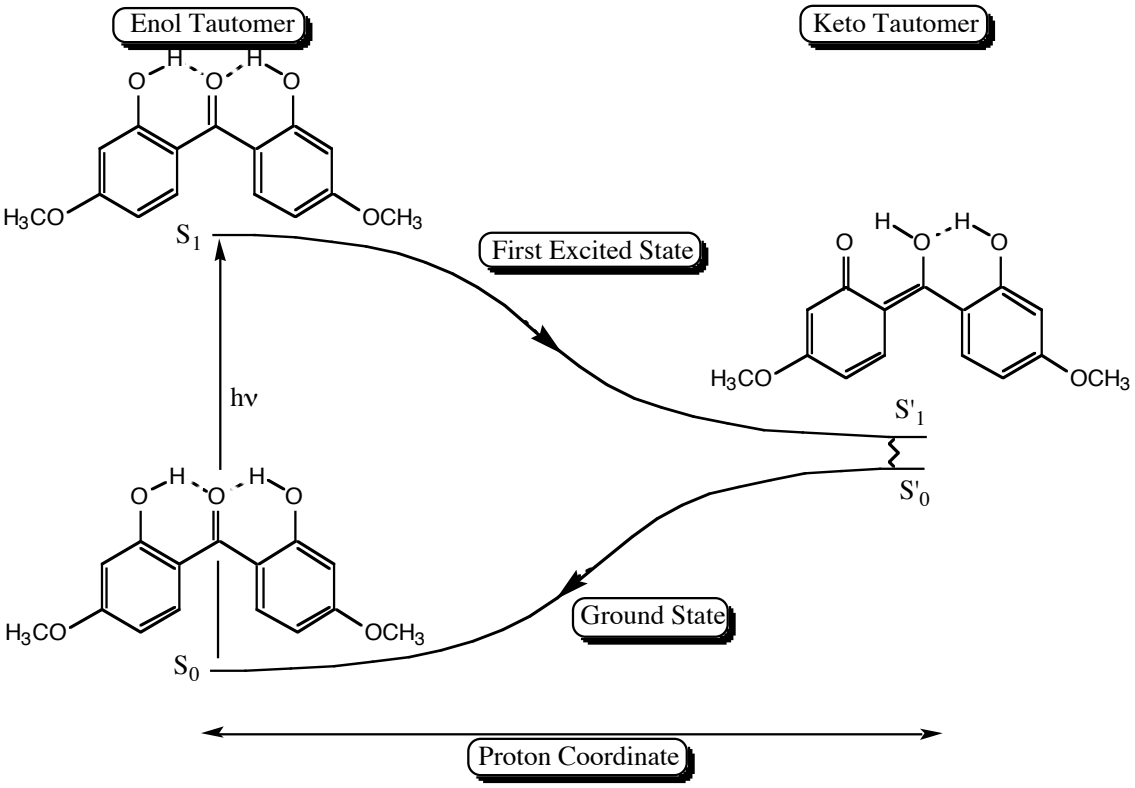

Figure 1.16 *Internal conversion of absorbed energy via excited state intramolecular proton transfer (tautomerism) by hydroxybenzophenones.*

1.7.2 HYDROXYBENZOTRIAZOLES

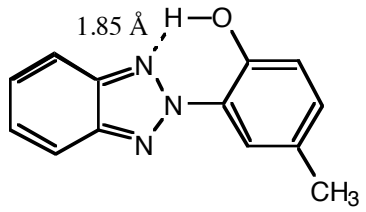

25

Another type of photostabilizer that has generated much commercial and academic interest is the 2'-hydroxyphenylbenzotriazole class such as Tinuvin P (**25**) from Ciba-Geigy. The photostability of these compounds has been attributed to an intramolecular hydrogen bond which forces the molecule into a planar geometry [lxxxiii, lxxxvi, lxxxvii, lxxxviii]. If the hydrogen bond is broken, by for example, polar solvents or ionization, the molecule becomes non-planar, phosphorescent, and subject to photodegradation [lxxxiii, lxxxix, xc].

Woessner *et al*. [lxxxvi] confirmed both the planar geometry of **25**, and the presence of a strong intramolecular hydrogen bond, by solving the x-ray structure. This study also confirmed the high degree of bond alternation in the benzotriazole moiety. The authors proposed a proton transfer mechanism, (Figure 1.19) which operated both in crystals and in frozen hydrocarbon matrices, to account for the extremely long Stoke's shift that they had observed [lxxxvi].

Woessner's tautomerism mechanism was generally accepted [lxxxiii] until Catalan *et al*. [xci] proposed an alternative stabilizing mechanism, based upon results from molecular modeling studies. Computations performed at the INDO semi-empirical level suggested that the keto tautomer did not form and hydrogen transfer did not take place in the $^1(\pi, \pi^*)$ state because the excited molecule was non-planar. The group used CNDO/S to locate the energy levels of triplet states and calculated that the lowest triplet state was located at 35 kcal.mol^{-1}, and that this state was not associated with proton transfer [xci]. They proposed that **25** physically quenched photoexcited impurities in the

polymer (e.g. carbonyl compounds) by accepting energy before degradative processes were initiated [xci].

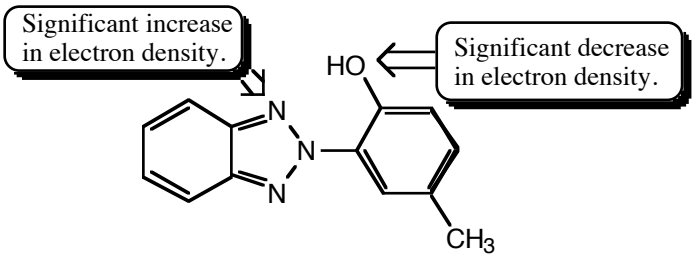

Figure 1.17 *Calculated electron density changes upon excitation.*

Although not discussed in the paper, close examination of the authors results, and in particular, the coefficients of the MOs involved in the longest wavelength absorption, revealed that the electron density redistributed in a manner that could facilitate proton transfer from oxygen to nitrogen upon excitation [xci] (Figure 1.17). The controversy was finally ended by Allan *et al.* [xcii], who showed that the lowest triplet state of **25** lies at approximately 70 kcal.mol^{-1}, and was therefore unlikely to act as a quencher.

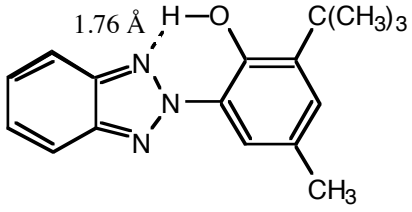

26

Introduction of a *t*-butyl group *ortho* to the hydroxy group of Tinuvin P was found to improve the photostability of this compound (**26**). Greenwood, Mackay and Wilshire [lxxxvii] showed from x-ray studies that the *t*-butyl group increased the strength of the hydrogen bond, reducing the H…N distance by almost 0.1 Å (**26** cf. **25**). In the same year, workers investigated the stabilizing role of the *t*-butyl group [lxxxix]. They assumed that photodegradation of this compound would take place from an open conformation, which arose after breaking the hydrogen bond. Catalan *et al*. [lxxxix] proposed that polar solvent could disrupt the intramolecular hydrogen bond by twisting the OH group, thus allowing relative rotation of the two ring systems (Figure 1.18) .

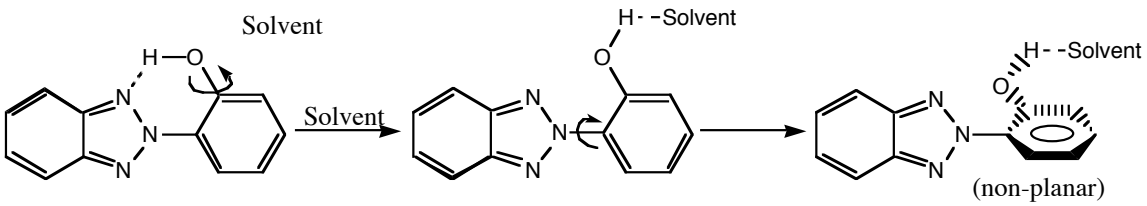

Figure 1.18 *Proposed generation of non-planar conformations of **25** by the presence of polar solvents.*

The authors proposed that the role of the *t*-butyl group was two fold: i) its bulk shielded the hydroxy group from solvent molecules approaching from the rear of the OH group, and ii) it prevented rotation of the OH group out of its hydrogen bonding position. Phosphorescence data was also collected [lxxxix] which showed that the lifetime of the first triplet state was not influenced by the presence of the *t*-butyl group, and so the higher stability of **26** compared to **25** could not be attributed to any extra degrees of freedom introduced into the system which could assist internal conversion from the T_1 state. Access to the triplet state of **26** was more restricted, however, as more efficient internal conversion of energy due to the contrived positioning of the hydroxy group in **26** competed more effectively with intersystem crossing events.

Interestingly, the assumptions of Catalan *et al*. [lxxxix] concerning photodegradation of Tinuvin P were later confirmed [xc]. Basing their results on spectroscopic evidence, Catalan and coworkers [xc] estimated that in DMSO, 56% of **25** existed in a non-planar, conformation. Researchers realized that as the excitation wavelength was reduced, the quantum efficiency of phosphorescence and photodegradation increased and furthermore, the phosphorescence excitation spectrum matched the quantum yield curve for photodegradation [xc], suggesting that the triplet state was involved in photodegradation. The authors also examined interactions between **25** and singlet oxygen, concluding that:

1) the closed (planar, hydrogen bonded) conformation of **25** was inert to $^1O_2$,

1) the open (twisted) conformation of **25** did not chemically react with $^1O_2$, but physically quenched it,

1) ionized Tinuvin P (**25**) photofaded rapidly in the presence of $^1O_2$,

1) photodegradation of **25** occurred from the triplet state of the open conformer.

Wiechmann *et al*. [lxxxviii] have undertaken an extensive spectroscopic investigation of the photochemistry of **25**. Infrared spectroscopy showed the presence of hydrogen bonding in the molecule which was weakened by polar solvents [lxxxviii]. UV-Visible spectroscopy showed two absorption bands - one at 345 nm associated with electron density changes over the entire molecule, and one at 300 nm which involved orbitals centered on the triazole ring (see Figure 1.21). Steady state emission and excitation studies showed that absorption at 345 nm led to fluorescence emission at 640 nm ($\phi = 10^{-5}$), however absorption at 300 nm led to fluorescence at 425 nm. After considering the Stokes shifts from each, the absorption band centered at 300 nm was assigned to the non-planar form of the molecule which predominates in polar solutions [lxxxviii].

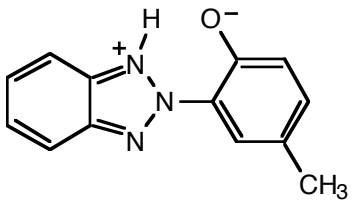

27

The red emission was thought to be due to the zwitterionic structure **27**, which has very loosely been termed the keto tautomer. Time resolved fluorimetry showed the red emission to be very short lived (< 5 picoseconds) in non-polar solvents, and independent of the viscosity of the local environment [lxxxviii]. The blue emission lifetime was found to be on the order of 10^3 times longer than the red emission lifetime [lxxxviii].

Femtosecond pump and probe techniques use the principle of stimulated emission to monitor structural changes in the excited states of molecules, and this technique was used to measure the time required to generate the proposed red emitting tautomer after initial light absorption [lxxxviii]. A high intensity

pump pulse at 310 nm was used to excite a solution of **25**. Low intensity probe pulses at 600 - 700 nm were then used to probe the buildup of the red emitting tautomer. The intensity of emission stimulated by the weak probe pulses reached a maximum after 200 femtoseconds in polar solvents and 100 femtoseconds in non-polar solvents. The experiment was repeated in polystyrene, which showed that the local viscosity did not interfere with the ESIPT process [lxxxviii]. The experiments allowed the authors to measure the timescales of the processes that occurred after excitation and construct the following diagram to describe the reaction [lxxxviii].

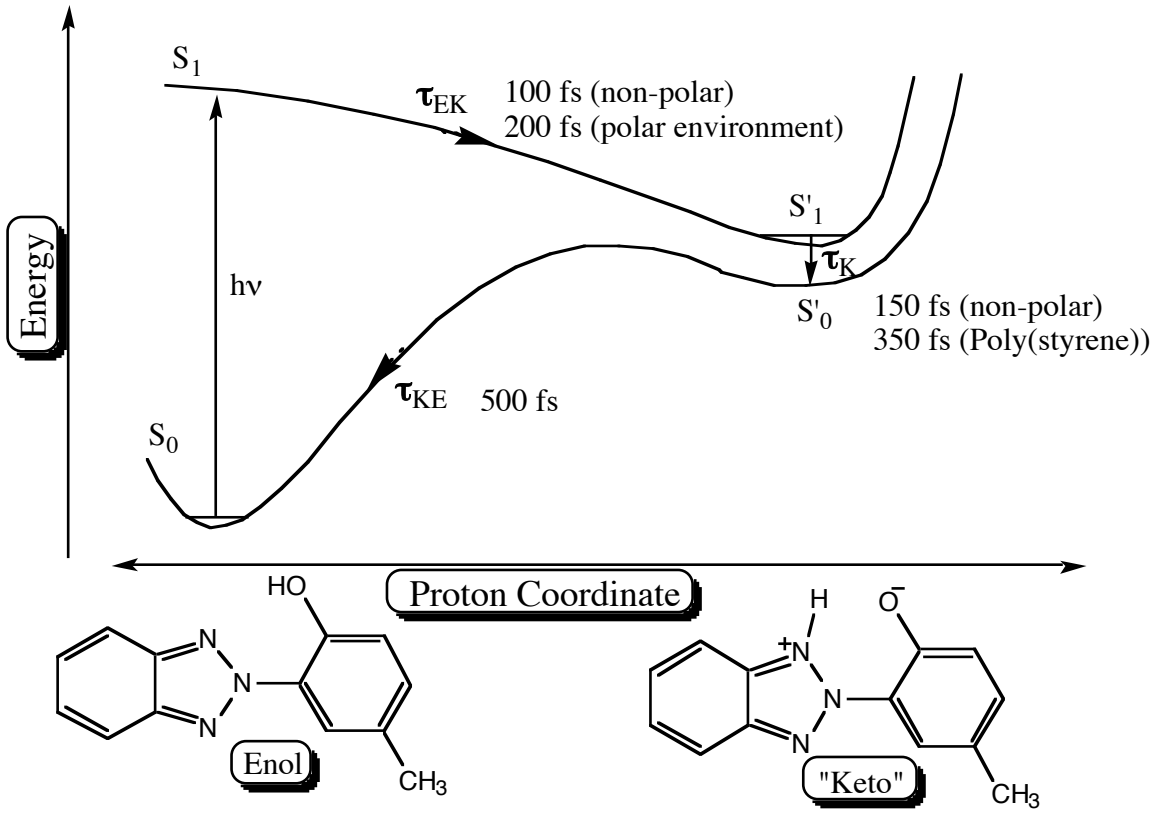

Figure 1.19 *Internal conversion of absorbed energy by ESIPT in hydroxybenzotriazoles showing experimental timescales for the transfer processes.*

The excited state surface allows a barrierless transition from the enol to the so-called keto tautomer, which explains the very short timescale τ_{EK} for

excited state enol → keto tautomerism. τ_K is also very fast. Keto Tinuvin (**25**) is thought to contain an essentially single bond between the phenyl ring and the benzotriazole moiety [lxxxviii]. The authors proposed that the single bond character allows low frequency vibrational modes about this bond, which most probably enhanced internal conversion (S'_1 - S'_0 .) Molecules arrive on the ground state surface extremely hot (800 - 1000 K) and as cooling time is estimated at 5 - 50 picoseconds, and proton transfer in the ground state was measured to take only 500 femtoseconds (0.5 ps), there is ample time for the kinetic energy to be used to overcome the small energy barrier in the ground state surface [lxxxviii]. The results of Wiechmann *et al*. showed that the complete reaction cycle takes place on a sub-picosecond timescale, independent of solvent polarity.

Enchev [xciii] modeled the ground state proton transfer from the keto tautomer to the enol tautomer of **25** using the MOPAC 6.0 implementation of AM1. Interestingly, and in disagreement with x-ray data [lxxxvi, lxxxvii], the two ring systems in Enchev's AM1 optimized geometries were non-coplanar, although the energy barrier to rotation about the phenyl-triazine bond was calculated to be extremely low (1.1 - 0.9 kcal.mol.$^{-1}$). A literature search revealed that AM1 tends to slightly underestimate π-system resonance energy [xciv], which could be a contributing factor to the calculated planar geometry in the ground state of this molecule. Aspersions have been cast regarding the ability of AM1 to reproduce hydrogen bond geometries with fidelity [xcv, xcvi]. Enchev [xciii] used the TS (transition state) routine of MOPAC 6.0 to optimize the transition state of **25** for proton transfer, using vibrational analysis to confirm that the structure was in fact a true transition state. The optimized transition state was found to be planar, and from Enchev's results, it is possible to construct the ground state reaction co-ordinate diagram shown in Figure 1.20 [xciii]. Enchev obtained the enthalpy and entropy change of reaction from MOPAC AM1 and then used the Eyring equation to obtain a calculated rate

constant for proton transfer of $2.24x10^6$ s^{-1} [xciii]. It is likely that the actual value for k is much higher, as comparison with *ab initio* methods suggests that the AM1 method may overestimate energy barriers to proton tunneling by as much as 300% [xciv].

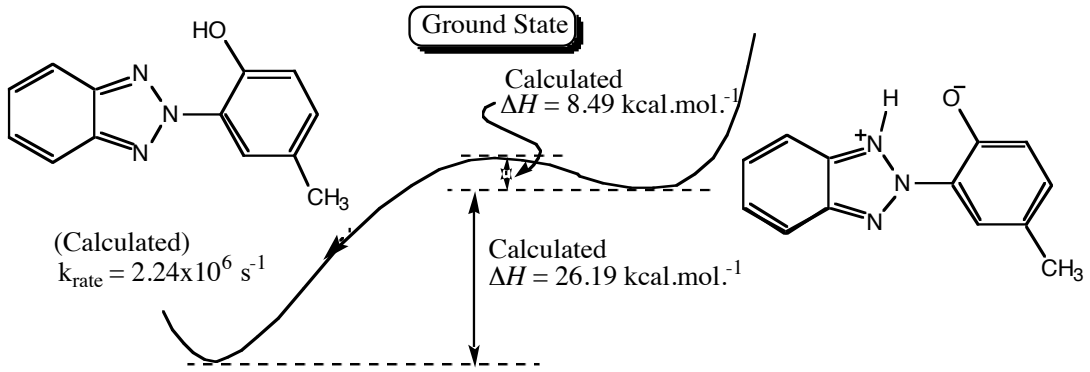

Figure 1.20 *Ground state reaction coordinate diagram for the tautomerism of TIN P, as calculated by Enchev (AM1).*

Sublimation of photostabilizers from treated surfaces inside cars can cause the buildup of an undesirable yellow oily film on the inside of car windshields. Morigana [xcvii] has developed substituted hydroxybenzotriazole photostabilizers which do not sublime (see **28**). The nature of R was not discussed, but the presence of the ester group had a pronounced effect on the UV spectrum of the compound. The two characteristic transitions of **26** were replaced by a single absorption band when the ester group was added onto the benzene ring.

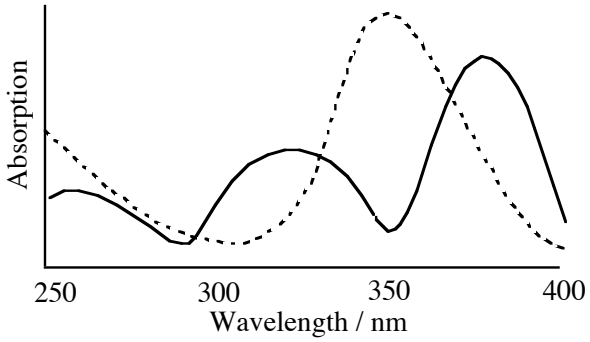

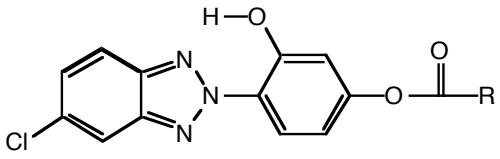

28

Figure 1.21 *Effect of substitution on the UV spectrum of hydroxy-benzotriazoles. Solid line is spectrum of **26**, dashed line shows spectra of **28**.*

1.8 DYES CONTAINING UV ABSORBING MOIETIES

US Patent 4,902,787 by Freeman [xcviii] discloses examples of nitro and azo dye structures into which hydroxybenzophenone and hydroxybenzotriazole photostabilizers had been incorporated. Freeman's approach was to identify structures common to both the parent dye and the parent photostabilizer, and then to combine the two structures to make a hybrid compound:

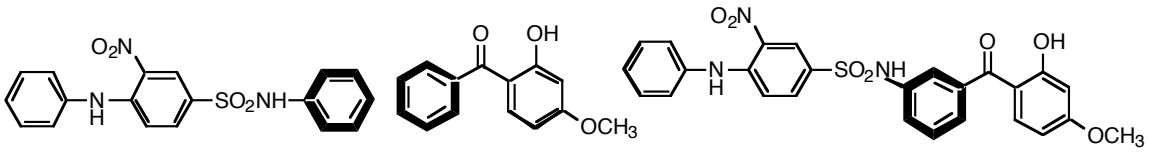

22 **29** **30**

In this case, CI Disperse Yellow 42 (**22**) is combined with a hydroxybenzophenone (**29**) to form a bichromophoric dye (**30**) in which the two systems share a common benzene ring. Another example arises when **22** is combined with the hydroxybenzotriazole structure, **31**:

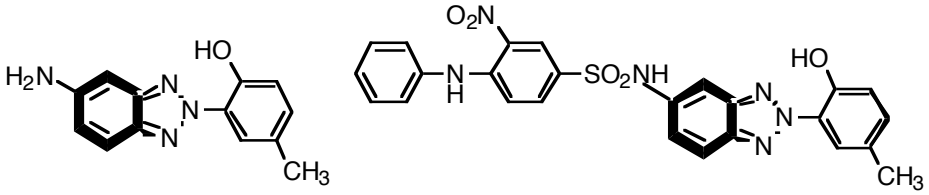

31 **32**

Mason, Posey and Freeman [lxxxv] later published papers which described Disperse Yellow 42 analogs containing hydroxybenzophenone, hydroxybenzotriazole and oxalanilide groups, The authors concluded that:

1) by making a composite molecule, the photostability of Disperse Yellow 42 could be improved; and

1) co-exhaustion of a commercial photostabilizer with the "composite" dye led to further improvement in photostability; and

1) the location of the photostabilizer moiety (i.e., sulfonamide link vs. diphenylamine residue) had variable effects on the LF ratings.

Later results involving Yellow 42 analogs containing oxanalanide photostabilizers allowed the Freeman group to rank photostabilizer effectiveness for use as the second chromophore in the order of oxanalanide > hydroxybenzophenone > hydroxybenzotriazole [xcix]. With the passage of time, more dyes containing built in UV absorbers were prepared by the Freeman group [c, ci, cii]. Freeman and Posey [cii] showed that in the case of CI Disperse Yellow 86, both the ring into which the stabilizer was placed and the type of stabilizer incorporated had a dramatic influence on [lxxxv]. This group was able to synthesize three dyes that were more stable than a physical mixture of the parent dye and commercial photostabilizer, viz., **30**, **33**, and **34**. In addition, dye **35** possessed slightly improved lightfastness over the parent dye.

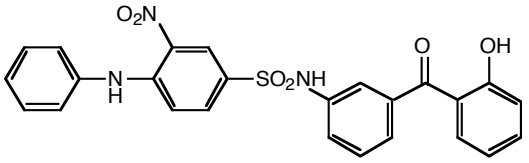

33

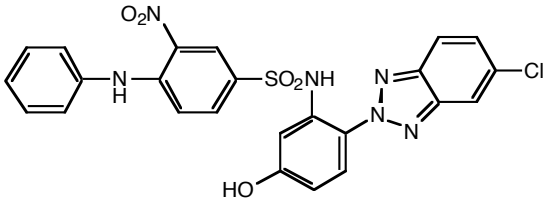

34

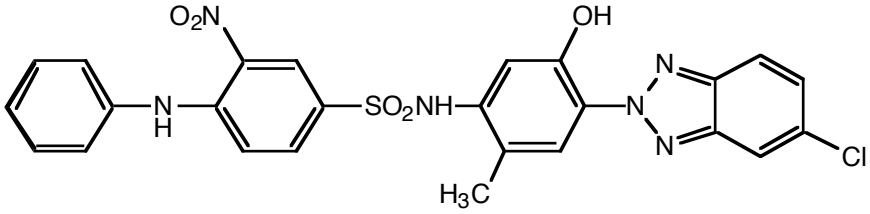

35

In the case of Yellow 86, the analogs prepared were found to have lightfastness that varied widely with structure [c]. For example, **36** and **37** are structurally similar and yet the lightfastness was found to be very different. Some Disperse Yellow 42 analogs were also found which exhibited similar substituent sensitivity. Although the pair of dyes represented by **38a** and **38b**

differ by only a methyl group, their lightfastness ratings were different. Furthermore, the addition of the ethoxy group (see **39a** and **39b**) caused a reversal of the effect of incorporating a methyl group into the structure.

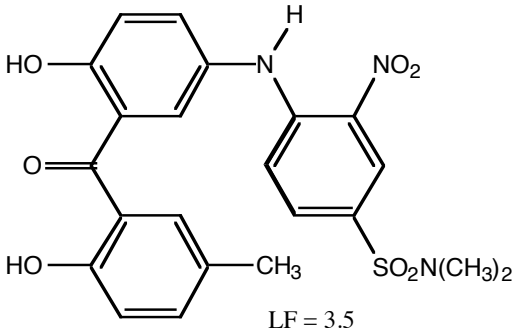

LF = 3.5

36

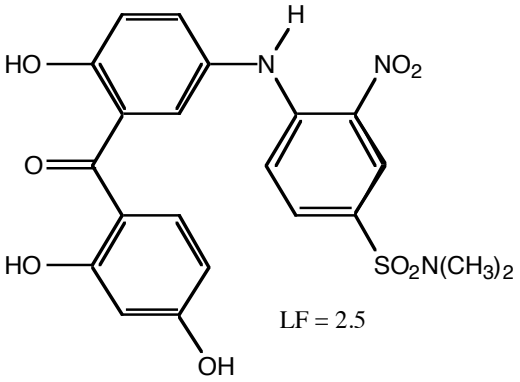

LF = 2.5

37

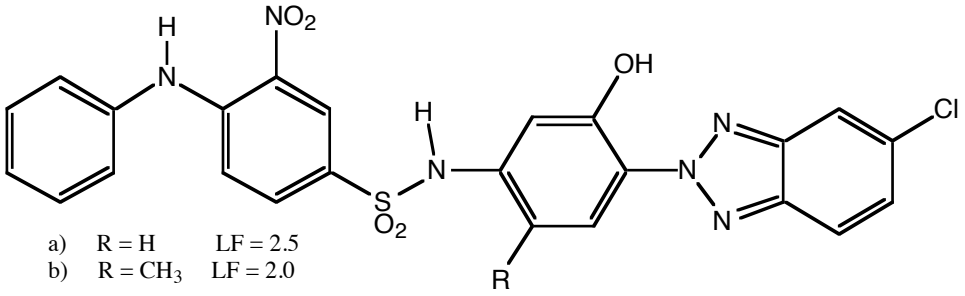

a) R = H LF = 2.5
b) R = CH_3 LF = 2.0

38

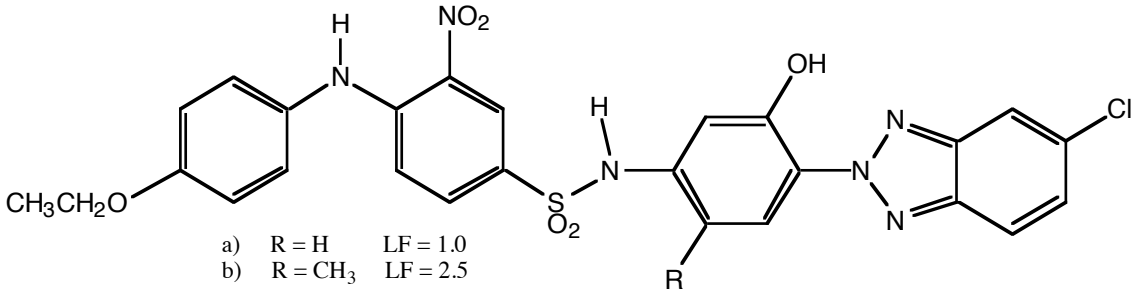

a) R = H LF = 1.0
b) R = CH_3 LF = 2.5

39

A similar approach was adopted by the same authors in an attempt to prepare lightfast CI Disperse Red 167 analogs [ci] containing a benzophenone type photostabilizer. Examples are **40** and **41**. All of the analogs prepared had lower lightfastness than the parent dye.

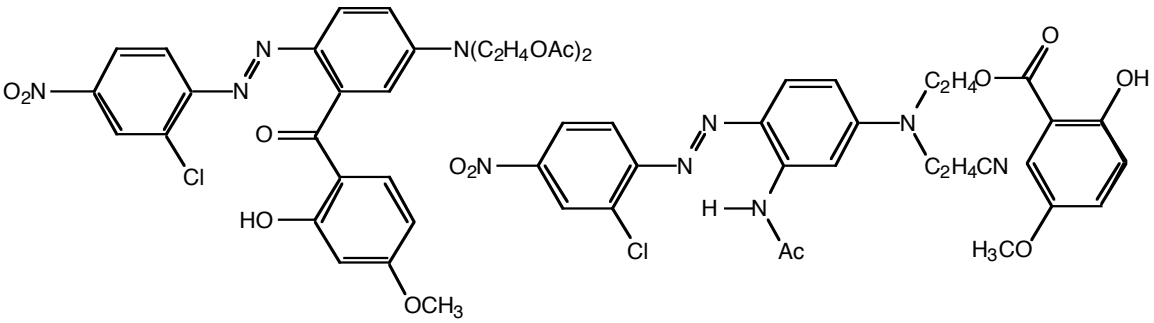

40 **41**

Although red and yellow stabilized dyes were prepared during the study, attempts to prepare anthraquinone blue dyes possessing higher lightfastness than CI Disperse Blue 27 were unsuccessful.

The dyes prepared by Freeman and coworkers fall into the category of bichromophoric dyes. A search of US patent documents revealed 58 documents which mentioned the key words *bi-* or *multiple-* and *-chromophore-* in the abstract. These patents disclosed mostly UV stabilizers for polymers. Such compounds have been examined both theoretically and experimentally in the past by various authors, thus warranting the preparation of a discrete subsection to cover the theory of bichromophoric compounds.

1.8.1 BICHROMOPHORIC EFFECTS AND INTERACTIONS

Public domain documentation reminds us that discrete or contiguous chromophores separated by less than about 50 Å can and often will interact through bonds, through solvent media, and also through space [ciii]. Indeed, it can be shown that MO wavefunctions have non-zero values at all points in space. Chromophore interactions may lead to shifts and splitting of absorption bands [civ, cv, cvi, cvii], excitation energy transfer, and light-induced electron transfer.

1.8.1.1 Energy Transfer Between Chromophores

1.8.1.1.1 Conjugated Chromophores

The case of the nitrodiphenylamine-azo dye **23**, in which it appears that excitation energy could be dissipated by either chromophore [lxxii], has already been discussed (page 22)

1.8.1.1.2 Non-Conjugated Chromophores

Excitation energy transfer (see Figure 1.22) between chromophores separated by distances exceeding ca. 5 Å are adequately described using Förster's theory. This theory depicts energy transfer as an interaction between the emission S_1-S_0 transition dipole of the donor chromophore and the absorption transition dipole of the acceptor chromophore [ciii] (see Figure 1.23). The excitation energy is transferred from the donor chromophore to the acceptor chromophore through space or through bonds, at a rate determined by the distance separating the two chromophores and their relative orientations in space.

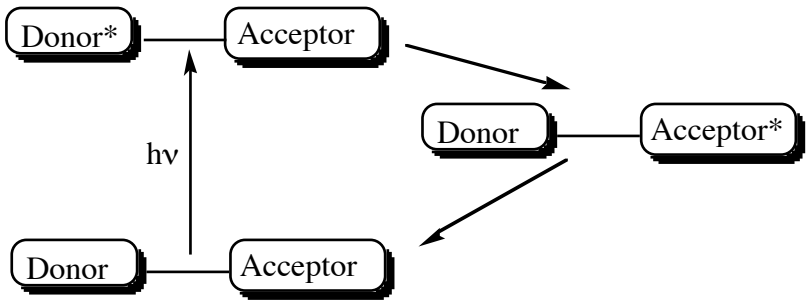

Figure 1.22 *Representation of excitation energy transfer between non-conjugated chromophores.*

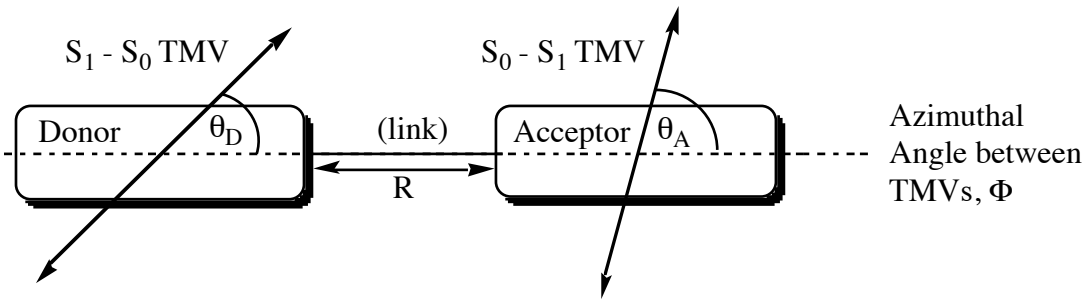

$$\text{Rate } k = (3/2)\ K^2\tau_D^{-1}(R_0/R)^6$$

Figure 1.23 *Rate of energy transfer between two non-conjugated chromophores.*

The term τ_D in Figure 1.23 is the lifetime of the donor excited state in isolation, and

$$K^2 = \sin\theta_D\sin\theta_A\cos\Phi - 2\cos\theta_A\cos\theta_D$$

which takes the relative orientations of the transition dipoles into account. The critical transfer distance R_o is related to the spectral overlap between the emission band of the isolated donor and the absorption band of the isolated acceptor. For fast efficient transfer of energy between chromophores, the absorption and emission transitions should be allowed, and there should be good spectral overlap between the emission band of the donor and the absorption band of the acceptor [ciii].

Förster's interaction has recently been utilized to improve the efficiency of laser dyes, by effectively increasing the absorption bandwidth of the emitting dye [cviii]. Fluorescence by the acceptor group of **42** (Figure 1.24) is enhanced by the additional input of excitation energy from the donor moiety. Femtosecond pump and probe spectroscopy showed that the energy transfer took place between 1 and 20 picosecond after excitation of the donor moiety [cviii].

In the case of chromogens separated by less than 5Å, energy transfer is better described by Dexter's theory [ciii, cix]. This is not a dipole interaction type transfer, and so energy may also take place between disallowed states. The rate of transfer is given by:

$$\text{Rate } k = (2\pi/h)\mathrm{K}J\exp(-2R/L)$$

Where K and L reflect the ease of electron tunneling between the two chromophores and J is the spectral overlap integral between the donor and acceptor chromophore. L is the average orbital radius - the rate of attenuation of the MO wavefunction with distance. Dexter energy transfer can be triplet-triplet, and can also be slightly endothermic. Triplet excited state energy transfer from benzophenone to 1-methylnaphthalene has been observed on a

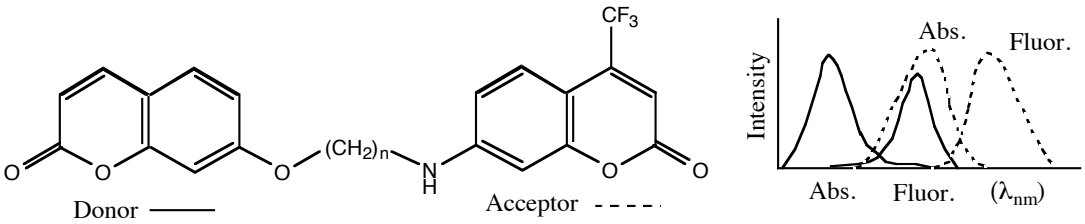

42

Figure 1.24 *Donor-acceptor type bichromophoric laser dye and spectrograph showing desirable overlap between the emission envelope of the donor moiety and the absorption envelope of the acceptor chromogen.*

timescale of 10^{-11} s (10 picoseconds) [ciii].

Levy, Rubin and Speiser [cx] have shown that Dexter intramolecular excitation energy transfer can take place between linked chromophores, even when spectral overlap is low. The authors showed that energy could be transferred between both singlet [cx] and triplet [cxi] states. Other workers have demonstrated that excitation energy may be transferred from a high triplet state into the triplet system of the donor through 4 σ-bonds [cxii]. Excitation energy

from the long lived T_2 state of an anthracene (donor) moiety **43a** was transferred to the triplet state of a diene acceptor **43b**. Back transfer from the acceptor to the lower triplet state of the anthracene was prevented because the acceptor underwent a conformation change which relieved strain.

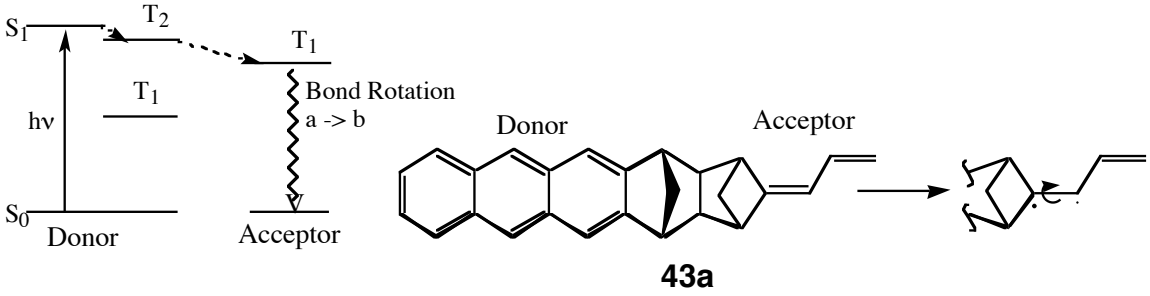

43a

b

Figure 1.25 *Excitation energy transfer from an upper triplet state.*

1.8.1.1.3 THE "WATER TANK" MODEL

The processes that dissipate photoexcitation energy are competitive, and can be visualized as a system of water tanks and drains. In Figure 1.26, the donor chromophore is photoexcited (process a) which fills the top tank. Competitive processes (b, c, d, and e, depicted as holes in the water tank) then operate to dissipate energy, and return the molecule to the ground state. Process b could represent internal conversion, c, fluorescence, and d, phosphorescence. Process e represents energy transfer from the donor chromophore to the acceptor chromophore.

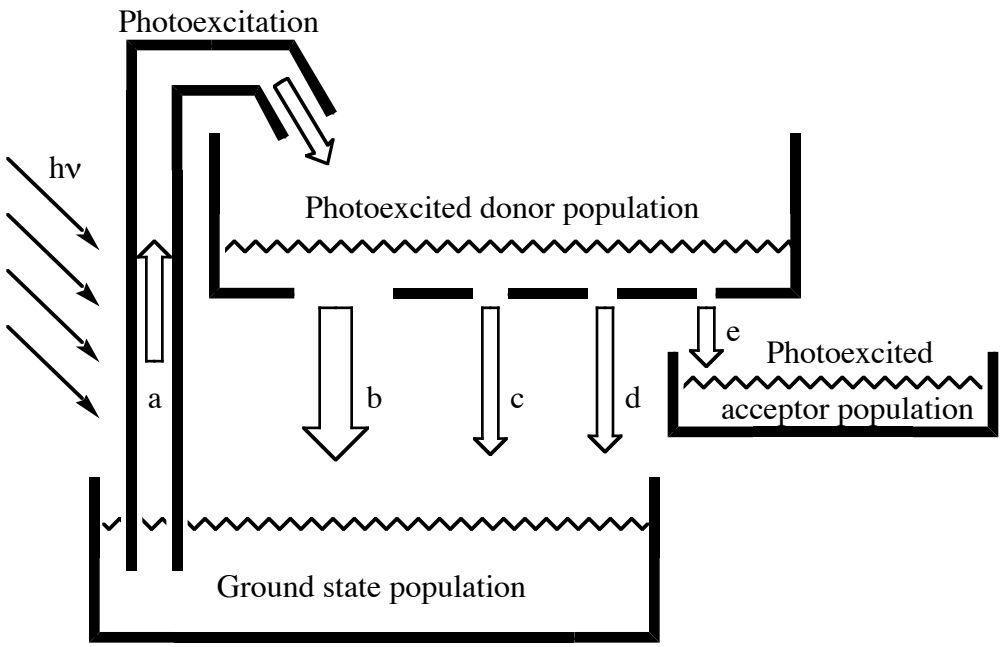

Figure 1.26 *A working analogy to photoexcitation energy transfer and loss processes in bichromophoric dyes using tanks of water.*

As these processes are competitive, increasing the size of the internal conversion hole (b) will automatically reduce the volume (energy) which escapes from all the other holes, even though the diameters of the remaining holes is not changed. The diameter of the intramolecular energy transfer hole (e) may be increased by optimizing factors which facilitate Dexter or Förster energy transfer.

1.8.1.2 ELECTRON TRANSFER BETWEEN CHROMOPHORES

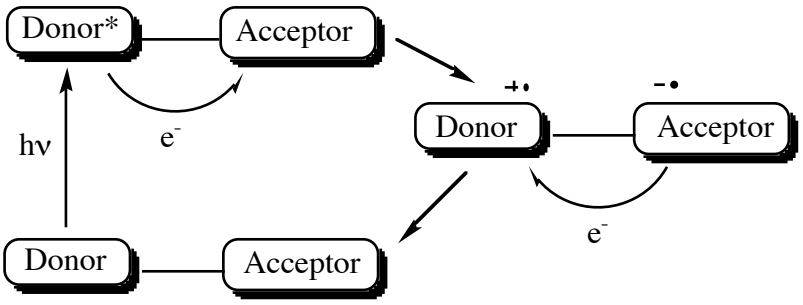

Figure 1.27 *Light-induced electron transfer between chromophores.*

An alternative process to energy transfer involves the migration of an electron from one chromophore to another to form a charge transfer state (cf. Figure 1.27). Light-induced electron transfer may be spin-allowed or disallowed, radiative or non-radiative, through bonds, solvent media, or space [ciii]. Since non-radiative transfer is Franck-Condon in nature, if the nuclear positions have to change significantly to make the transfer exothermic, it is unlikely to occur. According to theory, chromophores i) come into close proximity and ii) when thermal fluctuations make the state energies of the donor and acceptor similar, rapid electron transfer takes place, producing a charge separated state [ciii, cxiii].

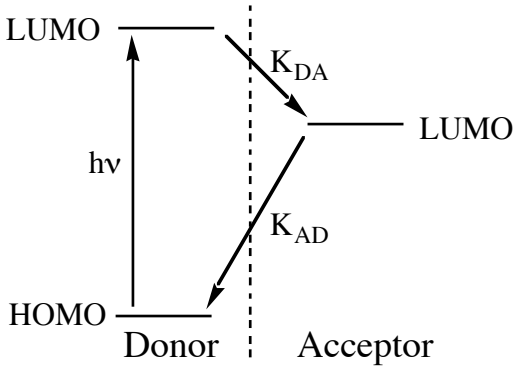

In non-contiguous chromophores, the rate of transfer follows a Dexter type relationship, depending upon ease of electron tunneling. Studies involving light-induced electron transfer and back transfer between chromophores have shown that the rate of transfer depends upon the distance between the donor and acceptor chromophores in a bichromophoric system [cxiii]. Non-radiative

Dexter-type back transfer has been observed and attributed to relaxation via conformational changes, in some systems [cxiv].

Bichromophoric systems producing charge separated states via an electron transfer process find practical application as organic photoconductors. Photoconductors have been produced by co-crystallizing light-induced electron donors and acceptors into a rigid lattice [cxv, cxvi].

1.9 Molecular Modeling and Computational Chemistry of Dyes

Arguably the simplest tangible molecular model might consist of a set of spheres, to represent atomic centers, connected via thin bars that represent chemical bonds. Such a model may provide the chemist with insight into steric effects giving rise to regiochemical and conformational effects. More nebulous concepts such as those introduced when quantum mechanical principles are considered often test the limits of our modeling capability.

Computational chemistry may be defined as any application in which a computer aids our calculation and visualization of chemical effects. Rigorous modeling of molecules takes into account all interactions that involve a given molecule in a given system. However, due to the practicalities of computational power demand and a number of deficiencies in mathematical and physical theory, simplifying assumptions are always made. Three basic families of methods have evolved over the history of computational chemistry. *Ab Initio* (Latin for "from the beginning") methods assume very little about atomic structure, and are the most computationally intensive. It is generally accepted that they are also the most accurate. Molecular mechanical calculations are the most basic, as these essentially consider strain and steric effects, although modern molecular mechanical forcefields now consider certain stereoelectronic effects in structural moieties, where these effects have been documented. Semi-empirical methods are intermediate in that the methods are developed within the framework of rigorous quantum mechanics; but, many assumptions and mathematical shortcuts are made in these methods to expedite calculations.

1.9.1 Overview of Molecular Modeling Tools

Although it is not the author's intention to explain the modeling methods in great detail; a qualitative overview of the methods most commonly used will

be presented. More detailed descriptions of the methods are given in excellent texts [lxiii, cxvii, cxviii].

1.9.1.1 Molecular Mechanics

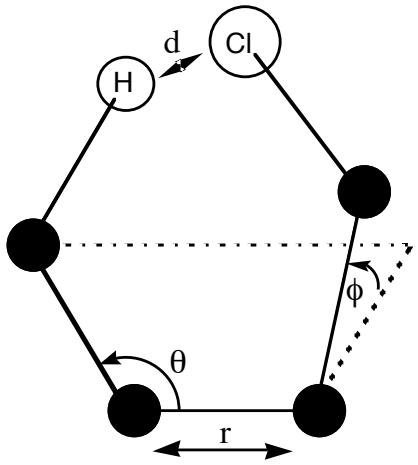

Figure 1.28 *Interactions considered in molecular mechanical calculations.*

Molecular mechanics calculations are based on the premise that molecules behave as hard spheres joined by Hookian springs. Molecular mechanical methods consider interactions between atoms in terms of bond length (r), bond angle (θ), dihedral angle (ϕ) and non-bonding distance (d) see Figure 1.28. Deviations from set bond lengths and angles give rise to strain in the molecule, that can be minimized by iterative structural adjustments. Thus, several force-fields have been developed to describe how forces develop in a molecule as deviations from nominal values of r, θ, ϕ, and d increase. One of the most popular examples is the MM2 forcefield, originally developed by Allinger [cxix].

Molecular mechanical methods are fast, reliable methods for obtaining low energy structures of large molecules and systems, with minimal demand for computer power and time [cxvii]. The steric energy in the molecule is given as a sum of functions of bond compressive-stretch (r), bond angle (θ), dihedral angle (ϕ), and non-bonding interactions (d):

$$E_{\text{Total Strain}} = \sum E_{(r)} + \sum E_{(\theta)} + \sum E_{(\phi)} + \sum E_{(d)}$$

1.9.1.2 Semi-empirical Self Consistent Field (SCF) Methods

SCF methods attempt to solve the Schrödinger equation for valid MO wavefunctions for a single electron moving in a virtual potential field. The virtual potential field arises from a combination of the nuclei and “an average” of the

complex influences of the remaining electrons [cxvii], and is iteratively adjusted until further small adjustments no longer reduce the energy of the single electron wavefunction. All SCF procedures attempt to iteratively reduce the energy of the molecular wavefunction to a minimum.

Semi-empirical methods take advantage of the fact that the Schrödinger equation, which describes a molecule in terms of MOs, can be algebraically manipulated to give a number of integrals that have physical significance. Some of the integrals of interest for this discussion are shown in diagram form in Figure 1.29. The main differences between the various semi-empirical methods involve the manner or depth in which these, and some additional integrals are treated.

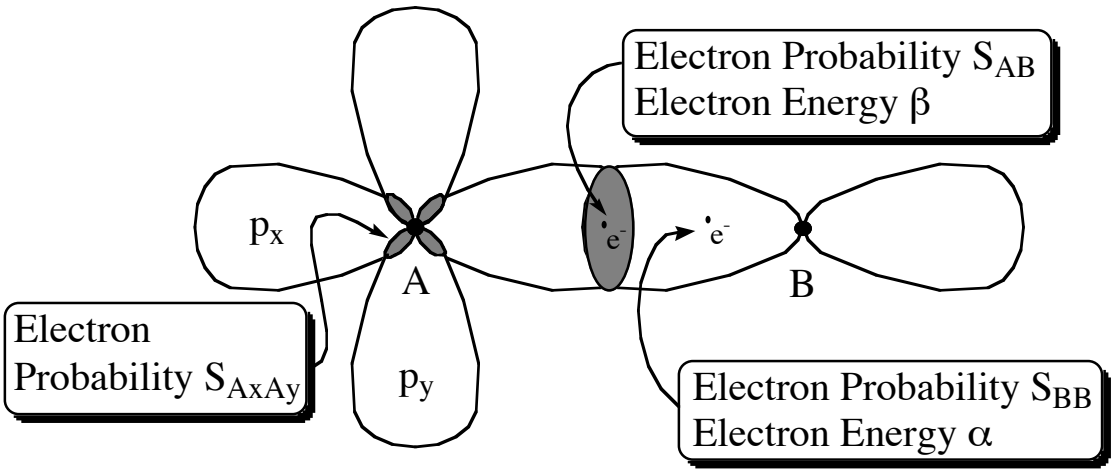

Figure 1.29 *Bonding between two atom centers A and B showing several important energy and integral quantities needed to calculate the MO wavefunction.*

Here, α is the energy of an electron when it is associated with a given atom. This energy quantity can be taken as the valence state ionization potential (VSIP) and is sometimes referred to as the *Coulomb Integral*;

β is the energy of an electron when it is associated with a bond between two atoms and is sometimes referred to as the *Resonance Integral*;

S_{BB} is the probability of finding an electron in the region of overlap between two orbitals on the same atom. In some of the more complex methods, many one center overlap integrals are included so that overlap between all orbitals on the same atom are considered. An example is S_{AxAy};

S_{AB} is the probability of finding an electron occupying the region of overlap between orbitals associated with different atom centers;

γ (not shown in Figure 1.29) is also worthy of note as it represents repulsion integrals which give the energy of the repulsion between the valence electrons when the SCF is calculated.

The numerous semi-empirical methods that have been developed treat these integrals in a variety of ways, depending upon the degree of rigor. Although not a SCF method, the Hückel method was probably the first semi-empirical approach to obtaining valid MO wavefunctions for polyatomic systems, and as such is worthy of note. The Hückel procedure, which considers only α and β for π-electrons and has been used since the 1930s.

The Extended Hückel method was developed as an SCF method and included consideration of the σ-framework, some of the atomic orbital overlap integrals, and also non-adjacent atom β terms [cxx, cxxi]. Electron interaction was assumed to be canceled out by nuclear repulsion [cxxi].

Pariser and Parr [cxxii, cxxiii] and Pople [cxxiv] were the first to attempt to include a rigorous treatment of electronic interactions into their method, now commonly referred to as the PPP method. These workers used a π-electron only, "zero differential overlap" (i.e. $S_{AB} = 0$ and $S_{AA} = S_{BB} = 1$) approach. However, they also included separate adjustment terms in α and β, which took account of electron-core (attractive) and electron-electron (repulsive) effects. Also, non-nearest neighbor β values were considered, which gave the method geometry dependence. Because the repulsion (γ) terms used in the adjustment of α and β depend upon electron densities, the PPP calculation is always

preceded with a simple Hückel calculation. This gives a crude value for electron densities on atom centers, from which electron repulsion terms can be derived for the first cycle of the SCF calculation. Griffiths has written a very lucid description of the PPP method [lxiii].

Over the years, the PPP method has been improved by various workers. Nishimoto and Mataga [cxxv] published an improved calculation of the electron repulsion term, and Hammond [cxxvi] showed how atomic parameters could be adjusted systematically to account for highly polarized σ-frameworks in heterocyclic compounds. Nishimoto and Forster [cxxvii] introduced the variable β approximation which adjusted β terms iteratively as the bond order was calculated, and Flurry, Stout and Bell [cxxviii] introduced β terms for non-nearest neighbor atoms.

Pople *et al.* developed the CNDO (Complete Neglect of Differential Overlap (i.e., $S_{AB} = 0$)) method in the 1960s [cxxix, cxxx]. This method considered all valence electrons in the system ($\sigma + \pi$.) The method was improved to give the CNDO/2 method [cxxxi], after adjustment of the α-parameters and incorporation of minor changes. Del Bene and Jaffé then modified the CNDO method to make it applicable to spectroscopy, giving rise to the CNDO/S method [cxxxii, cxxxiii, cxxxiv].

Pople *et al*. [cxxxv] and Dixon [cxxxvi] gave consideration to the S_{AxAy} terms when they formulated the Intermediate Neglect of Differential Overlap (INDO) method. Computer technology at that time afforded the possibility of Unrestricted Hartree-Fock calculations. Since such calculations did not assume that electrons were necessarily coupled, the INDO method could distinguish singlet and triplet states. In the case of restricted Hartree-Fock calculations, triplet state energy can be estimated indirectly from a knowledge of the singlet state energy and the calculated exchange energy [lxiii]. Later, Ridley and Zerner [cxxxvii] modified the method to give the INDO/S method for spectroscopic calculations. Bacon and Zerner [cxxxviii, cxxxix] extended the

INDO method so that transition metal complexes could be considered. Modifications included a more rigorous treatment of one center metal exchange integrals, implicit consideration of d-orbitals, reparameterizations, and the incorporation of a ground state configuration interaction calculation, in order to resolve the many weak interactions found in transition metal complexes.

Before 1969, with the exception of the PPP method, parameters α, β, S_{AA} etc. were calculated from the Schrödinger equation using *ab initio* methods. Baird and Dewar [cxl] reparameterized the original INDO method by fitting the atomic parameters in such a way that the calculated enthalpies of formation matched experimental atomic spectra. Thus, the MINDO (Modified INDO) method was born. The Dewar group later re-optimized the parameters of the MINDO method to give MINDO/2 [cxli]. This group also incorporated additional improvements to the treatment of the core repulsion integrals and treated overlap integrals more rigorously so that overlap between 2s and 2p orbitals was differentiated, producing MINDO/3 [cxlii].

The Dewar group proposed a second modification of the former INDO method in 1977, described as the MNDO (modified Neglect of Differential Overlap) method [cxliii]. This method reportedly gave better treatment of two-center repulsion integrals.

Eventually, there were so many similarly sounding acronyms in use to differentiate the various semi-empirical methods and procedures that the Dewar group named a modification and reparameterization of the former MNDO method the Austin Model 1 (AM1) method, presumably after Austin University, Texas, where the Dewar group was based. The AM1 method incorporated modified core repulsion integrals and was found to be the first method capable of reproducing hydrogen bonding interactions [cxliv], although not always with high fidelity [cxlv]. A former member of the Dewar group, Stewart then reparameterized AM1 and developed the latest semi-empirical method - PM3 (Parametric Model 3) [cxlvi, cxlvii]. PM3 parameters were optimized using a set

of 657 compounds, whereas parameters of the AM1 method were developed from a study of 167 compounds.

Discussions among computational chemists over the internet have brought to light a few subtle differences in the performances of PM3 and AM1 [cxlv]. Specifically, many researchers have determined that PM3 is better at predicting the geometry of nitro compounds. However, PM3 is not as good as AM1 for predicting the geometry of conjugated amino groups, as this method tends to pyramidalize these planar N-atoms. PM3 gives much better geometries for hydrogen bonded dimers [cxlvii], and bond lengths are reported to be significantly better than those predicted by AM1. PM3 is not useful for predicting orbital shapes or atomic charges, unlike the AM1 method [cxlv]. Also, PM3 does not correctly account for steric interactions involving hydrogen atoms (including hydrogen-hydrogen interactions) at distances smaller than 2Å. As a consequence, some crowded systems for instance cyclobutane, and the boat conformer of cyclohexane, are predicted to be unrealistically stable by PM3 [cxlv]. Both methods tend to grossly overestimate proton transfer barriers in calculations involving the transition states of tautomeric structures. Proton transfer transition state energy errors approaching 300% have been reported, and this has been attributed to the very high heat of formation for the proton in both AM1 and PM3 [cxlv, cxlviii, cxlix]. AM1 tends to slightly underestimate π system resonance energy [xciv]

PM3, AM1, MNDO and MINDO/3 have been collected and implemented in a public domain software package called MOPAC [cl] by Stewart. The package incorporates algorithms that use these semi-empirical methods to calculate heats of formation, from which searches for low-energy conformations and also reaction transition state structures can be made. In addition, the program also contains algorithms for calculating reaction coordinates, vibrational spectra, and also a configuration interaction routine for the calculation of excited state energy and structure. The CNDO and INDO

methods have been implemented in ZINDO, which incorporates routines for geometry optimization, SCF energy, transition state location and configuration interaction, as well as conformational searches.

The PPP method has been implemented in the commercial package PISYSTEM [cli], which incorporates routines for performing two-dimensional mechanical geometry optimizations on input structures, and for predicting absorption spectra, reactivity and the effects of a variety of perturbations, including aromatic ring substitutions and bond rotations.

1.9.1.3 RHF, UHF AND ROHF CALCULATIONS

Thus far, we have assumed that two electrons of antiparrallel spin occupy each filled MO. The Restricted Hartree-Fock (RHF) method assumes that paired electrons of antiparrallel spin occupy orbitals of identical energy and spatial distribution. For systems with an odd number of electrons, or those containing uncoupled electrons, the Unrestricted Hartree-Fock (UHF) method can be used, as it designates each electron to an individual MO. MOs containing electrons of spin α are derived separately from those containing electrons of spin β. Unfortunately, spin contamination of the molecular wavefunction may arise in the UHF calculation, and the final MO wavefunction may appear to have taken on some of the character of other spin states. In cases where this is anticipated to be a problem, the Restricted Open-shell Hartree Fock matrix may be used instead. Two types of MOs are solved separately in the ROHF method; one set of MOs holds two electrons, while the second set comprises one-electron orbitals that are similar to those used in the UHF method. Sophisticated mathematics are then used to resolve the interactions between the coupled and uncoupled electrons.

1.9.1.4 GEOMETRY OPTIMIZATION

Geometry optimization is an iterative process by which a structure of interest is manipulated or adjusted. Energy calculations before and after

adjustment determine the effect of changes to the structure. The structure is deemed to be optimized when further small changes to the structure do not reduce the energy. Automated optimization algorithms, such as those included in CAChe Mechanics, CAChe MOPAC and CAChe ZINDO, are limited in that the minimum energy structure returned from an optimization calculation could correspond to one of a number of local minima, as opposed to the global minimum. As an example, consider the optimization of n-butane. If the starting structure for the optimization corresponds to the eclipsed rotomer A (Figure 1.30), the first minima to be located will be the gauche rotomer B, as a large change in atomic coordinates is required to surmount the energy barrier between B and the global minima E (due to the high-energy rotomer C). If the rotomer corresponding to position D is used as the starting structure, then optimization will return the global minimum E.

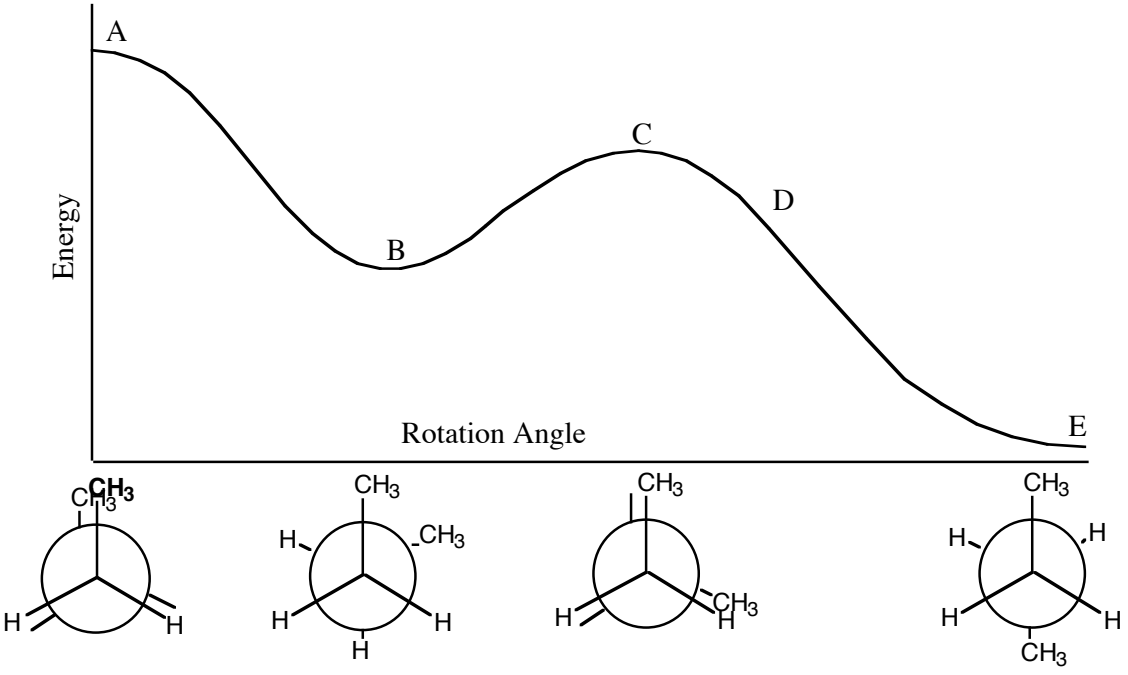

Figure 1.30 *Local and global minima of n-butane.*

1.9.1.5 Configuration Interaction Calculations

Energy values from all semi-empirical methods refer to the electronic ground state of the molecule. The PPP method gives the ground state π-electron energy, ZINDO methods give total energy (i.e. electronic and nuclear) of the system, and MOPAC methods give the thermodynamic heat of formation at zero Kelvin. The calculation of excited state energy involves a configuration interaction calculation to obtain useful results.

An excited state can be approximated by considering the energy of a system in which one of the HOMO electrons has been promoted to the LUMO. This is a poor description of the first excited state for most compounds, which is more accurately described in terms of a weighted mixture of a series of excited configurations, such as shown in Figure 1.31.

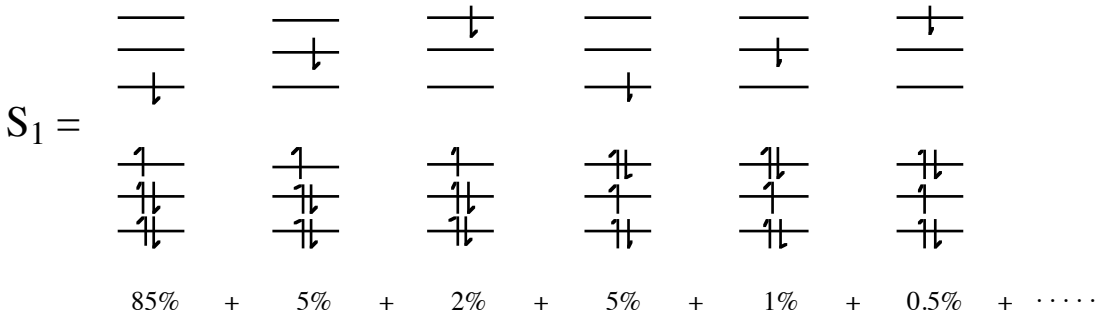

Figure 1.31 *Excited state represented as a weighted mixture of several excited configurations. The mixing coefficients are obtained from a CI calculation.*

Representing the excited state in this way is analogous to using resonance theory to describe a structure in terms of the relative contributions of a series of canonical forms, with higher energy canonical forms contributing less to the overall structure. The percentage values underneath each of the excited configurations in Figure 1.31 represent the relative contribution of each to the excited state, which in this case is principally HOMO→LUMO in character.

During a CI calculation, a manifold of configurations are considered. Choosing the manifold requires judgment. Degenerate configurations must be either all considered or all excluded from the CI calculation and the manifold should include all of the major contributing configurations [cliii]. The mixing coefficients (i.e., the relative contributions that each configuration makes) for each configuration are calculated simultaneously using the variation principle. The method is similar to the iterative calculation of the atomic orbital coefficients of the molecular orbitals.

An important parameter from CI calculations is the transition moment vector (TMV), which results from consideration of time-dependent quantum mechanics. The TMV is a transient dipole that arises as the molecule undergoes a transition from one electronic state to another during light absorption or emission. During absorption, the electrical vector of the incident light wave interacts with the TMV, thus light is selectively absorbed in one polarization plane by the molecule.

1.9.1.6 *Ab Initio* Calculations

Ab Initio calculations involve the highest level of quantum theory, although as with all of the quantum mechanical methods, the integrals from manipulation of the Shrödinger equation are made tractable by observing the Borne-Oppenheimer approximation. Although *ab initio* calculations are computationaly very intensive, they are reportedly more accurate than semi-empirical methods [cliii].

1.9.2 Dyestuff computations

1.9.2.1 Prediction of UV-Visible Spectra

Because of flexibility, reliability, and low demand on computer power, the PPP method has enjoyed a renaissance during the past two decades, despite the availability of more rigorous computational methods during that time. The main use of PPP has been in the prediction of λ_{max} and ε_{max} for which it excels

[lxiii, cli, cliv, clv, clvi, clvii]. The PPP method was implemented on an Apple home microcomputer developed in the 1980s as an educational tool, which demonstrates the amenability of these calculations to modest computer systems [clviii].

The PPP method has proved to be extremely adaptable, and has found utility for predicting the light absorption characteristics of most chromophoric systems [cli, cliv, clv, clvi, clix, clx, clxi, clxii, clxiii], and a generalized parameter set has been developed by Griffiths [clxii]. However, the PPP method does not take hydrogen bonding or d-orbital interactions into account, nor does it have parameters for metals [clxii].

INDO/S and CNDO/S methods give the energy difference between the ground and excited state for a fixed geometry [cxxxviii, cxxxix, clxiv]. The CNDO/S method with CI was used to study a series of polyenes, cyanines, and the protonated Schiff's base of retinal, a natural pigment [clxv]. Researchers found that CNDO/S could reproduce the spectrum of polyene dye, however, agreement between predicted and experimental spectra for cyanine dyes and retinal was poor [clxv]. In the case of the cyanine dyes studied, the authors chose to replace *N*-methyl groups in the structures with hydrogen when conducting their calculations [clxv]. Presumably, this substitution was carried out in order to save computation time and memory, both of which were at a premium in the 1980s. It should be pointed out that this substitution may have had a deleterious effect on the calculation of state energies. In fact, methylation of the nitrogen atoms in a cyanine dye would result in a convergence of, and a possible re-ordering of the higher excited states of the dye, as the pseudo-π (Walsh) orbitals of the methyl group contribute to the π-system. The HOMO would also be destabilized by methylation, leading to a bathochromic shift [clxvi]. Consequently, it is not surprising that agreement was poor. The authors attributed the poor agreement between retinal color and predicted absorption to

the possible presence of polar/ionic groups in the protein environment of the compound which act as external perturbations [clxv].

The INDO/S method has been used to study the excited states of *cis* and *trans* cyanine dyes, with and without methylated nitrogen atoms [clxvi]. The authors found good agreement between experimental and predicted results, and were able to explain the effects of *cis-trans* isomerism and methylation on the color of the dyes [clxvi]. Hinks *et al*. have also shown that the INDO/S method is useful for predicting the color of cyanine and polyene dyes [clxvii, clxviii].

The INDO/S method has also been used to examine porphyrin macrocycles and their nickel and copper complexes [clxix]. Geometry optimizations and energy calculations confirmed the multiplicity of the complexes, and a Mulliken population analysis of orbital occupancy after CI was used to assess bonding between the central metal atom and the macrocycle. This method was able to reproduce the spectra of these complexes [clxix]. A similar approach was used to account for the redox activity of a large, square planar tetradentate cobalt (II) complex [clxx]. The authors found strong d-π mixing in the cobalt (II) complex, and concluded that the reductive properties of cobalt (I) are a consequence of the availability of d-electrons [clxx].

No accounts were found which suggested that AM1 or PM3 were useful for predicting the absorption spectra, although these methods are reported to give much better geometries and heats of formation [clxxi]. However, AM1 CI implemented in Hyperchem [clxxii] has been used to construct ground state and excited state potential hypersurfaces along bond-rotation reaction coordinates in order to explain *cis-trans* isomerism in cyanine dyes [clxxiii]. Time resolved spectroscopy with picosecond resolution showed that the surface shapes were consistent with observed results, except for the presence of an unexplained calculated minima and a small potential barrier in the case of the sulfur containing compounds. The presence of these unrealistic peaks in the

hypersurface was attributed to interactions between the lone pairs of the sulfur atom and the remainder of the dye molecule [clxxiii].

1.9.3 MODELING ESIPT PROCESSES

Although no papers were found that relate to modeling proton transfer processes in the excited state using semiempirical procedures, several were found that dealt with modeling ground state tautomerism [xciii, xciv, clxxiv, clxxv 195]. The general approach appears to be to optimize the two tautomers using AM1, followed by executing the 'TS' (transition state) routine in MOPAC to optimize the transition state structure. Vibrational analysis was then used to confirm that the structure obtained was a true transition state. A stationary state (minima or maxima) has 6 very low frequency vibrational modes, and a true transition state will have five low frequency and a single vibrational mode with a negative frequency. Furthermore, vibrational analysis gives values for the enthalpy and entropy of the transition state at 25°C (from statistical thermodynamics) from which Gibbs' free energy can be calculated [xciii, clxxvi].

Comparison of the semi-empirical energy results with those from *ab initio* revealed the proton tunneling energy barriers to be between 200 - 300% higher by semi-empirical methods, and this has been attributed mainly to the heat of formation of the proton being too high in these methods [xciv, cxlviii, cxlix, clxxiv, clxxvii]. Comparison of the heat of formation of the tautomers often agreed with experimental NMR or x-ray crystal data [xciii, clxxv, clxxvi,].

1.9.4 TEXTILE DYE DESIGN

Schumacher *et al.* [clxiii] recently described how molecular modeling (PPP) can be used to predict the color and dyeing behavior of reactive dyes. The authors suggested that docking optimized (MM2 and PM3) structures with the x-ray crystal structure of cellulose could be used to optimize dye-fiber interactions; however, no examples were given in the paper.

1.10 MO-Based Investigations in Dye Chemistry: Proposed Research

1.10.1 Molecular Modeling Systems

The goals of the present research are threefold: i) to demonstrate the utility of molecular modeling for synthetic dye design, ii) to establish unambiguous protocols applicable to a wide range of dye structures of interest to the textile and allied industries, and iii) to apply molecular modeling to a) explain the lightfastness behavior of known dyes and b) to design new dyes for use in applications requiring high lightfastness. Given the complexity of the systems to be studied and the quantity of previous work on the use of semi-empirical methods to model moderately sized systems, it seems reasonable to investigate the utility of semi-empirical molecular modeling as a first step. In order to assess the applicability of candidate software and hardware, all molecular models will be assessed in terms of their ability to consistently reproduce experimental data. Once the applications and limitations have been established, the models will be applied to hypothetical dyes prior to synthesis.

The PPP method will be implemented using PISYSTEM [cli]. MOPAC and ZINDO will be implemented using the CAChe Worksystem [178] commercial modeling software package.

1.10.2 Geometry Optimizations

The goal is to assess the ability of the semi-empirical methods implemented in MOPAC and ZINDO to optimize dye geometries. Specifically, a method which facilitates routine geometry optimization of dyes is sought.

The x-ray crystal structures of disperse dyes CI Disperse Red 167 and Disperse Yellow 86 have been solved [179, 180]. As these are two key dyes relevant to ongoing lightfastness research efforts, the ability of the various methods implemented in MOPAC and ZINDO to optimize the geometries of

nitrodiphenylamine and azo dyes will be determined by comparing the optimized geometries to x-ray crystal structures.

It is well known that the outcome of geometry optimizations are highly dependent upon the starting geometry because optimization methods currently available only locate local minima. Local minima generated may be significantly different from the desired global minima, and such deviations may have an appreciable effect on the outcome of further calculations. Thus, another objective of this study is to design a series of structural adjustments that can be performed on starting structures, to improve the final outcome of geometry optimizations.

1.10.3 Prediction of Dye Color and Strength

Dye color prediction for dyes of interest to our research program is a realistically attainable goal, given the prior work undertaken in this field by Griffiths and coworkers [lxiii]. Historically, three semi-empirical Hamiltonians have been used to estimate the colorimetric properties of dyes, *viz.*, the PPP (π-only), CNDO/S, and INDO/S methods. Adachi and Nakamura have shown that PPP is superior to INDO/S and CNDO/S for the prediction of dye color and strength [clvii]. However, the PPP method does not take into account the effects of hydrogen bonding. In addition, it does not consider d-orbital interactions, or have parameters for metal atoms. The methods implemented in ZINDO are designed to be applied to metallized systems. Thus, for the proposed investigation into the effects of metallization, the INDO method will be used.

1.10.4 *ORTHO*-SUBSTITUTED AZO DYES

The goal here is to model a series of aminoazobenzene dyes, searching for correlations between experimental lightfastness properties and data obtained from semi-empirical MO calculations.

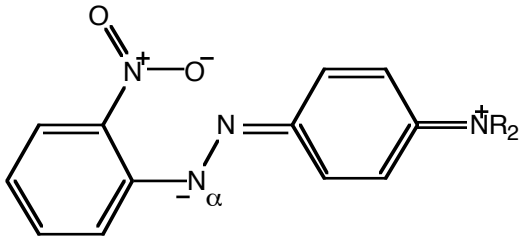

2b

Mehta and Peters [28] suggested that the α-nitrogen atom in **2b** may have a low pK_a in the first excited state. Bridgeman and Peters [9] showed that the reciprocal of the pK_a of this atom in a series of azo dyes was proportional to the rate of photodegradation.

Freeman *et al*. have characterized a series of *ortho*-substituted azo dyes in terms of lightfastness. As the pK_a may be estimated using SCF energy calculations for the protonated and unprotonated forms of these dyes, this study will serve as a group on which to test whether the reciprocal of the calculated pK_a value is useful as an indicator of light fastness.

1.10.5 DYE-POLYMER INTERACTIONS

The goal of this aspect of the research is to use molecular modeling to determine the extent to which the polymer matrix is involved in the photofading of disperse dyes. Studies will be directed towards investigating the electronic aspects of dye-polymer interactions.

The fading of dyes in PET often produces products arising from reduction. Indirect photoreduction can be initiated by photoelectron transfer from the photoexcited polymer to the ground state dye molecule. Arcoria coworkers found zeroth order kinetics for the photofading of **9**, suggesting that photofading was initiated by the polymer [53]. Thus, the electron affinity of the ground states of dyes, which have already been evaluated for lightfastness, will be calculated to determine whether there is a correlation between these

molecular descriptors and observed lightfastness. The electron affinity is defined by the energy difference between the neutral and anionic states of a given material. Thus, as the calculated electron affinity increases (i.e., becomes more positive), it becomes easier for the species in question to accept an electron and become an anion. The electron affinity corresponds to the negative of the LUMO energy, which will be calculated using MOPAC. MOPAC will also be used to examine the MO energy levels of PET to determine whether electron transfer from polymer to dye would be possible, in light of the discussion on bichromophoric dyes (page 43).

1.10.6 INVESTIGATION OF BICHROMOPHORIC DYES

The goal of this aspect of the research is focused upon investigating the lightfastness of previously synthesized dyes containing a UV absorbing moiety. It may be possible to explain the anomalous photostability of certain bichromophoric dyes if we assume that allowing the excitation energy from the UV-absorbing moiety of bichromophoric dyes to be transferred into the low energy (dye) chromophore (Figure 1.32.) will increase photodegradation. As discussed (Section 1.8.1.1.3), processes that dissipate photoexcitation energy are competitive, and can be visualized as a system of water tanks and drains. In Figure 1.26, the UV-absorbing chromophore is photoexcited (process a) which fills the top tank. Competitive processes (b, c, d, and e, depicted as holes in the water tank) then operate to dissipate energy, and return the molecule to the ground state. Process b could represent internal conversion, c fluorescence, and d, phosphorescence. Process e represents undesirable energy transfer from the donor chromophore to the acceptor chromophore. As these processes are

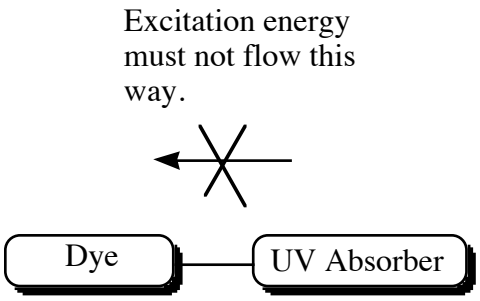

Figure 1.32. *Undesirable energy flow in experimental bichromophoric dyes.*

competitive, increasing the rate of internal conversion will automatically reduce the likelihood of other events.

Attempts to prevent energy flow from the UV absorber to the dye moiety will be two pronged. First, two approaches will be used to increase the rate of internal conversion of absorbed UV radiation by optimizing ESIPT efficiency in the stabilizing moiety. This may be achieved by i) reducing the hydrogen bonding distance between the phenol group and the triazole nitrogen by placing bulky groups *ortho* to the phenol group in hydroxybenzotriazoles, and ii) by reducing the pK_a of the phenolic group in the first excited state by the judicious selection of substituents. Second, a model of excitation energy will be developed along the lines of Dexter's intermolecular excitation energy transfer theory, to model the rate of excitation energy transfer from the UV absorber to the dye moiety. Dexter's equation describes the excitation energy transfer between proximal or contiguous chromophores in a mixture of both observable and theoretical terms. The rate of energy transfer is given by:

$$\text{Rate } k = (2\pi/h)KJ\exp(-2R/L)$$

where K and L reflect the ease of electron tunneling between the two chromophores and J is the spectral overlap integral between the absorption envelope of the accepting chromophore and the emission envelope of the donor chromophore. L is the average orbital radius - the rate of attenuation of the MO wavefunctions with distance, and R is the separation of the two chromophores.

As Dexter's model contains several terms that are challenging to estimate, attempts will be made to model excitation energy transfer in terms of quantities that can be estimated using semi-empirical methods. Namely, a method will be developed which incorporates such molecular descriptors as photoactive MO overlap and interchromophoric distance.

The unoccupied orbitals principally responsible for the UV and visible absorptions in bichromophoric dyes will be identified. The MO coefficients of

these orbitals on the atoms which link the two chromophores will be monitored. If the antinodes of these unoccupied orbitals coincide, it may be possible for excitation energy to tunnel from the unoccupied MO associated with the UV absorbing state into the MO associated with the visible absorption. This process is shown by example in Figure 1.33. In this hypothetical case, the UV absorption is associated with a HOMO - LUMO+1 transition, and the visible absorption is associated with a HOMO - LUMO transition. The MO coefficients are shown as circles on atoms; the diameter is proportional to the magnitude of the coefficient, and the color indicates the phase. In the hypothetical case shown, it would appear that there is a significant coincidence of phase and magnitude on several of the atoms shown in the link group.

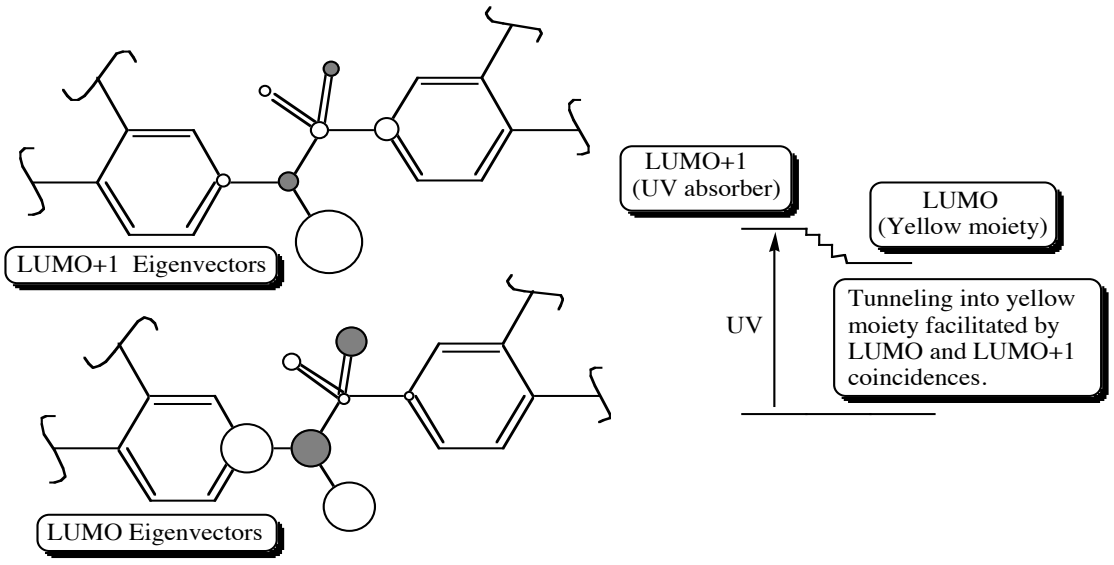

Figure 1.33 *Illustration of proposed excitation energy transfer between two chromophores, facilitated by coincidences of destination orbital antinodes, present on groups linking the two chromophores (not to scale).*

1.10.7 METAL COMPLEX DYES

The goal of this aspect of the present investigation is to establish why some metals e.g., Fe (III) usually give metal complexed dyes of lower lightfastness than their more toxic Cr (III) and Co (III) counterparts. Once the role of the central metal atom in such dyes has been determined, the results will

be used to design metal-free dyes for applications where currently only metallized dyes can be used.

As a first step to achieving this goal, molecular modeling protocols will be established for building metal complex dye structures and optimizing them. The semi-empirical ZINDO package is the only such method available in which parameters and the correct algorithms for calculating the optimum structure of metal complexes are found. Consequently, this package will be employed in these studies. It will be necessary to compute the multiplicity of the iron complexes. This can be achieved if one assumes that the sextet multiplicity complex will have longer bonds from the CMA to the ligand than the doublet multiplicity complex. Geometry optimizations of both the sextet and doublet structures will be performed. It is anticipated that the structure with the lowest SCF energy will give the multiplicity of the complex.

After geometry optimization, the results of the Mulliken population analysis will be used to assess the type of bonding that exists between the ligand and the CMA. In particular, d-electron interactions with the ligands will be examined. Also, the optimized geometry, will be used to examine the localization/delocalization and relative energies of the lower excited states of these dyes.

2. EXPERIMENTAL

2.1 COMPUTATIONAL METHODS:

2.1.1 HARDWARE AND SOFTWARE

Two molecular modeling systems were used to analyze dye structures. PISYSTEM [cli, 181], which is based upon the π-only SCF MO approach of Pariser, Parr [cxxii, cxxiii], and Pople [cxxiv], was executed on a 133 MHz Pentium-based PC system with 16MB of RAM. PISYSTEM retains the σ-π separation principle, and Nishimoto-Mataga two-center repulsion integrals of the original PPP method [cxxv]. However, non-planar systems are accommodated by adjustment of the β-resonance integrals [182], and σ–frame polarization is accommodated by the iterative variation of electronegativity [cxxvi]. CAChe Worksystem (Oxford Molecular [178]) running on an Apple Macintosh Quadra 950 equipped with a 40 MHz CXP RISC coprocessor, 64 MB RAM, and a 3D stereoscopic monitor was used for the remaining calculations. CAChe implementations of MOPAC 6.0 and ZINDO were used for all-valence electron quantum mechanical calculations.

2.1.2 STRUCTURE CONSTRUCTION

Structures were entered using a graphical editor (CAChe Editor); heavy atom centers were defined using a mouse to generate a topologically correct, crude starting structure. Formal atomic charges and electronic configurations were specified judiciously wherever required. A process designated by CAChe as “Beautification” then added electron lone pairs and hydrogen atoms wherever needed and converted the structure into a more realistic representation, using standard bond lengths and angles.

In the case of PISYSTEM, atoms contributing to the π-system of the dye were entered into a graphical editor, which then performed a two-dimensional geometry optimization routine (denoted as “Idealise” in PISYSTEM) before the PPP SCF CI calculation was started.

2.1.3 Structure SCF Energy Calculations

PM3, AM1, MNDO, and MINDO/3 Hamiltonians were used to calculate SCF energy in MOPAC using a RHF method and the default MOPAC SCF converger. The INDO/2 Hamiltonian was implemented in ZINDO using either a RHF, UHF, or an ORHF method for SCF energy, depending upon the electronic configuration of the system under study. PISYSTEM implemented the π-only PPP method (RHF) to obtain MO energies.

2.1.4 Geometry Optimizations

2.1.4.1 Manual Adjustments

Manual adjustments of structures using the graphical editor were often necessary to generate alternate starting structures (e.g., rotomers, isomers, and structures containing intramolecular Hydrogen bonds) and hence facilitate location of low-energy minima. This step went part way to overcoming the difficulty of locating global minima.

2.1.4.2 Classical Molecular Mechanics

CAChe Worksystem implemented an augmented MM2 forcefield and a conjugate gradient minimizer to reduce the energy of structures on the basis of molecular strain. Convergence was reached when further small changes in geometry would did not affect the structure energy by more than 0.001 kcal.mol^{-1}.

2.1.4.3 SEMI-EMPIRICAL QUANTUM MECHANICS

The Eigenvector Following function minimizer was used to iteratively reduce SCF energy in MOPAC calculations. Extra MOPAC keywords were used to further control the calculation, *viz.*:

EF To use the eigenvector following minimizer

HESS=1 To generate a matrix consisting of the derivative of the atomic coordinate displacement with respect to SCF energy before beginning the first optimization cycle. (Makes EF optimizations more efficient.)

GNORM=2 To continue to optimize the geometry until the conjugate gradient fell below 2.0

XYZ To use Cartesian coordinates in the optimization calculation. (Makes the calculation more robust, especially for linear systems.)

In some MOPAC optimizations, the default Broyden-Fletcher-Goldfarb-Shanno function minimizer was used. In these cases, the geometry was optimized to the satisfaction of Herbert's test. Herbert's test was satisfied when the estimated distance from the current point to the minimum was less than a specified constant.

For ZINDO optimizations, the Newton-Raphson converger was used unless convergence problems arose, in which cases, an Augmented Hessian converger was used instead. The Augmented Hessian converger took the first and second derivatives of atomic coordinates with respect to energy into account, and so was a more stable converger. Convergence criteria were satisfied when the largest component of the gradient was less than 0.001 $kcal.mol^{-1}$.

2.1.5 SOLUBILITY PREDICTION

CAChe ProjectLeader contains an implementation of a calculation that allows estimation of the water-octanol partition coefficient (Log P) for structures amenable to AM1. COSMO (Conductor-like Screening Model) is used in conjunction with AM1 to simulate the effect of a continuous dielectric medium on the structure SCF energy. The log P calculation used by CAChe ProjectLeader is based on the Blog P technique of Bodor *et al*. [183, 184], which utilizes a regression equation to estimate log P from a series of molecular descriptors, including atomic partial charges from MOPAC, heats of solvation (MOPAC AM1 COSMO model [185]), and solvent accessible surface area. A correction for heteroatoms and nitro groups present in the structure is also made.

2.1.6 CONFORMATIONAL ANALYSIS

It is conceivable that certain MO based properties associated with bichromophoric dyes depend upon the relative orientation of the two chromophores. In an attempt to accommodate the conformational freedom of bichromophoric dyes, conformational analysis was carried out. Care was taken to treat intramolecular hydrogen bonds within each chromophore as if they were covalent bonds, thus preserving the planarity of the chromogen.

In the case of bichromophoric dyes containing a sulfonamide linkage, two dihedral angle geometry search labels were attached - the first set to rotate groups about the bond between the carbon and sulfonamide S atoms, and the second set to search while rotating about the N-C bond of the sulfonamide link (Figure 2.1). In the case of chromophores connected via a diphenylamine, only one search label was attached (Figure 2.1).

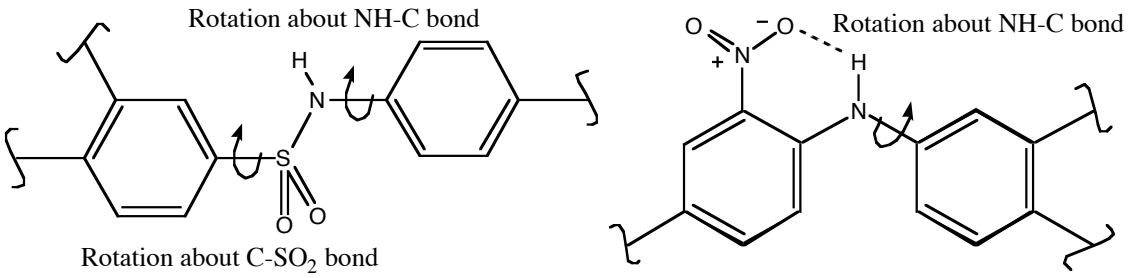

Figure 2.1 *Positioning of geometry search labels for conformational analysis of bichromophoric dyes.*

Structures were submitted for rigid searches using the MM2 augmented forcefield. In other words, phenyl groups attached to bonds identified with a search label were incrementally rotated in 24 steps of 15° about the identified bond. After each incremental rotation, the mechanical strain energy was calculated. Plotting the strain energy against the dihedral angle gave a pseudo reaction coordinate diagram for dyes containing only one search label (**80**, **81**, **86**, **92-94**, page 119), and an energy contour map (essentially a Ramachandran diagram) for containing two search angles (**77-79**, **82-85**, **87-91**, page 119). A true reaction coordinate diagram shows a reaction progressing through a saddle point. However, as the molecules were held rigid during rigid searches, we cannot assume that the reaction coordinate diagram produced passes through a saddle point. Optimized MM2 geometry searches were attempted in which a geometry optimization was conducted after each increment. However, as the MM2 forcefield does not treat hydrogen bonding rigorously, the optimization often returned non-planar minima. In addition, searches were attempted using MOPAC PM3 to calculate the energy after each incremental bond rotation. The MOPAC search took approximately 8 hours to construct energy contour maps for each structure, whereas MM2 searches typically took 10 minutes per structure to identify essentially the same minima.

Unique minima for each structure were identified using the energy contour maps and reaction coordinate diagrams and saved to separate files.

These crude minima were then optimized using MOPAC PM3 using usual settings and keywords to control the calculation. The SCF energies of the optimized minima were recorded, and Boltzmann's distribution (1) was then used to calculate the relative population of each conformer. The populations were then normalized to unity, so that results to which conformational analyses were applied were not skewed by structures with differing numbers of accessible low energy conformers. The Boltzmann distribution (1), where N_i/N_j

$$\frac{N_i}{N_j} = e^{-\left(\frac{E_i - E_j}{R\,T}\right)} \qquad (1)$$

is the mole fraction of conformer i compared to j, E_i and E_j are the respective energies of conformer i and j respectively, R represents Boltzmann's constant, and T is the thermodynamic temperature in Kelvin.

2.1.7 CONFIGURATION INTERACTION (CI) CALCULATIONS

ZINDO CI calculations utilized INDO/S parameters, derived from spectroscopic data. The CI level determines the number of orbitals that are used to construct the excited configuration manifold. In each case, a CI level was chosen such that further increases to the CI level would not cause significant change in the predicted energy states of interest.

Spectroscopic predictions using PISYSTEM were made based upon the results of a limited configuration interaction calculation involving the 36 lowest energy singly excited configurations.

MOPAC CI was initiated and controlled using the following keywords: SINGLET OPEN(X,Y) ROOT=Z, where X=number electrons distributed in Y partially occupied MOs which constitutes the excited configuration manifold. SINGLET specifies singlet multiplicity and ROOT=Z specifies that the Zth root of the molecular wavefunction should be optimized (ground=1, first excited=2, etc.). For example, to optimize the geometry of a structure in the 1st excited

singlet state, one could use the following additional keywords in the calculation settings:

SINGLET OPEN(2,7) ROOT=2 EF XYZ HESS=1 GNORM=2

Although values for X and Y were chosen through trial and error, to obtain consistent results, the MOPAC CI calculation failed if only part of a set of degenerate MOs were included in the configuration manifold. The OPEN(X,Y) keyword was used to include or exclude all of the degenerate orbitals, after examining MO eigenvalues either in the MOPAC output file, or by accessing these data through the CAChe Editor Internals menu.

2.1.8 EXCITATION ENERGY TRANSFER ESTIMATIONS

As the separation between the two chromophores of bichromophoric dyes (**77-94**) was less than 5 Å, excitation energy transfer would most likely follow a Dexter type relationship. Dexter's equation contains many terms that would be difficult to estimate using molecular modeling tools at hand. However, an attempt was made to formulate a model describing possible excitation energy transfer from the UV absorber moiety to the nitrodiphenylamine moiety. The mathematical model resembled Dexter's equation (Section 1.8.1.1.2), in that consideration was given to MO overlap and interchromophore separation.

Conformational analysis was used to establish populations of possible conformers. ZINDO configuration interaction was used to identify the most significant MOs involved in the first five transitions (including forbidden transitions) of each conformer of each dye. The chromophores associated with the MOs were then identified by examining representations using CAChe Visualizer. Hence, MOs responsible for UV absorption and those giving rise to absorption of visible light were identified. The MO coefficients (eigenvectors obtained from the CI calculation) of the LUMO+x destination orbitals for the transitions were then recorded for each atom in the groups linking the two chromophores. This included 7 atoms in the case of chromophores linked by a

sulfonamide group angles (**77-79**, **82-85**, **87-91**), and 4 in the case of those linked by an amino group. This process involved opening the structure in CAChe Editor and accessing the INDO/S eigenvector data stored in the molecule file by editing the file “Internals”.

MO eigenvectors on any given atom were multiplied together, and the eigenvector products for the individual atoms were then summed for the set of atoms in the link group. In this way, both the phase and magnitude of the overlap were included in the calculation. Our analogy for the quantity K in Dexter’s equation for a two atom link now becomes:

$$K = x_a \left(c_1\phi_1 \, c_1\phi_2 + c_2\phi_1 \, c_2\phi_2 \right) + x_b \left(c_1\phi_1 \, c_1\phi_2 + c_2\phi_1 \, c_2\phi_2 \right) + \ldots$$

where x_a is the normalized population of conformer a, $c_1\phi_1$ is the eigenvector of MO1 ($c\phi_1$), located on atom 1, and $c_1\phi_2$ is the eigenvector of MO2 ($c\phi_2$), located on atom 1.

In some cases more than one UV transition was found. As the probability of an absorption event occurring is proportional to the oscillator strength, cases involving more than one UV transition, the squares of the transition moment vectors for each transition were divided by 100 (to prevent skewing of data) and normalized to unity. These values were then used to weight the results of two separate calculations of K.

The value of R was taken from the measurement of the distance between atoms in conjugation with the chromophores and directly connected to linking group from the PM3 optimized structure. The quantity L (average orbital radius in Dexter’s equation) was included in this model by totaling the modulus of both (LUMO and LUMO+x) eigenvectors on each atom in the linking group and multiplying by 50. The quantity J (spectral overlap integral) was assumed to be a constant, and as such not included in this model.

2.2 MAGNETIC SUSCEPTIBILITY MEASUREMENTS

Magnetic susceptibility measurements were conducted on 20-30mg samples using a 4-inch electromagnet with Faraday pole pieces, powered by a Varian 2901 regulated magnet power supply [186]. A Cahn model RG microbalence [187] was used to measure sample weight changes.

$Hg[Co(NCS)_4]$ was used to characterize the magnetic field parameter, $(H.\partial H/\partial y)$ and to standardize magnetic susceptibility measurements. The diamagnetic contribution of the constituent atoms and ions were estimated from Pascale's constant tables, and subtracted from the measured total molar magnetic susceptibility, the difference being the paramagnetic susceptibility.

3. Results And Discussion

3.1 Geometry Optimization of Dyes

3.1.1 Development of a Protocol for Generating Starting Structures for Optimizations

It is well known that the outcome of geometry optimizations is highly dependent upon the starting geometry. As there is no test to confirm that an optimized structure is a global minimum, protocols aimed at refining the starting structure were developed. During the course of this investigation, it became clear that a number of routine manual adjustments could be made to azo dye structures which gave minima that were lower in energy and less distorted after optimization than if certain adjustments were not conducted.

3.1.1.1 Lone Pair Interactions in *Ortho* Substituted Azo Dyes

In the case of azo dyes possessing a substituent *ortho* to the azo bond, a lower energy structure was returned from the optimizer if the geometry of the substituent was adjusted such that it was positioned in alignment with the lone pair on the α-azo nitrogen (e.g. **44**). In the case of rotomer **45**, the *ortho* substituent can interact through space with the lone pair on the azo β-nitrogen atom. This interaction is avoided in rotomer **44**.

Rotomers **44** and **45** were optimized in MOPAC using AM1 and PM3. Table 1 gives the energy of the optimized structures in kcal.mol^{-1}. The results

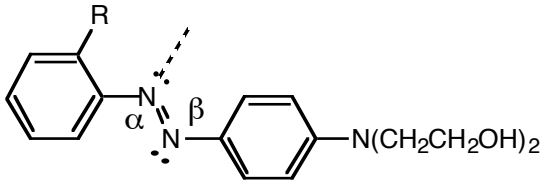

44

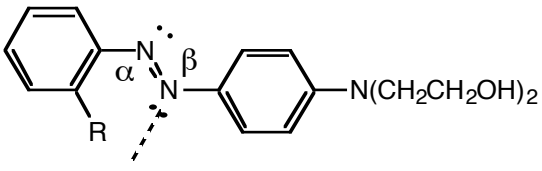

45

Table 1 *Final SCF energy values for optimized azo rotomers **44** and **45**.*

Structure and Method Used	Rotomer **44** Energy ($kcal.mol^{-1}$)	Rotomer **45** Energy ($kcal.mol^{-1}$)
R=Cl (AM1 Method)	2.9	3.9
R=Cl (PM3 Method)	-5.1	-5.3
$R=CH_3$ (AM1 Method)	2.0	5.4
$R=CH_3$ (PM3 Method)	-6.6	-6.4
R=CN (AM1 Method)	41.2	41.5
R=CN (PM3 Method)	35.9	36.7

showed that manual adjustments of the azo structure from rotomer **44** to **45** gave rise to a lower energy optimized structure. The case of the cyano derivative is worthy of comment. The shape of the cyano group is rod-like, whereas methyl and chloro groups are essentially spherical. It is possible that the rod-like shape of the cyano group presents interacts with the azo β-nitrogen lone electron pair to a lesser extent than spherical groups. This resulted in a smaller difference in the energy of the two rotomers using AM1.

In some cases, the minima produced by optimization of rotomer **45** were distorted, i.e. the optimizer distorted the chromophore while attempting to optimize the structure. Figure 3.1 shows a lateral view of the result of optimization of rotomer **45** ($R=CH_3$) using PM3. The azo group was twisted out of plane of the two phenyl rings. Such an arrangement would reduce π-orbital overlap across the chromophore, which would have a deleterious effect on color prediction calculations. Distortions such as these are consistent with underestimation of π overlap energy by AM1 and PM3, as also suspected by Redington and Bock [xciv].

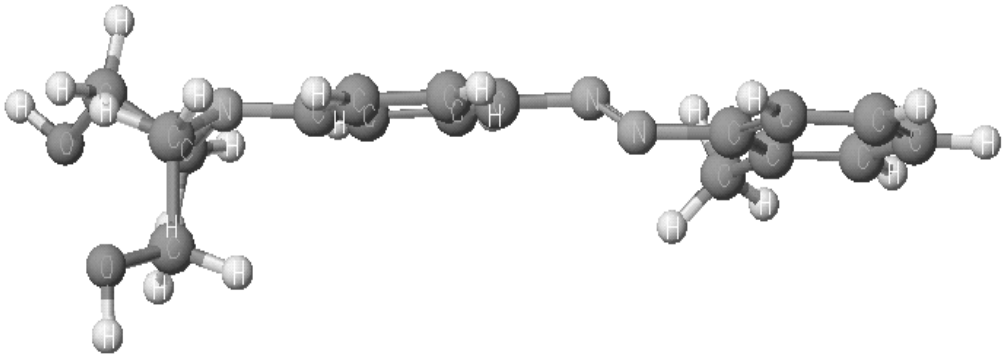

Figure 3.1 *Lateral view of rotomer **45** (R=CH_3) after optimization using PM3, showing distortions at the azo group.*

3.1.1.2 AZO DYES CONTAINING HETEROCYCLIC GROUPS

Lone pair interactions need also be considered in azo dyes containing heterocyclic rings. The lone pairs of the heteroatom in the heterocyclic moiety of **46** may interact weakly but unfavorably with the β-nitrogen lone pair and this interaction should be alleviated by bond rotation (**46** to **47**) prior to optimization. In the case of the sulfur atom, the lone pairs are in a tetrahedral configuration, and as such avoid clash with the azo lone pair by residing above and below them in **47**. The calculated energy differences between optimized **46** and optimized **47** are small; AM1 incorrectly predicts **46** to be more stable than **47**

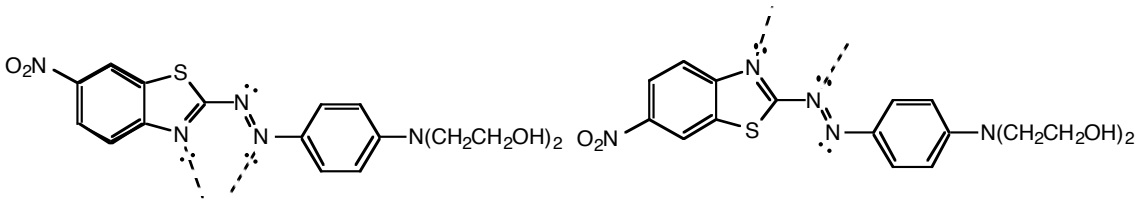

46 **47**

by 3.6 kcal.mol^{-1}, while PM3 predicts **47** to be more stable than **46** by 0.2 kcal.mol^{-1}.

3.1.1.3 HYDROGEN BONDS

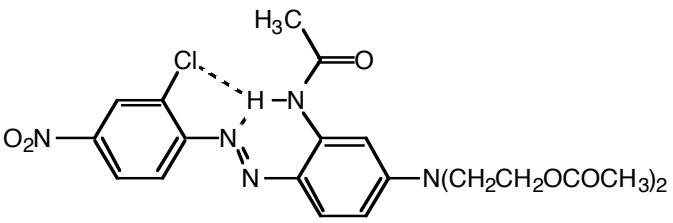

12

An exception to above findings occurs when the substituent is an acylamine, such as in **12**. Amide groups in this position are known to participate in hydrogen bonding with the β-azo nitrogen atom [179].

During the course of optimization protocol development, it became clear that structures had to be manually adjusted before semi-empirical optimization in such a way that the optimizer could then utilize the energy-reducing effects of hydrogen bonds in a given structure. If the atoms were not placed in a position such that they may form hydrogen bonds, the optimizer would often not include this interaction. An illustration of this potential shortcoming is provided by rotomers of a hydroxybenzotriazole (see **25a** and **25b**). The benzotriazole ring in **25b** is non-coplanar with the phenol ring, and the hydroxy hydrogen was rotated out of possible hydrogen bonding distance to the triazole nitrogens. These two rotomers were optimized in MOPAC using both AM1 and PM3. The SCF energies of the optimized structures are given in
Table 2. In this case, the PM3 method was more sensitive to the presence of hydrogen bonding than the AM1 method. The final optimized structures of **25b** from both AM1 and PM3 did not contain hydrogen bonding interactions and were non-planar, whereas the optimized structures for **25a** did contain hydrogen bonding interactions, and were planar.

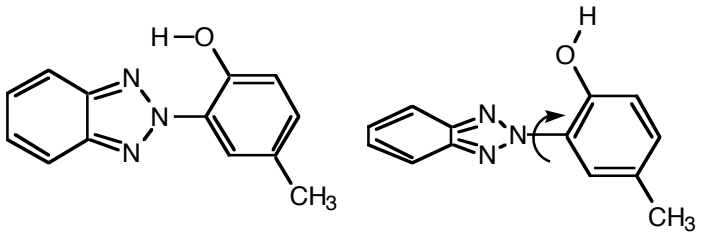

25a **25b**

Table 2 *Final SCF energy of **25a** and **25b** after optimization.*

Method Used	Structure **25 a**	Structure **25 b**
AM1 Energy	109.396 kcal/mol	109.607 kcal/mol
PM3 Energy	68.683 kcal/mol	71.903 kcal./mol

These results highlight the significance of the starting geometry in modern semi-empirical methods. Clearly, if hydrogen bonding plays significant roles in the conformation of a compound, the possibilities for hydrogen bonding in a structure need to be identified prior to semi-empirical optimization.

3.1.1.4 Amino Substituent Adjustment

Results of optimizations showed that if both alkyl chains of dialkylamino groups were co-planar in the starting structure, in most cases the optimizer retained this co-planarity even if it meant pyramidalization of the amino nitrogen in order to relieve steric strain. A less distorted final structure was returned when one of the alkyl groups was rotated out of plane before the optimizer was started, as shown in Figure 3.2. The energy difference between the two rotomers was on the order of 10 kcal/mol, before optimization.

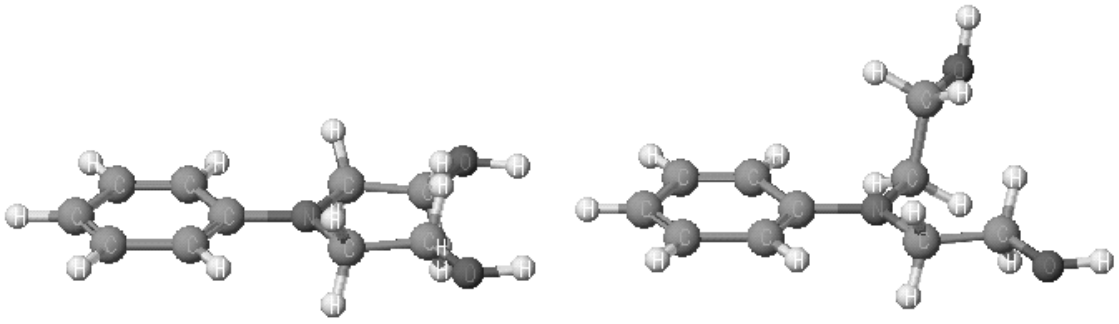

a **b**

Figure 3.2 *Routine adjustment of alkylamino groups in **a** to give **b** prior to semi-empirical optimization.*

Structures **48a-b** and **49a-b** were optimized using AM1 and PM3. The N-alkyl groups in structures **48b** and **49b** had been altered to resemble rotomers **a** and **b** in Figure 3.2. Table 3 shows that the energy of the final

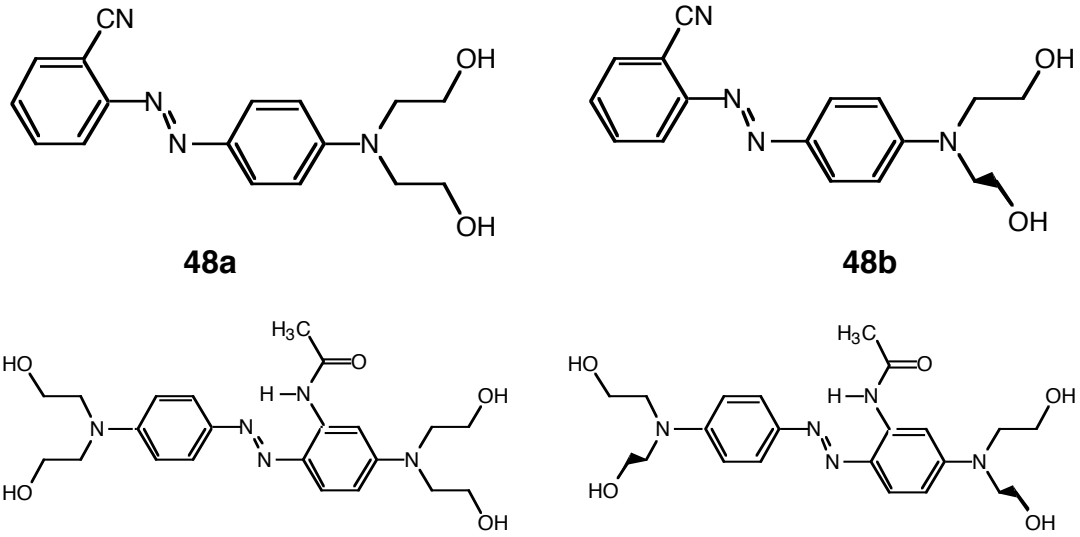

48a **48b**

49a **49b**

structure was only slightly affected by adjusting the N-alkyl groups. However, calculation times were reduced in most cases. Figure 3.3 demonstrates the distortions that were found in **48a** and **48b** amino groups when manual rotation of N-alkyl groups were not conducted.

Table 3 *SCF energy values (kcal.mol^{-1}) of compounds **48** and **49** before and after optimization. Calculation times are given in parenthesis.*

	48a	**48b**	**49a**	**49b**
AM1 Starting Structure Energy	89.224	46.468	471.154	222.597
PM3 Starting Structure Energy	85.738	51.008	322.555	132.256
AM1 Final Structure Energy	41.067 (38 min.)	41.408 (18 min.)	59.919 (1 h. 31 min.)	59.894 (49 min.)
PM3 Final Structure Energy	36.035 (28 min.)	35.726 (26 min.)	21.059 (1 h. 26 min.)	21.630 (1 h.)

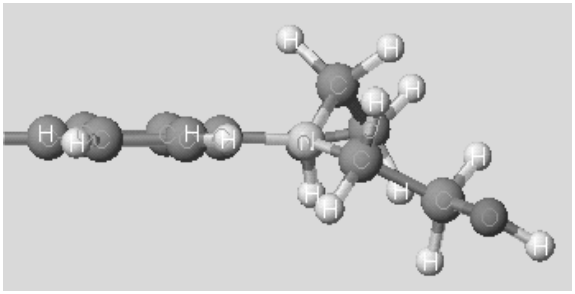

AM1-optimized alkylamino groups of **48a**.

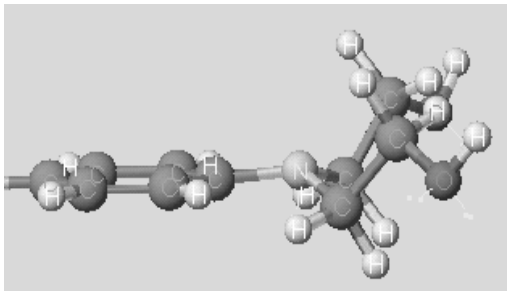

PM3-optimized alkylamino groups of **48a**.

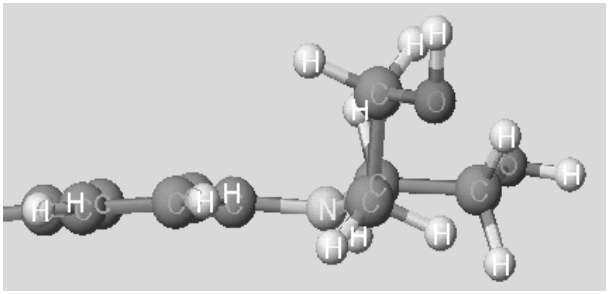

AM1-optimized alkylamino groups of **48b**.

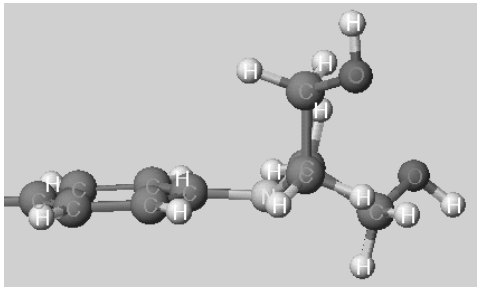

PM3-optimized alkylamino groups of **48b**.

Figure 3.3 *Distortions of amino groups are reduced if N-alkyl groups are adjusted prior to optimization.*

Clearly, distortions to the amino nitrogen atom were reduced when the alkyl groups were adjusted as shown in Figure 3.2. PM3 had a tendency to pyramidalize amino nitrogen atoms, as seen in Figure 3.3. Pyramidalization was noticeably worse in the case of PM3-optimized **48a**. AM1 also twisted the amino group out of the plane of the phenyl ring in the case of **48a**. However, in the adjusted structure **48b**, AM1 appeared to cause the least distortion to the amino group.

Consistent with an underestimation of π overlap energy, **48a** in Figure 3.3 shows that the amino group was twisted out of conjugation during the optimization. These results also highlight the impact of the starting geometry on the final structure obtained from geometry optimizations. Clearly, it is necessary to adjust N-alkyl groups (as shown in Figure 3.2, structure **b**) present in candidate structures before proceeding with optimizations.

3.1.1.5 METAL COMPLEX DYES

Optimizations involving metal complexes were found to be particularly sensitive to the initial starting geometry. A protocol was developed by which metal complex dyes could be optimized routinely. The protocol is based upon ensuring that the central metal atom (CMA) of the starting structure is placed at the center of a regular octahedron formed by the six electron donating atoms of the ligands. It became apparent that if short-cuts were taken, and the metal atom was not centralized, the "optimized" structure would usually contain severe distortions in the region of the CMA after optimization using ZINDO. The types of distortions observed included bond lengths in excess of 2Å, metal atoms dislocated far from the center of the molecule, and distortions to the ligands including bending planar azo dyes into butterfly shapes.

1) The ligands of the metal complex dye were built using CAChe Editor, and "beautified". The configurations of the ligands were adjusted to bring the groups that would be involved in bonding to the CMA onto the same side of each ligand. The two ligands were then positioned on the screen in the same plane

(Figure 3.4). The CMA was then added and bonds to the appropriate azo nitrogen atoms (in this case, the α-nitrogen atoms) were also added. At this stage, none of the atoms were assigned formal charges.

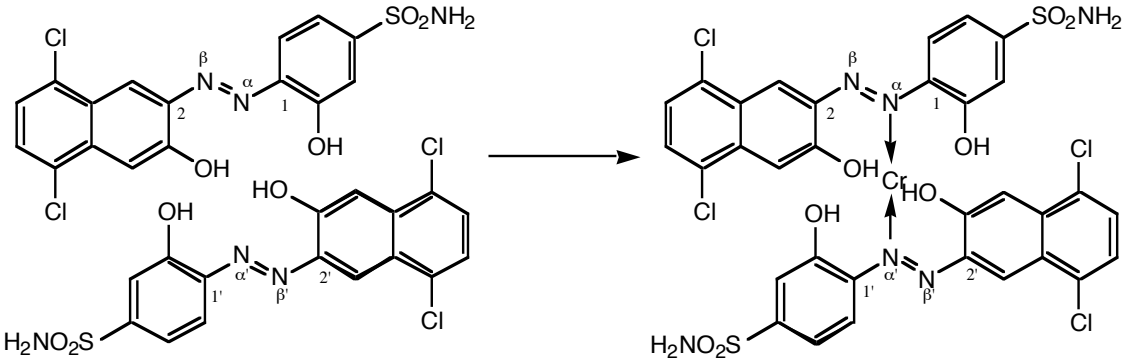

Figure 3.4 *Initial linkage of a central metal atom to ligand structures using CAChe Editor.*

2) The CMA-Nα bond lengths were adjusted to 1.9 Å, by clicking on the azo nitrogen followed by the CMA.

3) The Nα-CMA-Nα‘ bond angle was set to 180°.

4) The Nβ-Nα-CMA bond angle was adjusted to 120° for both azo groups.

5) The C1-Nα-CMA bond angle on each azo group was set to 120°.

6) The improper torsion angle between the CMA and the plane of the azo dyes was set to 0° by selecting atoms in the sequence CMA-Nα-Nβ-C1, and adjusting the improper torsion angle to 0°. This was repeated for both azo moieties. At this stage, the entire molecule was co-planar.

7) The two azo chromophores were set perpendicular by selecting atoms in the order Nβ-Nα-Nα’-Nβ’, and adjusting the dihedral angle to 90°.

8) Bonds were then added from the oxygen atoms to the CMA. The azo-CMA bonds were changed to coordinate bonds. With the entire molecule selected, the valence (and only the valence) was “beautified” using the “Beautify” utility of the Editor. This structure was saved.

9) A mechanics optimization was run on this structure. Figure 3.5 shows an example of a mechanics-optimized chromium complex.

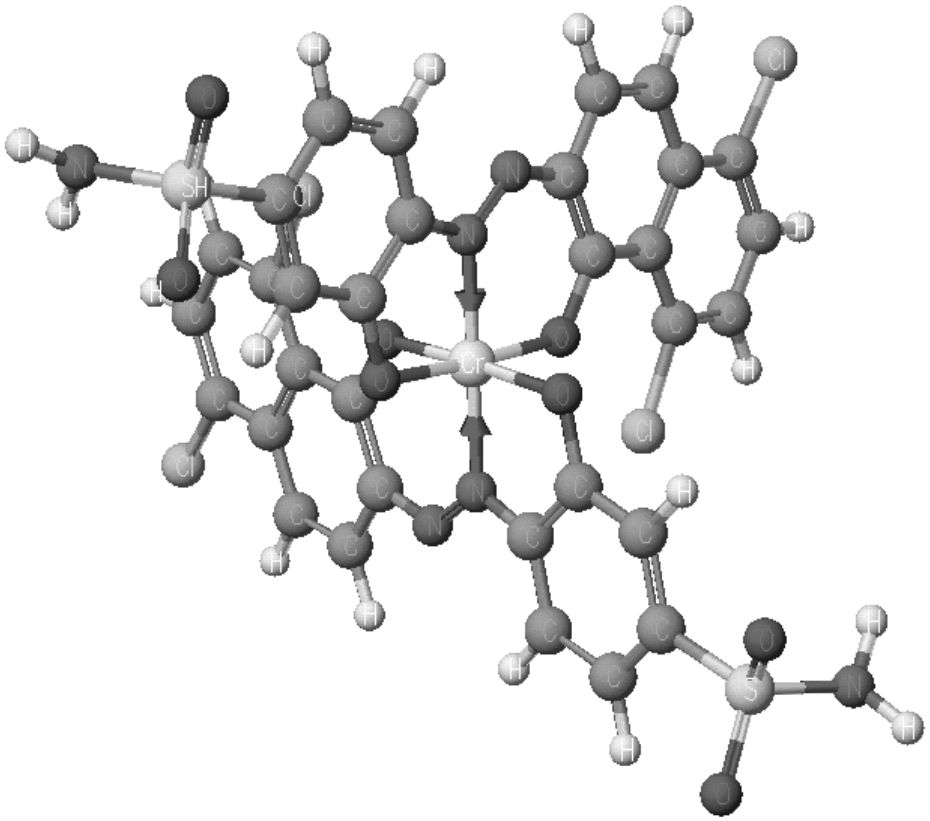

Figure 3.5 *A mechanically optimized metal complex dye structure.*

10) The mechanically optimized structure was re-opened in the Editor, and all bonds to the CMA were deleted. The oxygen atoms were changed to sp^2 oxygen atoms with a charge of -1. The central metal atom was also given an appropriate charge (e.g.: +3) and hybridization (e.g.: d^2sp^3). This structure was saved, and used as the starting structure for ZINDO optimization. An example of a metal complex starting structure is given in Figure 3.6.

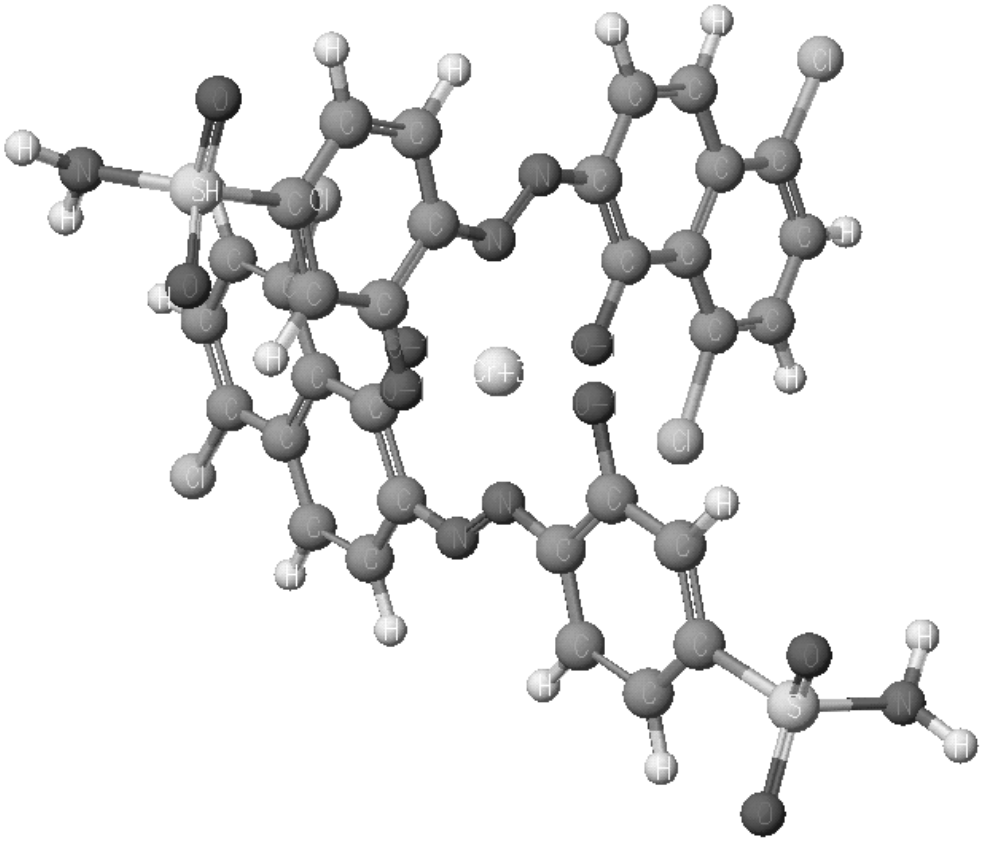

Figure 3.6 *Example of a starting structure for ZINDO optimizations. All bonds to the central metal atom have been removed following optimization using CAChe Mechanics, and atoms have been given an appropriate formal charge.*

3.2 GEOMETRY OPTIMIZATION OF DISPERSE DYES

This part of the study involved an examination of the ability of modern modeling methods to accurately predict the x-ray crystal structures of three disperse dyes, CI Disperse Yellow 86 (**21**), CI Disperse Red 167 (**12**), and CI Disperse Blue 27 (**50**). These three dyes are used in PET for applications requiring good lightfastness, and serve as prototypes in our research program aimed at designing lightfast analogs.

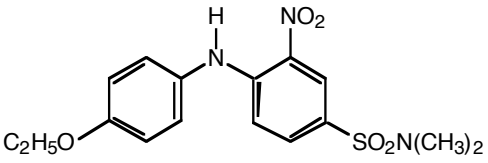

21

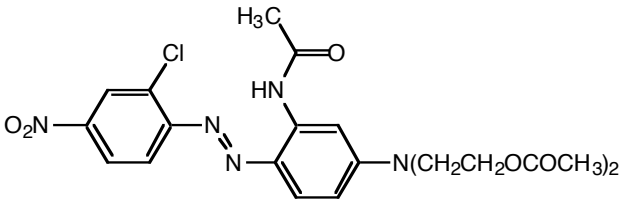

12

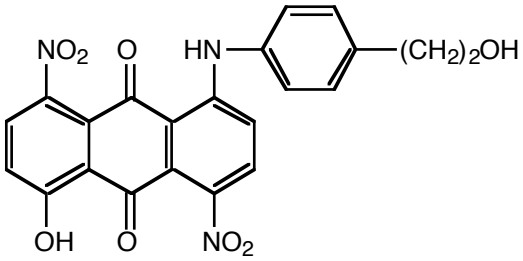

50

The x-ray crystal structures of **12** and **21** have already been determined by Freeman *et al.* [188, 189]. The presence of a hydrogen bonding interaction in **21** is believed to facilitate excited state intramolecular proton transfer [2], thus providing a mechanism for rapid deactivation of the photoexcited dye. With this point in mind, we sought to assess the ability of molecular modeling methods to accurately predict hydrogen bond distances. Similarly, in the case of **12**, x-ray studies have shown that a bifurcated hydrogen bond exists between the acylamino hydrogen atom, one of the nitrogen atoms of the azo group, and the chlorine atom [188]. The presence of such hydrogen bonding is thought to impart photostability to this dye. A literature search did not reveal the x-ray crystal structure of any commercial anthraquinone dyes, however, x-ray crystal

data are available for a number of pharmaceuticals containing an anthraquinone moiety. An example is the cytotoxic antibiotic daunomycin **51**, a compound used for the treatment of acute lymphocytic leukemia [190, 191].

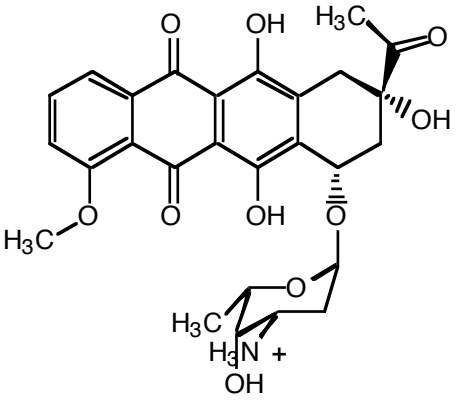

51

Structures **12**, **21**, and **50** were entered into the molecular mechanics package via the CAChe graphical Editor as planar structures. Initial optimization involved the use of a mechanical method (augmented MM2) to obtain a crude structure. A list of all of the non-hydrogen bond lengths was compiled and the mechanics-optimized geometry was then duplicated. Copies of the structure were fed into graphical interfaces to MOPAC and ZINDO. Geometry optimizations were then performed using MNDO, MINDO/3, AM1 and PM3 Hamiltonians, in the case of the four MOPAC calculations, and CNDO/1, CNDO/2, INDO/1, and INDO/2 were used for optimizations in the ZINDO package. In the case of optimizations run in MOPAC, the Broyden-Fletcher-Goldfarb-Shanno (BFGS) function minimization routine was used to optimize the geometry.

The outputs from the optimizations using the different Hamiltonians were then compared to the measured x-ray structures for dyes **12** and **21**. Initially, bond lengths were compared. The bond lengths of the N-alkyl ester chains of **12** were not included in the study, as these were ill-defined in the experimental data.

3.2.1 ANTHRAQUINONE DYES

It quickly became apparent that the semi-empirical modeling systems of CAChe were not capable of optimizing the structures of anthraquinone dyes. Although x-ray crystal data show the tricyclic system in these dyes to be planar [190, 191], each of the eight methods listed above distorted the geometry of the carbonyl groups and anthraquinone moiety so severely that investigations in

this area were terminated. Semi-empirical optimization tended to force the anthraquinone moiety into a non-planar "butterfly" shape. An example of an attempted anthraquinone optimization is shown in Figure 3.7, which shows the structure of CI Disperse Blue 56 after optimization using MM2 followed by AM1.

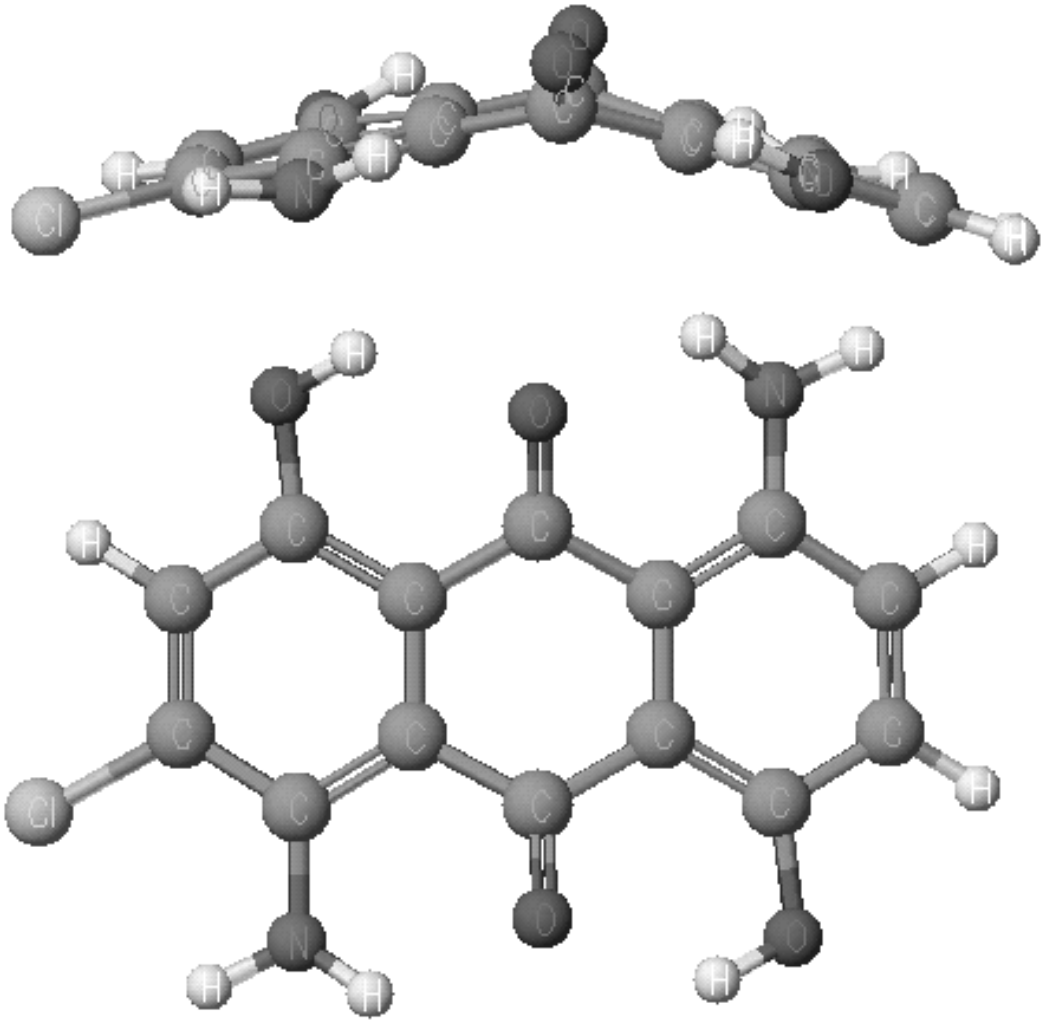

Figure 3.7 *Two views of CI Disperse Blue 56 after optimization using AM1. The butterfly-shaped distortions to the tricyclic anthraquinone system can be clearly seen in the lateral view of the molecule (top).*

3.2.2 ANOMALOUS HEAT OF FORMATION RESULTS FROM AM1

It came as a surprise to find that the AM1 method predicted the *cis* isomer of azobenzenes to be more stable than the *trans* isomer (Table 4). PM3

did not show the same flaw. Interestingly, this problem did not seem to apply to stilbene analogs **54** and **55** (Table 4), which were predicted to be most stable in the *trans* configurations by both methods. The (azo iso–π–electronic) stilbene dianion **56** was also optimized in AM1 and PM3. Interestingly, both methods suggested the *cis* and the *trans* isomers of the dianion to be degenerate. A search of the literature did not reveal any previous reports of this shortcoming of AM1. Although the source of this error is unclear, it would appear to be associated with the AM1 parameters for sp^2 hybridized double bonded nitrogen

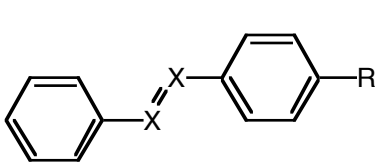

a *Trans*

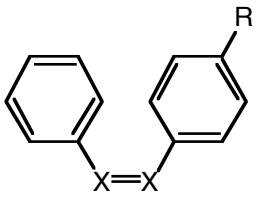

b *Cis*

52 R=H, X=N **53** R=N($CH_2CH_2OH)_2$, X=N

54 R=H, X=CH **55** R=N($CH_2CH_2OH)_2$, X=CH **56** R=H, X=C^-

atoms.

Table 4 *Calculated heats of formation for the cis and trans isomers of* ***52-56****.*

Structure	AM1 Energy (kcal.mol^{-1})	PM3 Energy (kcal.mol^{-1})
52a (*trans*)	100.1	90.7
52b (*cis*)	95.5	93.3
53a (*trans*)	6.8	-0.7
53b (*cis*)	2.3	2.6
54a (*trans*)	60.8	61.2
54b (*cis*)	64.2	65.4
55a (*trans*)	-30.1	-28.7
55b (*cis*)	-27.6	-23.3
56a (*trans*)	144.0	144.1

56b (*cis*)	144.1	144.1

3.2.3 NITRODIPHENYLAMINE AND AZO DYES

The structures obtained from geometry optimizations were compared to the x-ray crystal structures of **12** and **21** in terms of a) atomic bond lengths, b) intramolecular hydrogen bond distances, and c) molecular conformations, including the geometries of amino nitrogen atoms. A visual comparison of the x-ray crystal structure of **21** with the structure predicted by the AM1 method is presented in Figure 3.8. The structure obtained using PM3 was similar. The length of the intramolecular hydrogen bond is displayed in Å on both the predicted and x-ray crystal structures in Figure 3.8. It can be seen that the AM1 predicted structure is similar to the x-ray crystal structure, in terms of conformation and the presence of hydrogen bonding in the structure.

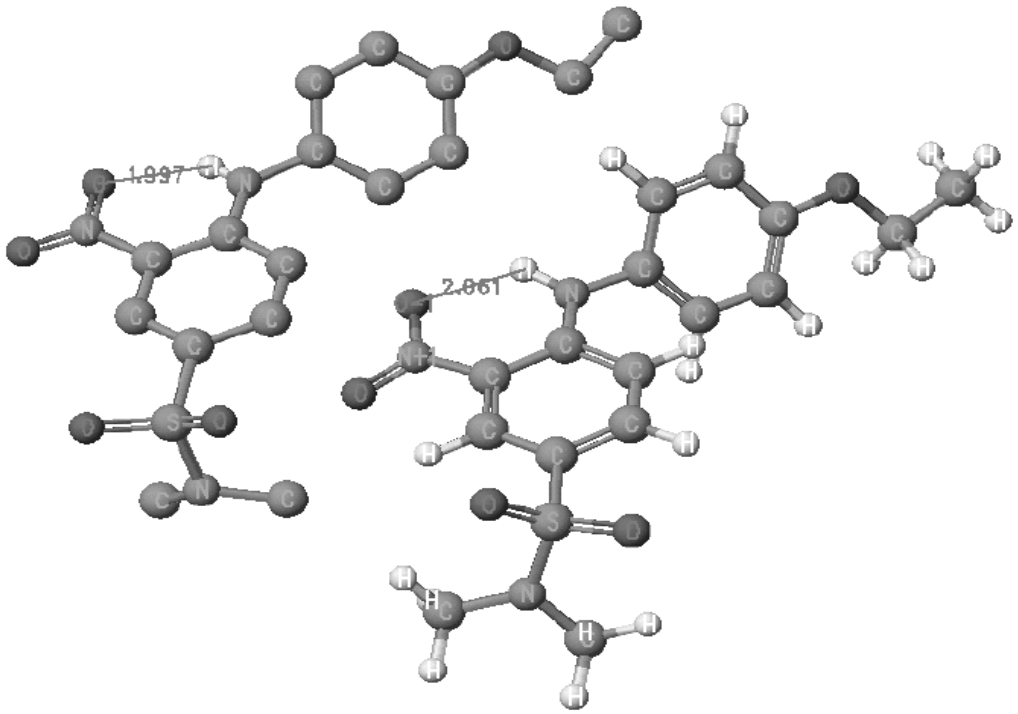

Figure 3.8 *Comparison of the x-ray crystal structure of CI Disperse Yellow 86 (top) with the AM1 predicted structure (bottom).*

The PM3 method gave similar results to the AM1 method for both **21** and **12**. Figure 3.9 shows a comparison of the x-ray crystal structure of **12** with the AM1 predicted geometry.

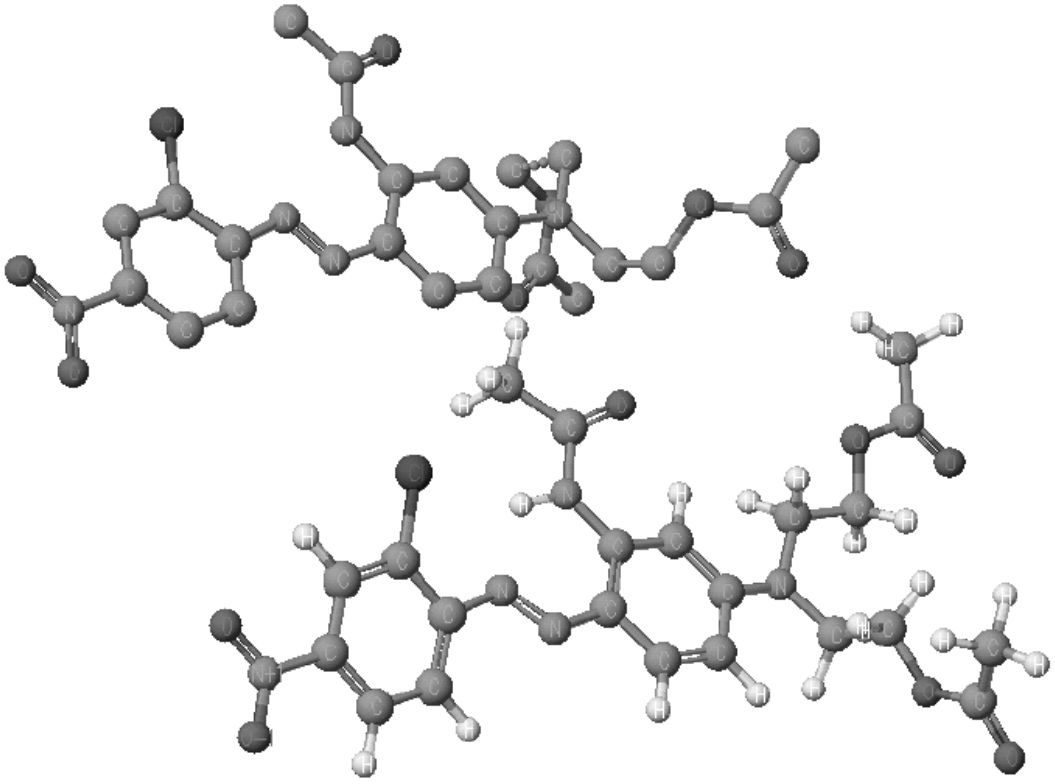

Figure 3.9 *Comparison of x-ray crystal structure of CI Disperse Red 167 (top) with the AM1 predicted structure (bottom).*

3.2.3.1 Bond Length Prediction

The experimental bond lengths of **12** and **21** were compared to those obtained for the structures after geometry optimizations, using the aforementioned eight semi-empirical methods and the Newtonian MM2 method. Representative data are provided in Figure 3.10 and show the relationship between experimental heavy atom bond lengths for dyes **12** and **21** and AM1 predicted bond lengths. The graph is similar to the graph obtained from the results of PM3 optimizations. Table 5 and Table 6 contain the root mean

square percent error, average end error, correlation coefficients, and largest bond-length error for each method employed.

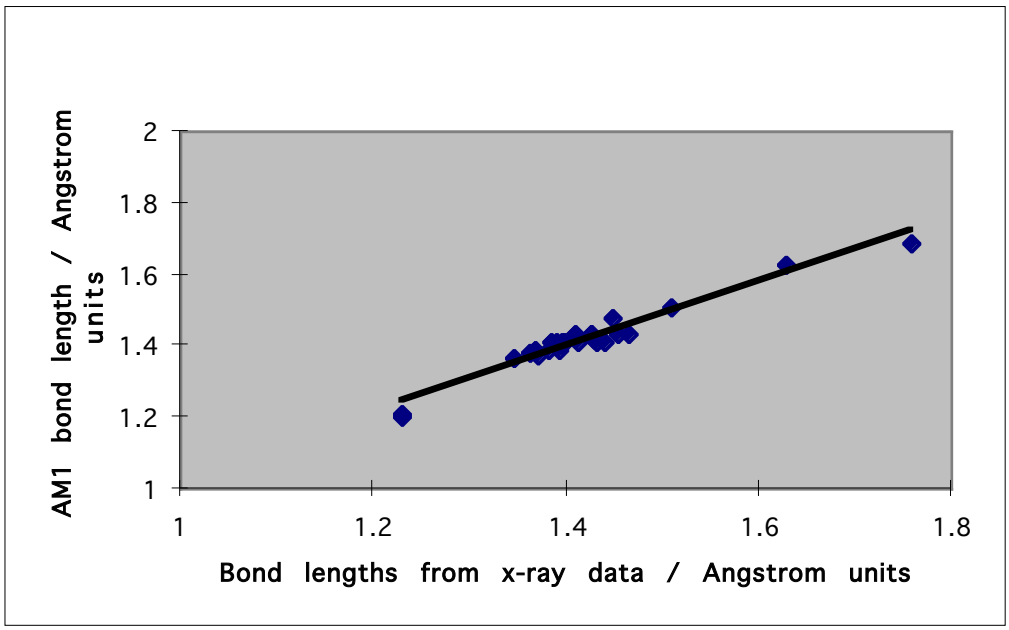

Figure 3.10 *Relationship between experimental and predicted (AM1) bond lengths in **21**. A similar graph was obtained when PM3 was used.*

Table 5 *Summary of results pertaining to the prediction of bond lengths of **21**.*

Method Used	Average RMS Error (%)	End Error (Å)	Correlation Coefficient	Largest Error (%)
MM2+	2.38	-0.340	0.928	11.19
CNDO/1	1.97	-0.079	0.957	5.51
CNDO/2	1.61	-0.017	0.961	3.87
INDO/1	1.65	-0.176	0.965	6.57
INDO/2	1.65	-0.031	0.961	4.55
MINDO/3	2.37	-0.249	0.948	5.05
MNDO	1.97	-0.069	0.973	6.42
AM1	1.18	0.172	0.977	4.04
PM3	1.16	-0.180	0.977	8.54

Table 6 *Summary of results pertaining to the prediction of bond lengths of **12.***

Method Used	Average RMS Error (%)	End Error (Å)	Correlation Coefficient	Largest Error (%)
MM2+	2.32	0.001	0.914	10.01
CNDO/1	1.76	0.148	0.961	4.33
CNDO/2	1.77	0.151	0.960	4.09

INDO/1	1.82	0.023	0.954	5.01
INDO/2	1.78	0.044	0.952	4.60
MINDO/3	2.35	-0.129	0.941	10.15
MNDO	1.77	<0.001	0.973	4.42
AM1	1.54	0.096	0.968	4.49
PM3	1.57	0.103	0.966	3.95

As anticipated, the Newtonian MM2+ method was the least accurate overall for modeling conjugated structures such as **21** and **12**. This method gave a level of random error that lowered the r^2 value to a modest 0.91 and 0.93 for **21** and **12**, respectively. While the causes of random error in this method are not certain, they could arise as a result of subtle molecular orbital interactions which were not taken into account. The MM2+ method is, however, accurate enough to warrant its use in obtaining a crude starting structure for more rigorous semi-empirical optimizations.

The r^2 values for the eight semi-empirical methods are comparable. The occurrence of random errors was progressively reduced in the most recent methods, as AM1 and PM3 showed the best consistency. Interestingly, the end errors for the estimation of bond lengths in nitrodiphenylamine dye **21** are much larger than those for azo dye **12**. While the cause of this effect was not established, it could be attributed to different crystal forces impacting the crystal lattices of the two dyes -- factors which were not taken into account by any of the methods employed in this study.

In the case of dye **21**, clearly, AM1 and PM3 gave the best correlation and the lowest mean errors. In the case of results pertaining to the azo dye **12**, it would appear that MNDO, AM1, and PM3 are suitable methods to use to estimate equilibrium bond lengths. In every case, the largest errors in bond length prediction were associated with prediction of bond lengths involving non-carbon atoms. This is illustrated in Table 7 which shows the largest bond length prediction errors for **21**. The errors associated with non-carbon bonds may be due to inadequate parameterizations for non-carbon atoms in the individual methods. In addition, the experimental data for this study were

obtained from x-ray crystal data. Crystal forces acting on the molecule in the crystal environment will have an influence on the conformation of the molecule; however, all of the modeling methods used considered the wavefunction of only a single, isolated molecule in a vacuum. Despite these differences, all of the methods gave surprisingly realistic bond length predictions.

Table 7 *Largest bond length prediction errors (%) for **21.***

Method	Largest Bond Length Error (%)	Bond Associated with Error
MM2	11.19	C6 - N1
CNDO/1	5.51	S - O5
CNDO/2	3.87	C12 - S
INDO/1	6.57	S - N3
INDO/2	4.55	C12 - S
MINDO/3	5.05	C2 - O1
MNDO	6.42	S - O5
AM1	4.04	C12 - S
PM3	8.54	S - N3

3.2.3.2 Prediction of Hydrogen Bond Distances

In view of the connection between hydrogen bonding in dye structures and lightfastness, it would be advantageous to predict the existence of this key feature. Table 8 provides a comparison of experimental hydrogen bond distances in **12** and **21** with those predicted by the four MOPAC methods. The results suggest that AM1 and PM3 were able to predict the presence of an intramolecular hydrogen bond in both structures. Dewar [cxliv] reported that the AM1 method was the first semi-empirical method to be able to simulate hydrogen bonding. However, Stewart [cl] suggested that the AM1 method was unreliable for the prediction of hydrogen bonds, and showed that the PM3 method reproduced hydrogen bonds with greater fidelity.

Table 8 *Comparison of predicted and experimental hydrogen bond distances (Å) in **21** and **12.***

Structure	X-ray	PM3	AM1	MNDO	MINDO/3
21	1.997	1.827	2.061	2.778	3.012

12	1.701	1.926	2.141	2.496	3.394

Figure 3.11 is a comparison of the conformation of the nitrodiphenylamine chromophore of **21** predicted by the MNDO method with the x-ray crystal structure. In this rendition, the x-ray structure is represented by solid spheres and the predicted (MNDO) structure is shown superimposed as dotted spheres. Note that the MNDO method predicts the nitro group to be twisted out of conjugation -- an arrangement that circumvents intramolecular hydrogen bonding.

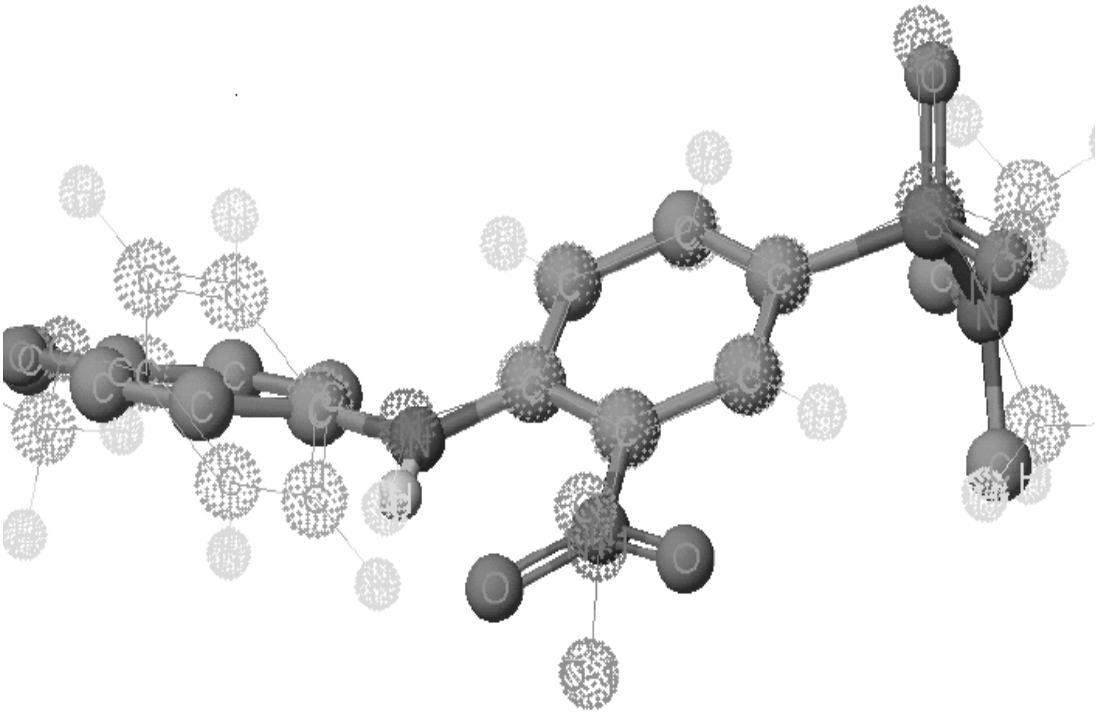

Figure 3.11 *Comparison of the x-ray crystal structure of **21** (solid atoms) to the MNDO-predicted conformation (dotted atoms).*

Figure 3.12 shows the x-ray structure (solid) docked with the PM3 predicted geometry (dotted) of **21** in the region of the chromophore. The structure predicted by this method was found to be very similar to the x-ray structure. The nitro group was predicted to be coplanar with the phenyl ring to which it is attached. Such planarity is conducive to a hydrogen bonding

interaction between the amino hydrogen atom and the nitro group. PM3 also predicted the two phenyl rings to be mutually twisted, in agreement with x-ray studies.

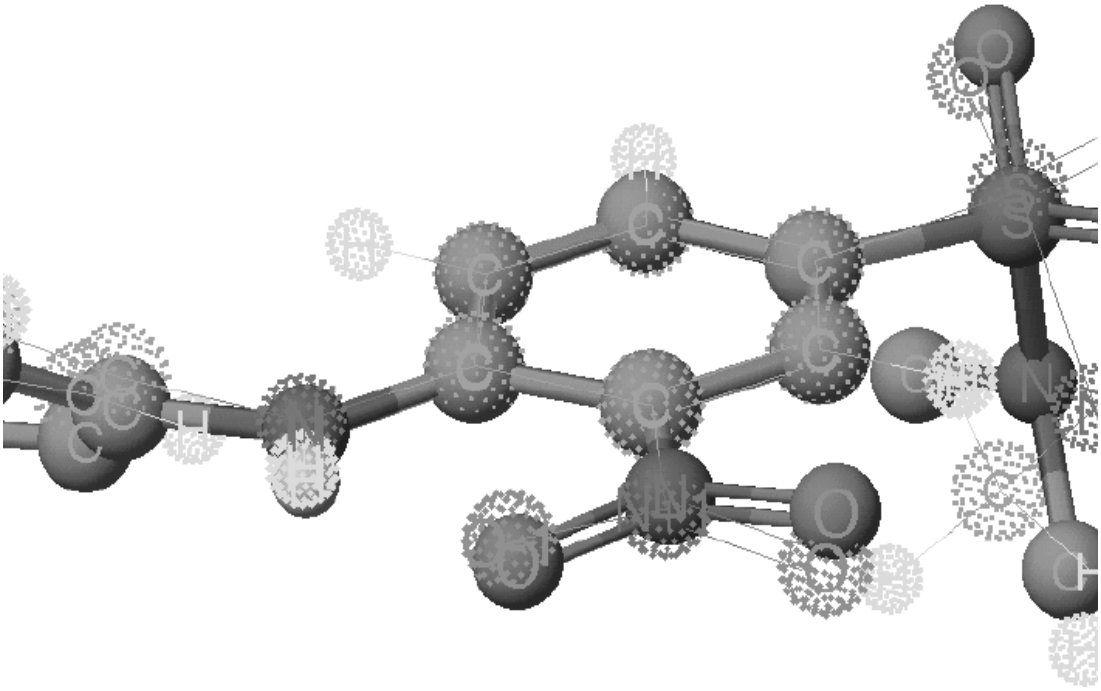

Figure 3.12 *Comparison of the x-ray crystal structure of **21** (solid atoms) with the PM3 predicted conformation (dotted atoms).*

3.2.3.3 Prediction of Molecular Conformations

The importance of molecular conformations tending to form intramolecular hydrogen bonds has been discussed (Figure 3.11 and Figure 3.12). In addition, it is known that molecular planarity effects the interaction of mesomeric donors with the π-electron system of the dye, which in turn has an effect on dye color [192]. Similarly, it is known that the electronic spectra of *cis* and *trans* azobenzenes differ [192, 193]. It has also been suggested that the PM3 method is better at predicting the geometry of nitro groups [194], and that AM1 tends to underestimate π-orbital overlap energy [195]. While these results,

together with its ability to predict hydrogen bond distances, suggests the routine use of PM3 for the geometry optimization of dyes, results from the present investigation showed that the PM3 method has a tendency to pyramidalize planar amino groups. Since such distortions could affect the results of color prediction using structures optimized using PM3, an assessment of the experimental and predicted improper torsion angle for the substituents around each of the amino groups in **21** and **12** was undertaken. The results are summarized in Table 9. For comparison, the improper torsion angle of a perfectly planar sp^2 hybridized atom would be 0°, and that of methane (which is centered by an sp^3 hybridized atom) would be 60°. The data in Table 9 suggest that pyramidalization of amino nitrogen atoms in **21** and **12** was less severe when AM1 was used instead of PM3.

Table 9 *Predicted and observed improper torsion angles (°) for amino groups in **21** and **12**.*

Structure	X-ray	PM3	AM1	MNDO	MINDO/3
21	3.08°	14.99°	1.71°	23.23°	2.85°
12	4.75°	32.08°	23.80°	3.87°	4.39°

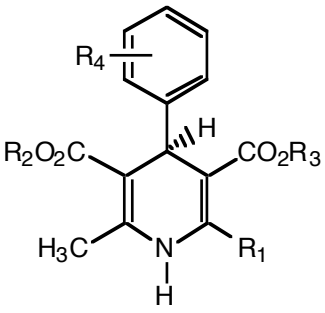

57

Although no published studies were found which evaluated the utility of semi-empirical methods in predicting the equilibrium geometries of dyes, several papers have been published in which semi-empirical methods were applied to conjugated systems of moderate size. The results are similar to our own. For instance, Bikker and Weaver [196] compared AM1, PM3 and MNDO for their ability to predict the x-ray structure of a series of eighteen dihydropyridine calcium channel modulators such as **57** (R_1=Me or CN, R_2 and R_3 = alkyl, R_4 = NO_2, F, OMe), using a BFGS minimizer in MOPAC. The authors concluded that AM1 was best suited to reproducing the crystal geometries of these compounds, followed by PM3 and then MNDO.

Aakeröy [197] calculated the minimum enthalpies of formation for 15 simple carboxylic acids, including 9 benzoic acid derivatives, using MNDO, AM1 and PM3 on structures optimized by a BFGS converger, and compared these values with those measured experimentally. Aakeröy also compared experimental proton affinities of the acid anion to those calculated using the same three methods and found PM3 to be superior to AM1 and MNDO, and AM1 to be better than MNDO for predicting heats of formation and proton affinities.

In a similar study, Karaman, Huang and Fry [198] showed AM1 and PM3 to be better than MNDO for calculating the heat of formation and gas phase acidity for 120 compounds, including phenols, anilines and benzoic acids. In fact, these workers concluded that AM1and PM3 were as good as *ab initio* methods for estimating the affects of substituents on gas phase acidity in aromatic systems.

Yates and Patel [199] used the MNDO method to optimize the structures of six tricyclic compounds (**58**) possessing interesting biological and colouristic properties. The authors calculated the heats of formation, dipole moments, and electron affinities of compounds **58a-f**. As no comparison was made with experimental data, the authors were unable to assess the applicability of the MNDO method for the prediction of dye geometries, dipole moments, and electron affinities.

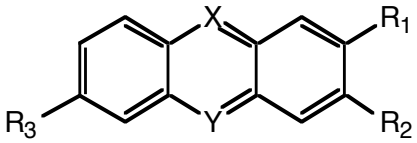

58

	a	**b**	**c**	**d**	**e**	**f**
R_1	CH_3	H	H	H	H	H
R_2	NH_2	$N(CH_3)_2$	NH_2	$NH(CH_3)$	$N(CH_3)_2$	NH_2
R_3	$N(CH_3)_2$	$N(CH_3)_2$	NH_2	$N(CH_3)_2$	$N(CH_3)_2$	NH_2
X	N	CH	CH	N	N	N
Y	N	N	N	S^+	S^+	S^+

3.2.4 HYDROXYBENZOTRIAZOLE PHOTOSTABILIZERS

It has been shown that the phenolic proton in **59** plays a key role in photo-excitation energy dissipation of this compound via excited state intramolecular proton transfer [lxxxvi]. Furthermore, the presence of the hydrogen bond in **59** and **60** has been shown to be a stabilizing factor for hydroxybenzotriazoles, which maintains a planar geometry, thus facilitating rapid ESIPT. X-ray crystal data was available for compounds **59** and **60** making it possible to assess the capability of MOPAC methods to predict hydrogen bonding.

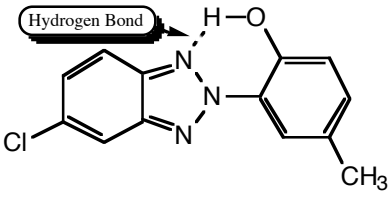

59

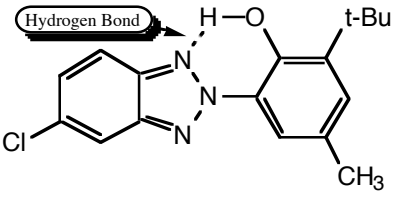

60

Compounds **59** and **60** were built using CAChe Editor, and optimized using AM1 and PM3 in CAChe MOPAC, implementing the protocols for generating starting structures for optimizations. Table 10 contains a comparison of predicted and experimental hydrogen bond lengths in **59** and **60**. The results showed that the AM1 method tended to

Table 10 *Comparison of experimental hydroxybenzotriazole hydrogen bond lengths with those predicted by AM1 and PM3 methods.*

Structure	Experimental H-bond length / Å	AM1 predicted H-bond length / Å	PM3 predicted H-bond length / Å
59	1.85	2.055	1.841
60	1.76	1.999	1.817

overestimate hydrogen bonding distances in these compounds, and that the effect exerted by the *tert.* butyl group on the hydrogen bond length is underestimated by AM1. While the PM3 method gave closer estimates of hydrogen bond lengths in these compounds, the impact of introducing the *tert*.

butyl group *ortho* to the phenolic hydrogen atom (cf. **59** and **60**) was somewhat understated.

3.2.5 METAL - LIGAND BOND LENGTHS

The x-ray crystal structure of the structurally isomeric 1:2 chromium complex dyes **19** and **20** have recently been solved [lxx]. In the present study, starting structures corresponding to the Nα, Nα‘ (**19**) and Nβ, Nβ‘ (**20**) chromium complex dyes were generated by following the protocols discussed in Section 3.1.1.5, and optimized as quartet multiplicity complexes in an INDO/2 UHF geometry optimization in CAChe ZINDO. Table 11 contains a comparison of the predicted and experimental metal-ligand bond lengths for **19** and **20**.

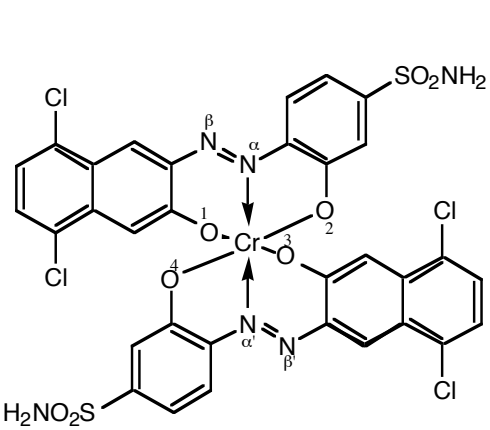

19

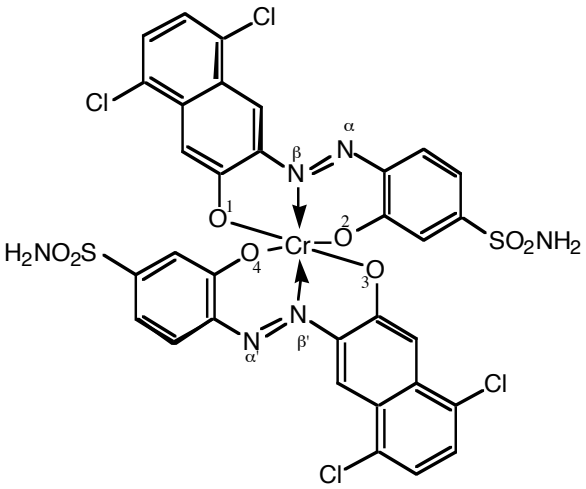

20

Table 11 *Comparison of predicted metal-ligand bond lengths with experimental data (from [lxx]). Numerals in parenthesis show the error in the last significant digit.*

Bond I.D.	Bond Lengths **19**		Bond Lengths **20**	
	Experimental (Å)	INDO/2 Predicted (Å)	Experimental (Å)	INDO/2 Predicted (Å)
N - Cr	2.00 (1)	1.915	2.005 (6)	1.916
O1 - Cr	1.947 (8)	1.902	1.961 (7)	1.881
O2 - Cr	1.978 (8)	1.965	1.944 (6)	1.981
N’ - Cr	1.97 (1)	1.914	2.021 (6)	1.915

O3 - Cr	1.938 (9)	1.904	1.956 (6)	1.879
O4 - Cr	1.970 (9)	1.966	1.917 (6)	1.980
Totals	11.803	11.566	11.804	11.552

In light of the assessments of the capability of ZINDO methods to predict atomic bond lengths (Section 3.2.3), inaccuracies in the prediction of absolute metal-ligand bond lengths were to be expected. However, particularly in the case of the Nα, Nα‘ isomer (**19**), the ZINDO results suggested that the INDO/2 method was effective in predicting the incidence of long vs. short bonds in these structures. Figure 3.13 and Figure 3.14 contain the optimized structures for **19** and **20** respectively. In these renditions the results of the ZINDO Mulliken population analysis were summarized graphically by CAChe Editor. Strong covalent bonds are displayed as cylinders, weak bonds are depicted by thick dotted lines, and essentially ionic interactions are represented by the absence of a directional bond.

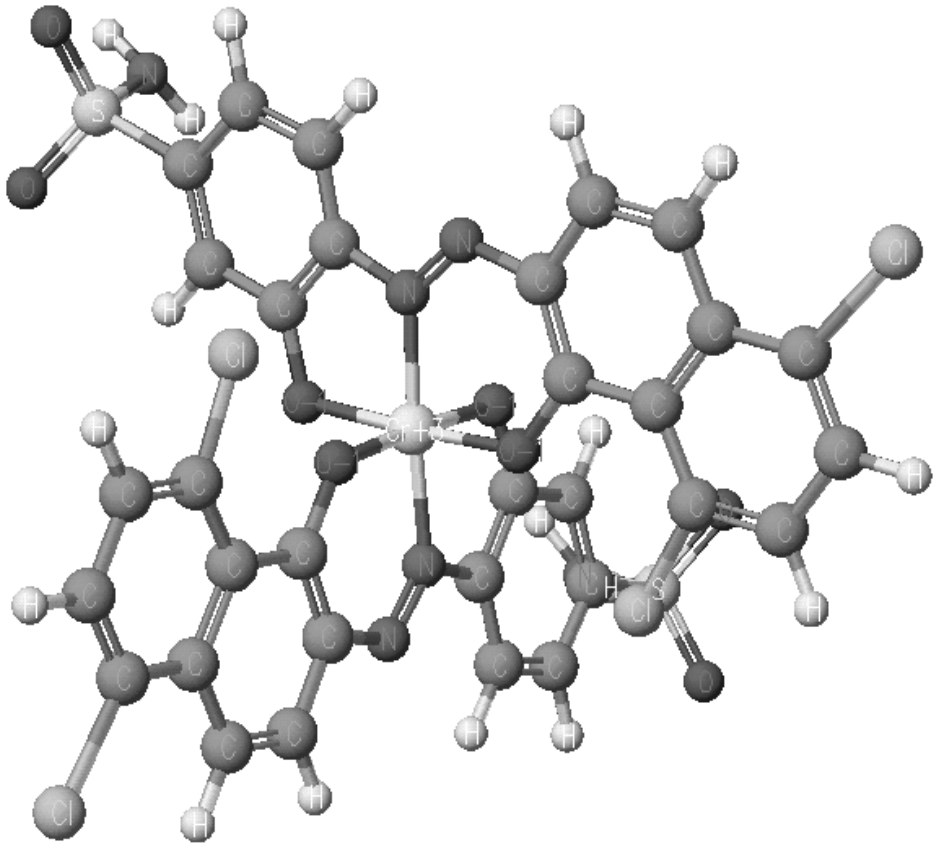

Figure 3.13 *Nα,Nα‘ chromium complex dye (**19**), optimized using the INDO/2 method.*

The Nα, Nα‘ isomer (**19**) was predicted to contain six strong bonds to the central metal atom, whereas the corresponding Nβ, Nβ‘ isomer (**20**, Figure 3.14) contained only two strong bonds and four weaker bonds. The Nα, Nβ‘ isomer was also optimized, and predicted to contain three strong and three weak bonds to the central chromium atom. Interestingly, the sums of the lengths of all of the bonds to the central chromium atoms of **19** and **20** (Table 11) were very similar, suggesting that bond length data alone may not be a reliable indication of bonding strength in these compounds.

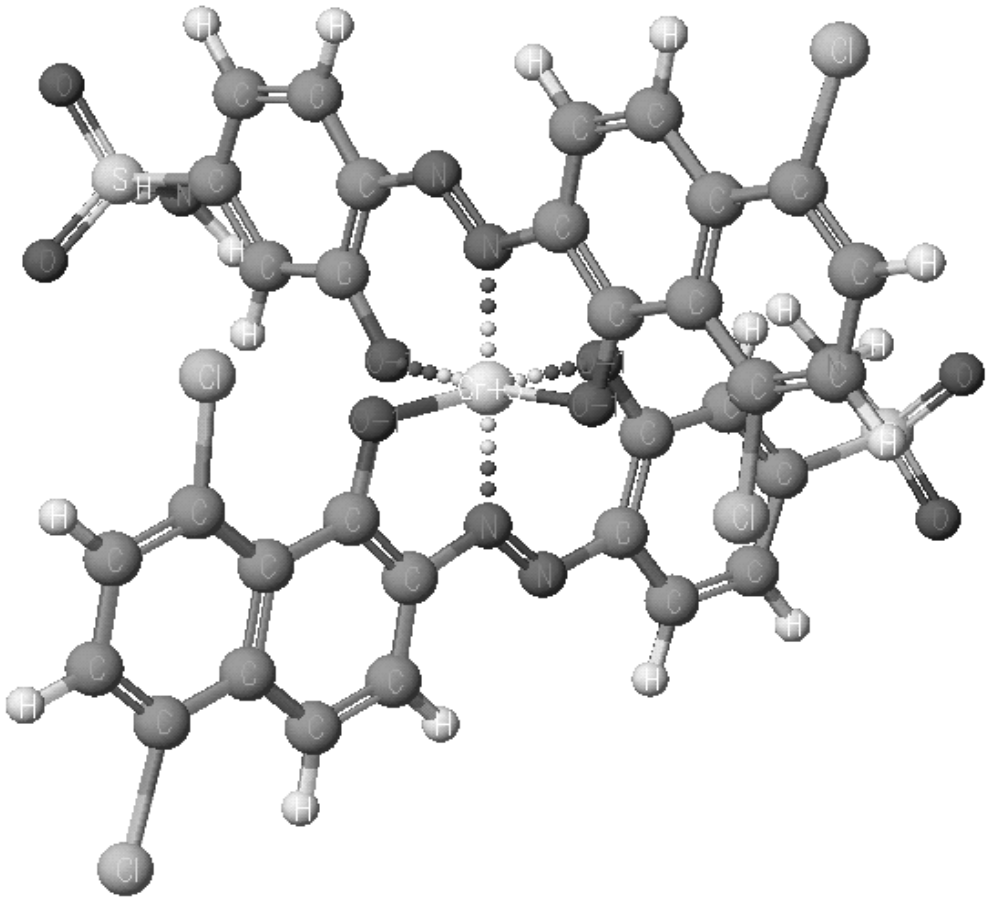

Figure 3.14 *NβNβ‘ chromium complex dye (**20**) optimized using the INDO/2 method.*

If the dye-metal bonding in the Nα, Nα‘ isomer (**19**) was stronger than that in the Nβ, Nβ‘ isomer (**20**), we might expect an equilibrium mixture of the two isomers to favor the Nα, Nα‘ isomer under thermodynamic conditions. Lehmann and Rihs used a combination of preparative HPLC and x-ray crystallography to establish that at 100°C and pH 9, equilibrium favors the Nα, Nα‘ isomer [lxx]. The presence of the Nα, Nβ‘ isomer was also detected in the mixture. Table 12 shows the initial (five minutes after complexation with chromium) and equilibrium isomer distribution between **19** an **20**. Thermodynamic equilibrium was reportedly established after 50 hours at 100°C, pH 9.

Table 12 *Experimental concentrations of **19** (Nα, Nα') and **20** (Nβ, Nβ') at equilibrium. (Results from Ref lxx).*

	Isomer	Distribution	INDO/2 Predicted
Isomer	Initial	Equilibrium	Number of Bonds
Nα, Nα'	23.6 %	78.7 %	6 strong
Nα, Nβ'	61.9 %	20.4 %	3 strong + 3 weak
Nβ, Nβ'	14.6 %	0.9 %	2 strong + 4 weak

Interestingly, the relative abundance of each isomer in the equilibrium mixture correlates with the predicted strength of the bonding to the central metal atom. It is a general principle in chemistry that compounds containing stronger (i.e., exothermic) bonds are thermodynamically favored over those containing weaker bonds. Thus, it was encouraging that ZINDO predicted the dominant isomer to contain the strongest bonds to the central metal atom.

The SCF energy values of the three isomers varied by +/- 0.0006% of the total. Given the modest ability of INDO/2 to predict bond lengths, it is unlikely that energy differences on the order of 0.0006% will prove to be useful indicators of thermodynamic stability. However, predicted bond strength appears to provide a useful inroad to predicting the relative thermodynamic stabilities of isomers.

3.2.6 SOLUBILITY PREDICTION

Experimental measurements of aqueous solubility are available for the series of monoazo dyes **61** - **72** [200, 201]. The structures were restricted to hydrophobic monoazo benzene-based dyes. Dyes based on anthraquinone were avoided because of a lack of confidence in the ability of MOPAC to compute these structures. Despite these limitations, dyes **61** - **72** are structurally diverse. The structures were prepared for the optimization by applying the protocols established in Section 3.1.1 before the BLogP calculation was initiated by using CAChe ProjectLeader.

Experimental aqueous solubility data for structures **61**-**68** at 25°C were obtained from the work of Baughman and Weber [200], and those for **69**-**72** were obtained from the work of Siddiqui [201], for aqueous solubilities at 21°C. Table 13 gives results of CAChe BLogP calculations. AM1 was used to optimize the geometries of the dyes and to calculate the energies of the structures in a vacuum and an aqueous environment.

As water-octanol partition coefficients were not available for many of the dyes, the natural log of the reciprocal of the aqueous solubility was compared to the calculated log P value. Figure 3.15 shows the correlation between the calculated water-octanol partition coefficient and the natural log of the reciprocal of experimental aqueous solubility. Despite the indirect relationship between aqueous solubility and water-octanol partition coefficient, the correlation appears to be useful for estimating the solubility of azo disperse dyes.

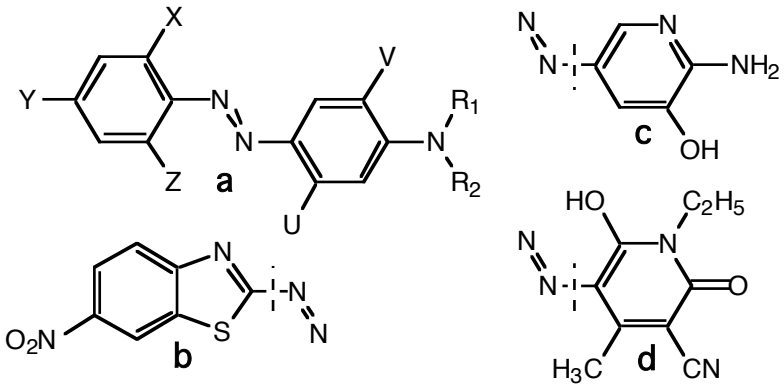

	Ring system	X	Y	Z	U	V	R_1	R_2	CI or CASS No.
61	**a**	H	H	H	H	H	C_2H_5	C_2H_4OH	11110
62	**a**	Cl	NO_2	H	CH_3	H	C_2H_4OH	C_2H_4OH	11215
63	**a**	CN	NO_2	CN	CH_3	H	C_4H_9	C_2H_4OAc	72828-64-9
64	**a**	Cl	NO_2	H	NHAc	Cl	$CH_2CHOHCH_3$	H	71617-28-2
65	**a**	Cl	NO_2	H	H	H	C_2H_4OH	C_2H_4CN	6657-33-6
66	**a**	Br	NO_2	NO_2	NHAc	OCH_3	C_3H_7	C_2H_4CN	68877-63-4
67	**a/b**	-	-	-	H	H	C_2H_4CN	C_2H_4OAc	-
68	**a/c**	NO_2	Cl	H	-	-	-	-	70528-90-4
69	**a/d**	H	NO_2	H	-	-	-	-	-
70	**a/d**	NO_2	NO_2	H	-	-	-	-	-
71	**a/d**	Cl	NO_2	H	-	-	-	-	-
72	**a/d**	Cl	NO_2	Cl	-	-	-	-	-

Table 13 *Log P calculation details and experimental solubilities for **61-72** in water.*

Structure	Hf in Vacuum (kcal mol^{-1})	SAS area ($Å^2$)	Hf in Water (kcal mol^{-1})	Calc. LogP	Expt. Solubility ($\mu g.l^{-1}$)	Log_e (reciprocal solubility)
61	53.087	139.631	36.919	2.76	160 *	-5.075
62	1.625	1.69594	-27.501	3.61	100 *	-4.605
63	68.381	205.702	35.4	4.89	0.590 *	0.528
64	1.6383	180.933	-28.434	3.80	16.0 *	-2.773
65	85.182	172.617	55.335	4.00	280 *	-5.635
66	74.507	209.989	35.526	5.58	0.69 *	0.371
67	88.641	200.770	48.748	4.51	7.9 *	-2.067
68	50.289	156.255	23.968	2.90	74 *	-4.304
69	71.189	124.957	42.977	1.66	4000 **	-8.294
70	81.640	135.516	44.870	2.53	7000 **	-8.854
71	66.888	134.160	39.787	2.13	2000 **	-7.601
72	62.598	142.222	34.433	2.48	8000 **	-8.987

* Experimental solubility data from [200]

** Experimental solubility data from [201]

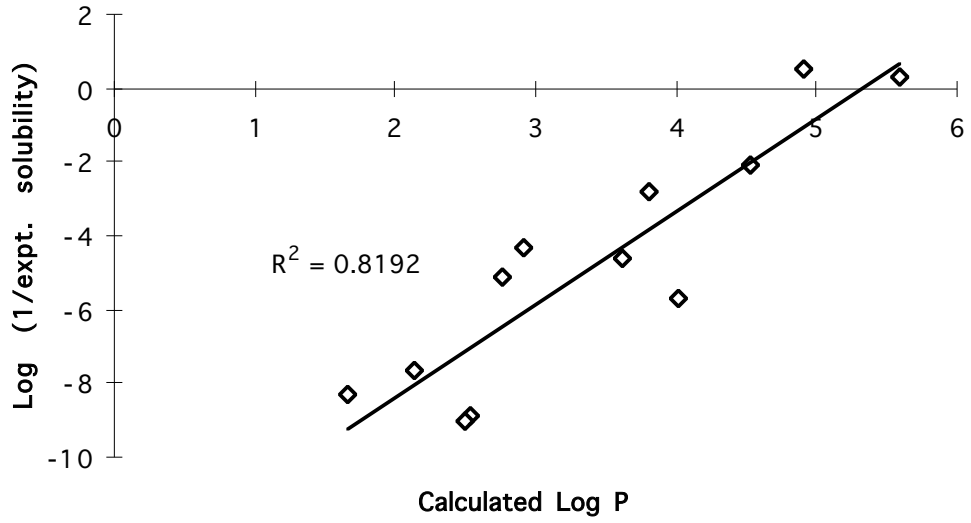

Figure 3.15 *Graph to show the relationship between the predicted Log P value and experimental solubility data for a series of azo dyes.*

3.2.7 PREDICTION OF DYE COLOR

The definitive work on the prediction of the color of organic dyes was produced by Griffiths [192]. Later, other workers found the PPP method more reliable for color prediction than the more recent CNDO and INDO methods, despite the advances and refinements incorporated into the latter methods [clvii]. However, the PPP method is restrictive, in that i) it does not consider d-orbitals, or ii) have atomic parameters for transition metals, or iii) take hydrogen bonding into account. It is also limited to closed shell systems containing even numbers of electrons, using RHF SCF calculations. In view of these limitations, it was deemed worthwhile to also briefly investigate the color predictive capabilities of ZINDO.

3.2.7.1 PREDICTION OF ABSORPTION MAXIMA

Structures **73a-h** were optimized in MOPAC (AM1) according to the protocols described in Section 3.1.1. The resulting structures were fed into ZINDO for configuration interaction calculations including excited configurations

formed from the nine lowest energy unfilled orbitals and the nine highest energy filled orbitals, which gave the longest wavelength allowed absorption band position (λ_{max}). Structures **73a**-**h** were also fed into the graphical interface of PISYSTEM, which subjected them to a two-dimensional geometry optimization. Experimental λ_{max} values for **73a**-**h** are quoted below each structure. In PISYSTEM, a PPP SCF CI calculation was then used to calculate λ_{max}. In all cases, the wavelength recorded was that corresponding to the first allowed transition. The results from PISYSTEM are presented in Figure 3.16, and those for ZINDO are presented in Figure 3.17.

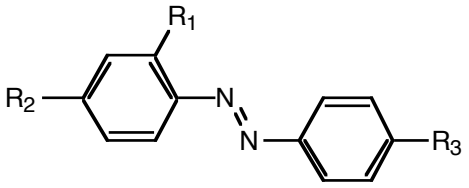

73

	a [202]	**b** [202]	**c** [202]	**d** [202]	**e** [202]	**f** [203]	**g** [204]	**h** [202]
R_1	H	H	H	H	H	NH_2	H	H
R_2	H	H	H	H	H	H	CN	NO_2
R_3	H	NO_2	NH_2	NMe_2	NEt_2	H	NEt_2	NEt_2
Expt. λ_{max}	318 nm	332 nm	385 nm	408 nm	415 nm	417 nm	466 nm	490 nm

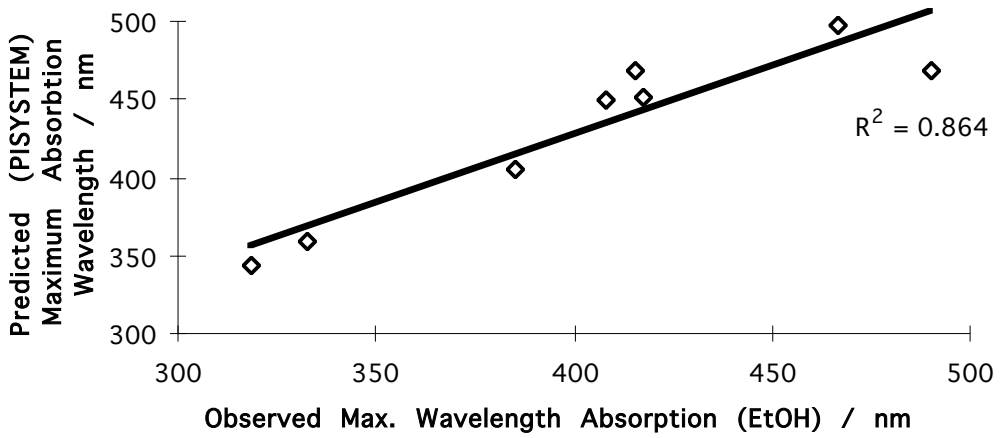

Figure 3.16 *Correlation between predicted (PISYSTEM) and experimental λ_{max} values for azo dyes series **73a-h**.*

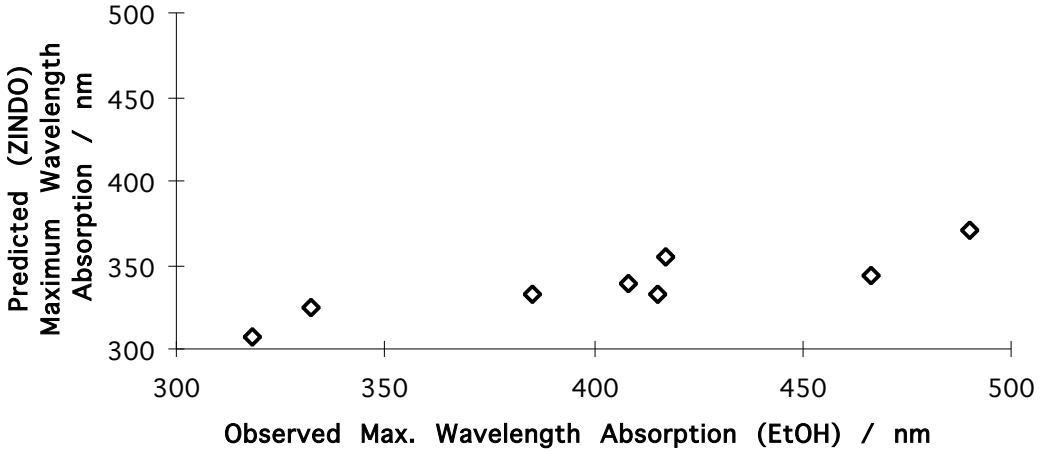

Figure 3.17 *Correlation between the predicted (ZINDO) and experimental maximum wavelength absorption for the series of azo dyes **73a-h**.*

In the case of the present azo dyes, predictions using the INDO/S method were unacceptably hypsochromic and generally less reliable than those from the PPP method (PISYSTEM). On the other hand, previous work has shown that the INDO/S method gave excellent predictions for the λ_{max} of polyene dyes (r^2=0.998) and cyanine dyes (r^2=0.996) [205]. The present results

are in general agreement with the work of Adachi and Nakamura [clvii] who found the INDO and CNDO methods less useful for predicting color than PPP based methods. The amenability of PPP to the prediction of absorption spectra may be due to extensive parameterization and high specialization of this method compared to the multi-purpose ZINDO package.

The spectroscopy of **25** has been studied in detail by Weichman *et al*. [lxxxviii], who reported absorptions in the UV region at 345nm and 300nm, and a fluorescence emission at 640nm, occurring with low quantum yield. The large Stoke's shift of 300nm has been ascribed to rapid proton transfer in the excited state (Figure 1.19). CAChe and PISYSTEM were used in an attempt to predict the Stoke's shift due to intramolecular proton transfer. Compounds **25** and **27** were submitted for calculation using PISYSTEM. Compound **25** was optimized using PM3. Several attempts to optimize the first excited state of **27** using various open shell configurations and other settings failed. Eventually, the ground state optimized structure **25** was carefully modified using CAChe Editor to generate the proton-transferred form **27** using standard N-H bond lengths, without disturbing the remainder of the structure. The structures were entered for ZINDO CI (level 14). Table 14 shows the results of these calculations. Clearly, both modeling systems predict a large Stokes shift arising from proton transfer.

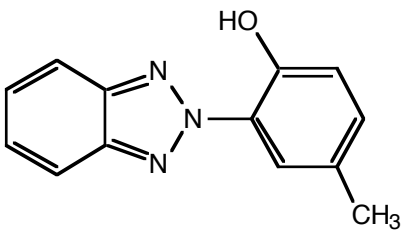

25

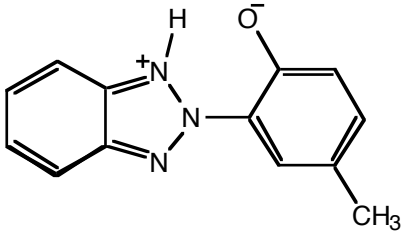

27

Table 14 *Results of attempts to predict the absorption and emission band of **25** and **27** using PISYSTEM and ZINDO.*

25			**27**		
Expt.	PISYSTEM	ZINDO	Expt.	PISYSTEM	ZINDO

[lxxxviii]			[lxxxviii]		
λ (nm)	λ (nm)	λ (nm)	λ (nm)	λ (nm)	λ (nm)
345	338.7	340	640	518	597
300	299.9	297			

3.2.7.2 MOLAR ABSORPTIVITY

Quantum mechanical calculations can be used to assess the probability of a light absorption event occurring by estimating the transition dipole moment, **M**. The oscillator strength, f is proportional to $\mathbf{M}^2$ multiplied by the average frequency of the light being absorbed:

$$f = k\nu\,\mathbf{M}^2$$

and, this value is related to the area beneath the absorption curve:

$$f = k' \int_{\nu_1}^{\nu_2} \varepsilon \, d\nu$$

where ε is the molar absorptivity of the compound at a given frequency of light.

Spectroscopists wishing to characterize a colored substance generally record the extinction coefficient (ε_{max}) of a dye, which is the molar absorptivity at the wavelength of maximum absorption. This particular quantity is difficult to predict from the oscillator strength without knowledge of the shape of the absorption curve, and normally only λ_{max} and ε_{max} are published. The INDO/S method gives a value for the transition dipole moment for the longest wavelength allowed transition, and from this, a value proportional to the oscillator strength can be calculated using the frequency of light corresponding to the transition (also estimated using the INDO/S method). PISYSTEM gives a value for the oscillator strength directly. The calculated oscillator strengths and observed ε_{max} values were compared; the errors associated with these calculations are presented in Table 15.

Table 15 *Summary of results pertaining to the color and molar absorptivity predictions for dyes **73a**-**h**.*

	λ_{max} Prediction			ε_{max} Prediction
	r^2	Error Range	RMS Error	r^2
PISYSTEM	0.864	-4 % / +13 %	8 %	0.873
ZINDO	0.792	-25 % / -2 %	15 %	0.863

The r^2 value for predicted oscillator strength is misleading because if the point due to structure **73f** is omitted from the data analysis, the r^2 value drops from 0.863 to 0.621, suggesting that this apparent correlation is false. In the case of values predicted by the PISYSTEM, removal of data from the set tended to increase the coefficient of determination. Clearly, the PPP method was more effective at predicting the extinction coefficient than the INDO/S method.

It is possible that the PPP method surpassed the INDO/S method in predicting λ_{max} and ε_{max} values of the azo dyes studied because the atomic and bond parameters used in the former method are not generalized. Different electronic configurations and oxidation states of the same atom are assigned different parameters, which have been refined to reproduce the spectra of moderately sized dye structures. The INDO/S method, on the other hand, uses generalized atomic parameters derived from spectroscopic analysis of small molecules and/or *ab initio* calculations. Thus, while one might expect ZINDO to be applicable to a more diverse range of compounds than the PPP method, the PPP method is actually better suited for moderately sized, non-metallized azo dyes.

3.3 Molecular Descriptors for the Prediction of Lightfastness

3.3.1 pKa of α-Nitrogen in Aminoazo Dyes

Bridgeman and Peters showed that the fading rate of a series of azo dyes was inversely proportional to the pKa of the α-azo nitrogen atom [25]. The propensity of a species to give up or accept a proton can be estimated using semi-empirical methods by assessing SCF energy on both sides of isodesmic reactions. The heat of formation of a proton may be obtained from experimental thermodynamic data [ccvi]. It follows that the pKa of the azo group would be related to the energy difference between protonated and unprotonated forms. As the pKb of a given atom increases, the calculated enthalpy of protonation should become more positive.

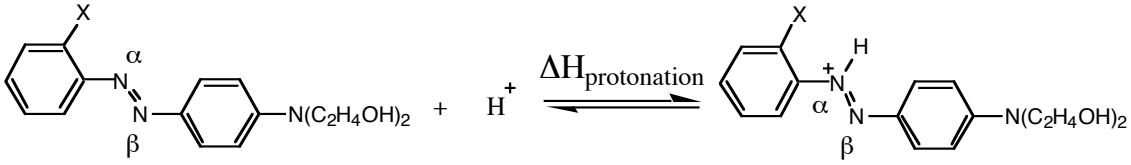

44 **74**

As the lightfastness of **44a-f** has been documented [ccvii], the dyes in this series offered themselves as useful candidates with which to test the potential of the calculated enthalpy of protonation as a molecular descriptor for predicting the lightfastness of azo dyes.

Structures **44a-f** were optimized using MOPAC AM1, following required manual adjustments and mechanical optimizations to obtain viable starting structures. The structures were then submitted to MOPAC for a PM3 SCF energy calculation. Each structure was then reopened in CAChe Editor, and a proton was added to the α-azo nitrogen atom by selecting only this atom, giving it a formal charge of +1, and then "beautifying" this atom only. In this way, a proton was added to the correct azo nitrogen using standard N-H bond lengths and angles without disturbing the rest of the molecule. The protonated

molecule was then submitted for a PM3 SCF energy calculation in MOPAC. Table 16 shows the results of these calculations, and the experimental lightfastness values. Entropy was neglected in these calculations. The enthalpy of formation for a proton was taken to be 365.6897 kcal.mol^{-1} (calculated from the enthalpy of atomization of H_2 plus the first ionization energy of hydrogen, both from [ccvi]).

Table 16 *Calculated (PM3) enthalpy of protonation for azo dyes **44a-f** compared to the experimental lightfastness.*

Substituent X	PM3 Energy -N=N- (kcal.mol^{-1})	Exptl. ΔHf H^+ (kcal.mol^{-1})	PM3 Energy -NH=N- $^+$ (kcal.mol^{-1})	PM3 ΔE protonation (kcal.mol^{-1})	Exptl LF [ccvii]
a NO_2	1.4	365.690	175.2	-191.9	1.0
b CH_3	0.1	365.690	163.1	-203.1	2.5
c OCH_3	-26.6	365.690	132.7	-206.4	2.0
d H	7.8	365.690	170.9	-202.5	3.5
e CN	44.4	365.690	211.2	-199.0	3.0
f Br	17.8	365.690	180.8	-202.8	3.0

If the calculated enthalpy of protonation of the dyes were a useful indicator of lightfastness, plotting the calculated enthalpy of protonation vs. lightfastness should give us a line with positive slope. Figure 3.18 shows such a plot of these data. Certainly, the outlying point due to the *ortho*-nitro derivative suggests that protonation dye is not a first step to degradation for this dye. While the data set is too small to draw firm conclusions, it is not clear that the calculated enthalpy of protonation of the α-azo nitrogen atom is a molecular descriptor that can be used to anticipate good or poor lightfastness.

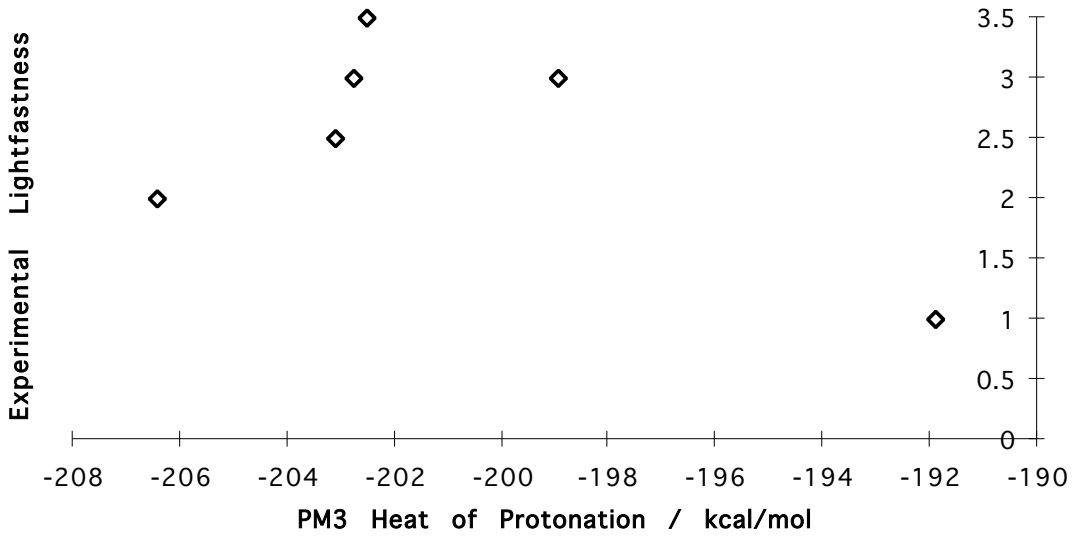

Figure 3.18 *Graph showing the relationship between the calculated enthalpy of protonation of a series of related azo dyes and experimental lightfastness.*

3.3.2 Electron Affinity of Protonated and Unprotonated Azo Dyes

Photodegradation in PET often proceeds via a photoreduction process. Such photoreduction can proceed from one electron transfer processes. PET absorbs UV radiation in the range 280-320 nm [ccviii] and if the LUMO energy of the dye approaches the energy of the photoexcited polymer, it is possible for a one electron transfer process to generate a free radical (Figure 3.19). If the dye happened to be protonated at the time, then electron acceptance from photoexcited polymer could form the hydrazine neutral radical **75**.

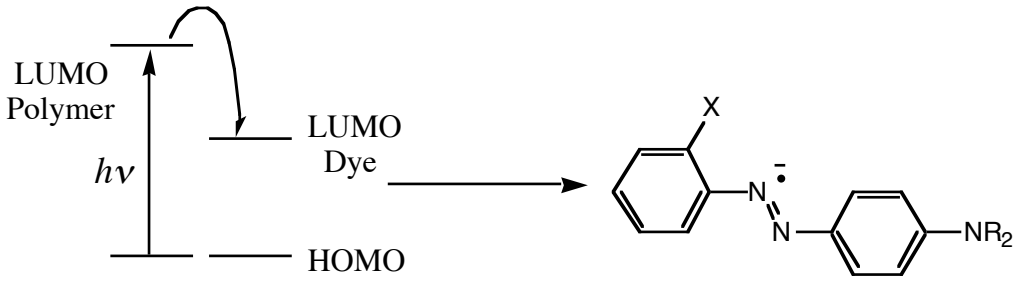

Figure 3.19 *Photoreduction of azo dyes: first step by one-electron transfer process from photoexcited polymer to form a radical anion.*

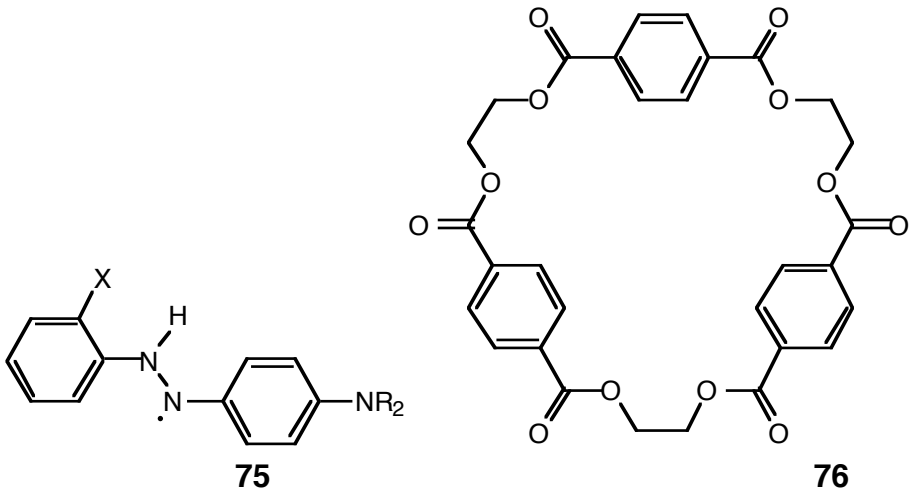

75 **76**

MOPAC is limited in the number of atoms that may be included in calculations. As PET is a high molecular weight polymer, a suitable model compound was sought that could be used to estimate the frontier orbitals of the polymer. As PET contains repeating ester units the cyclic trimer **76** was selected. The LUMO energy of PET was estimated by optimizing structure **76** using PM3. The starting structure for the PM3 optimization was the lowest energy conformer that arose from two 1 picosecond dynamics simulations. One simulation was run at 1500K, and the second at 2500K. The LUMO energy obtained after optimization was -1.361eV (PM3). This value was compared with the LUMO values for previously optimized structures of **44a-f** and their protonated forms. The calculated LUMO energy for the unprotonated dyes ranged from between -1.261 eV to -0.637 eV. The calculation of polymer LUMO was likely to be in error, as the LUMO energy of the polymer was

expected to be higher than that for the dye. It is possible that the high symmetry of **76** gave rise to a set of degenerate unoccupied orbitals, which stabilized the LUMO energy compared to PET. In the case of the protonated dye, the LUMO energy values ranged from -6.095 eV to -5.641eV. The LUMO energy has physical significance, as it corresponds to the negative of the electron affinity for the dye. Figure 3.20 shows the relationship between the calculated electron affinity and experimental lightfastness for dyes **44a-f**, while Figure 3.21 is a plot of lightfastness vs. calculated electron affinity of protonated **44a-f**.

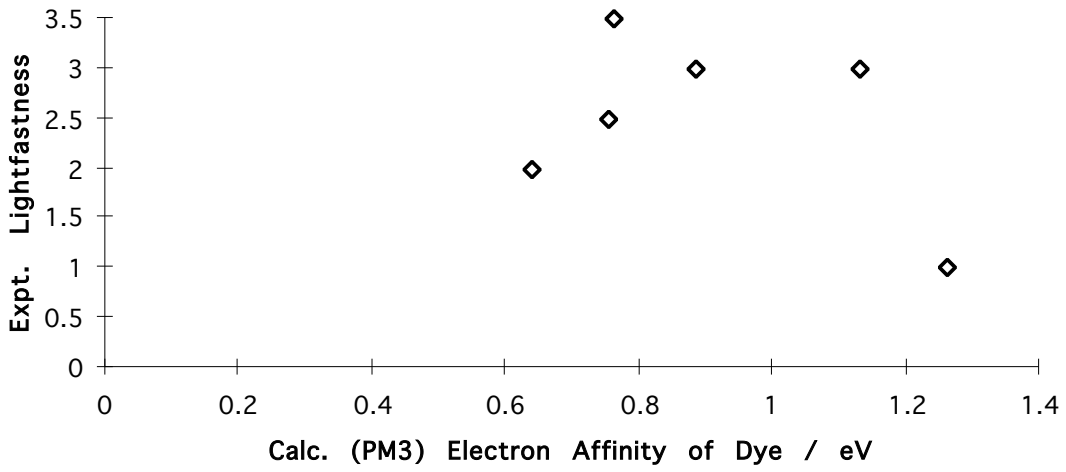

Figure 3.20 *PM3-calculated electron affinity (-ve of LUMO Energy) of azo dyes **44a-**f.*

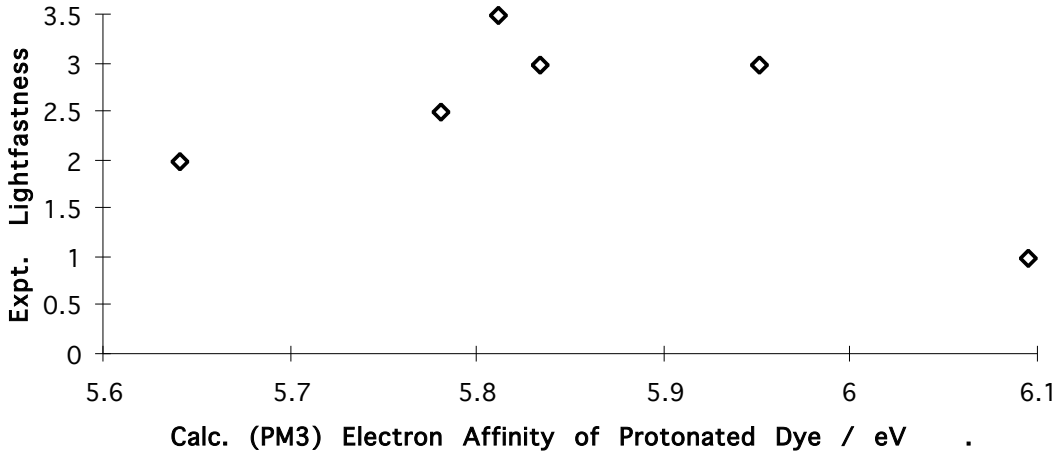

Figure 3.21 *PM3-calculated electron affinity of azo dyes **74a-f** protonated on the α-azo nitrogen atom.*

Probably because of the small number of compounds in the study group, the relationship between electron affinity and lightfastness is not clear for these dyes. Given reductive fading, and that electron affinity in this case is defined as the difference in energy between the neutral species and ion, one might expect that as the electron affinity increased, lightfastness would decrease. It is difficult to say from this small group whether calculated electron affinity is a good molecular descriptor indicative of lightfastness.

3.3.3 STUDIES INVOLVING BICHROMOPHORIC NITRO-DIPHENYLAMINES CONTAINING HYDROXYBENZOPHENONE OR HYDROXYBENZOTRIAZOLE MOIETIES

A range of CI Disperse Yellow 42 and Disperse Yellow 86 analogs containing hydroxybenzotriazole (**77**-**83**) or hydroxybenzophenone (**84**-**94**) UV absorbing moieties have been synthesized [xcviii]. Since the lightfastness of these compounds has been determined, they appeared to be represent a suitable group on which to test candidate molecular descriptors that could

indicate the lightfastness of hypothetical structures. (For clarity, previously mentioned structures in this group have been renumbered).

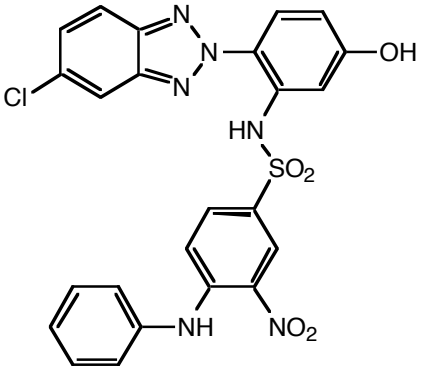

77

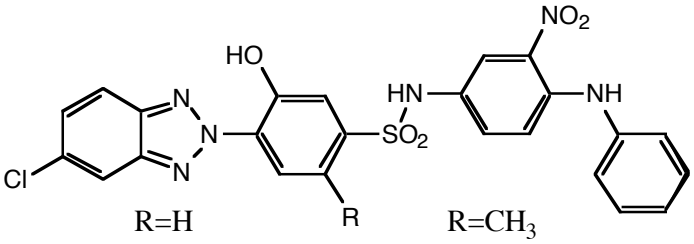

R=H R=CH_3

78 **79**

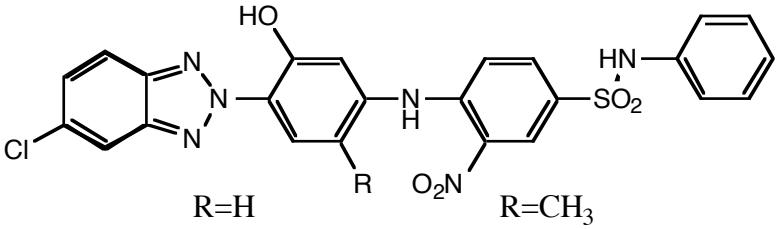

R=H R=CH_3

80 **81**

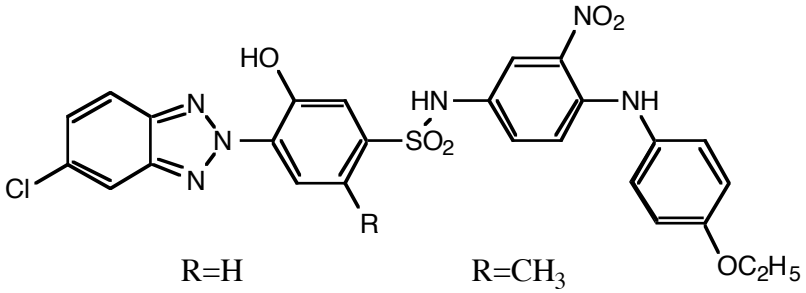

R=H R=CH_3

82 **83**

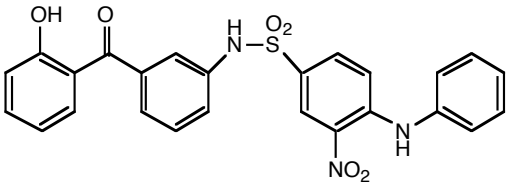

84

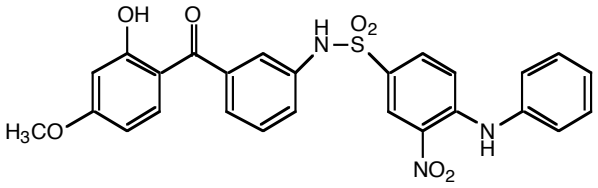

85

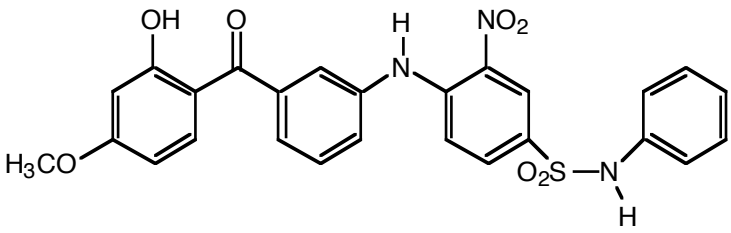

86

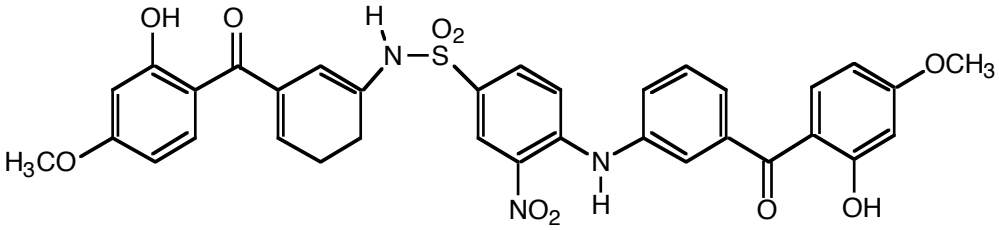

87

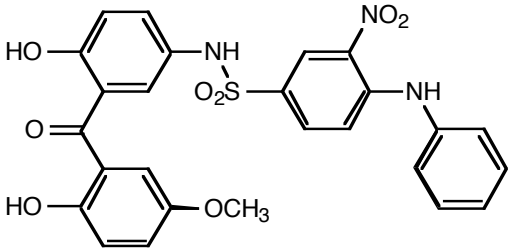

88

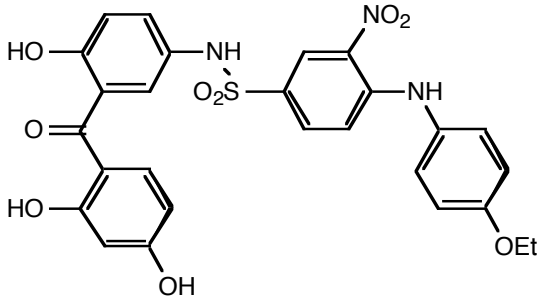

89

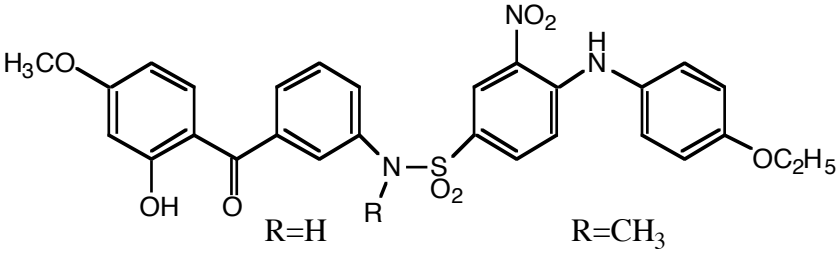

R=H R=CH_3

90 **91**

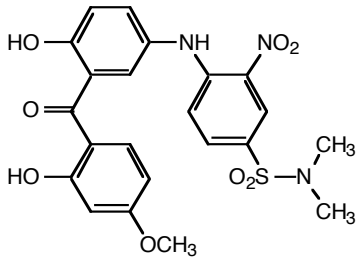

92

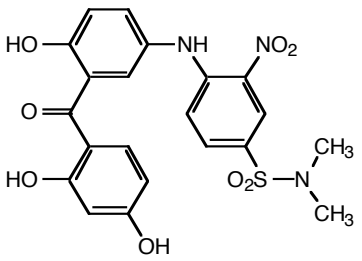

93

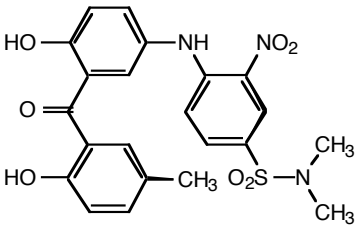

94

3.3.3.1 CONFORMATIONAL ANALYSIS

It is conceivable that certain MO based properties associated with these dyes depend upon the relative orientation of the two chromophores. In an attempt to accommodate the conformational freedom of these dyes, conformational analysis of **77**-**94** was carried out. Clear differences were observed in the strain energy maps for certain closely related dyes, for instance **82** and **83**. Four minima of approximately equal energy are accessible in the case of **82** (**a**, **b**, **c**, and **d**, Figure 3.22) whereas, the energy of two of the minima of **83** (**c** and **d**, Figure 3.23) are increased relative to those of **82**, and are hence less thermally accessible. The minima from the strain maps were optimized using PM3 before the Boltzmann equation was applied to determine the relative population of each minima.

Table 17 shows example calculations of normalized conformation populations for **82** and **83**. Note that the changes in conformational energy cause dramatic redistributions of microstate occupancies. Molecules of **82** are predicted to be distributed fairly evenly between two microstates (**c** and **d**), whereas those of **83** are predicted to be concentrated into one (**a**).

Table 17 *Example calculation of conformer populations using Boltzmann's distribution.*

Conformer ID	PM3 Energy J mol^{-1}	-(E_i-E_j) J mol^{-1}	Mole Fract. N_i/N_j	Normalized N_i/N_j
82 a	55853.346	-3730.287	0.22204736	0.10542128
82 b	60038.810	-7915.751	0.04103394	0.01948165
82 c	52123.059	0	1	0.47476932
82 d	52545.810	-422.75136	0.84320475	0.40032775
		Sum:	*2.10628605*	*1.000*
83 a	20933.556	0	1	0.98910575
83 b	34000.146	-13066.59	0.00513695	0.00508098
83 c	50319.671	-29386.115	0.00000710	0.00000703

83 d	33669.4011	-12735.845	0.00587019	0.00580624
		Sum:	*1.01101424*	*1.000*

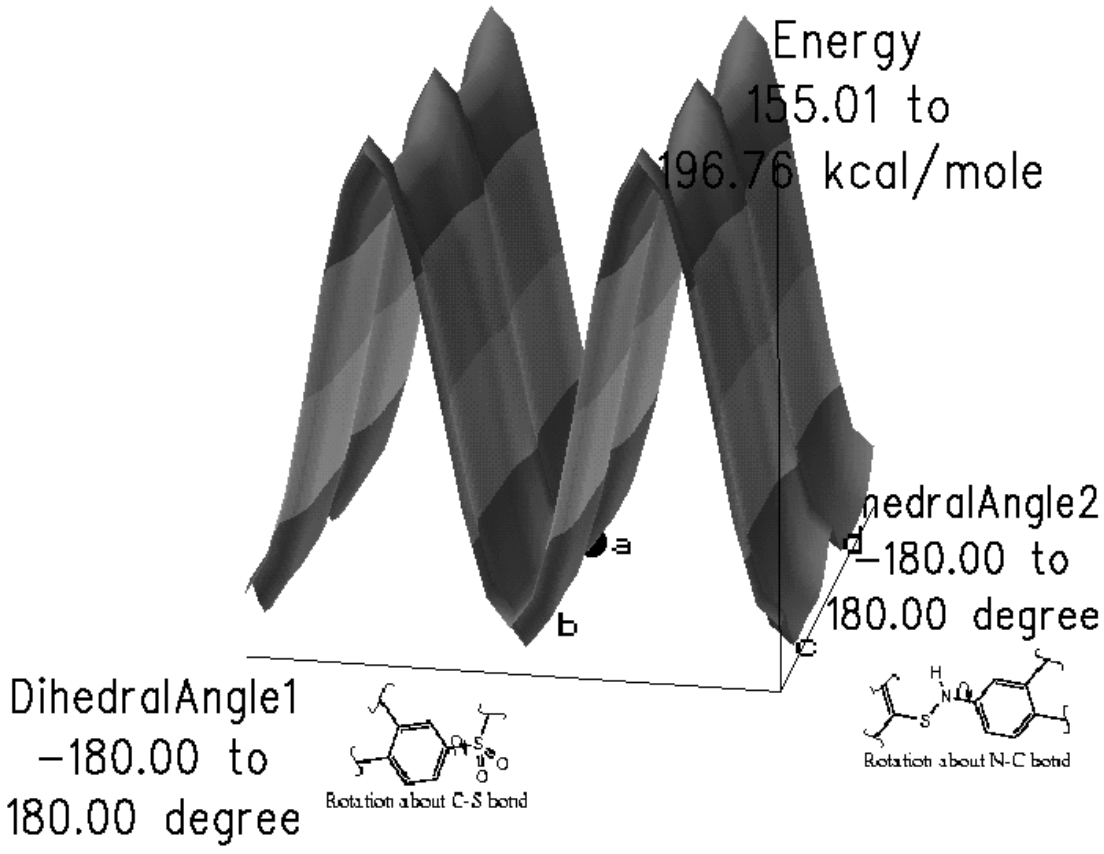

Figure 3.22 *Conformation search map showing strain energy changes associated with rotation of phenyl groups about the bonds indicated in structure **82**. The four minima found are denoted **a**, **b**, **c**, and **d**.*

Clearly, the conformation energy is lowered significantly after optimization using MOPAC PM3, highlighting the importance of a) interpreting conformation search maps, with caution and b) considering the calculation limitations. The observed relaxation of the minima found using the MM2 search during semi-empirical optimization also indicates that these diagrams are not true reaction coordinate diagrams. Although optimized MM2 searches were attempted, these tended to generate minima containing very long hydrogen bonds and non-planar chromophores. PM3 rigid searches were also attempted;

however these calculations required approximately eight hours per structure to obtain results similar to those obtained from the MM2 search, which took only ten minutes per structure.

Table 18 contains a summary of the normalized populations for each of the dyes **77**-**94**. These figures are basic data needed for further analyses of molecular properties.

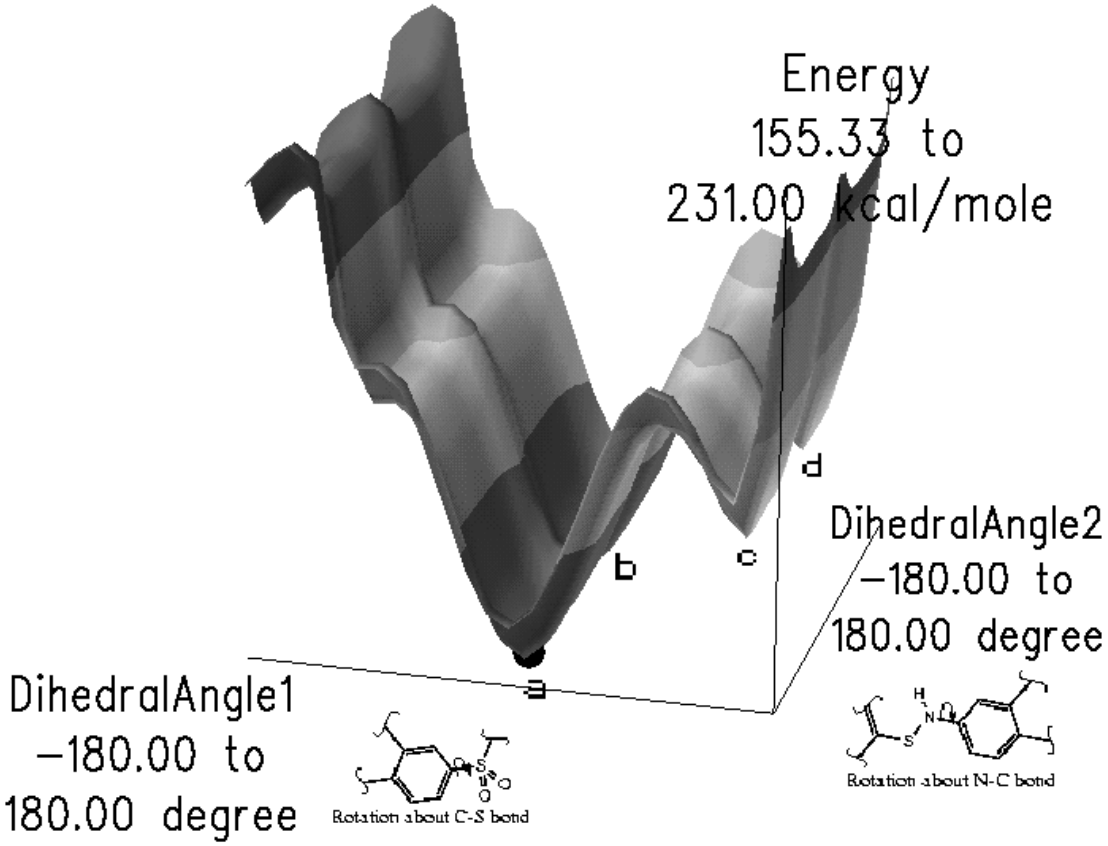

Figure 3.23 *Conformational search map showing MM2 strain energy changes associated with rotation of phenyl groups about bonds indicated in structure **83**. Four minima were found: **a**, **b**, **c**, and **d**. The presence of the methyl group increases the energy of minima **c** and **d** relative to **82**.*

Table 18 *PM3-calculated normalized microstate populations for **77-94**.*

	77	**78**	**79**	**80**	**81**	**82**
a	0.8388773	0.1419285	0.9047359	0.0742605	0.2101162	0.1054213
b	0.0071626	0.3941464	0.0950992	0.1490115	0.7898839	0.0194817
c	0.1444041	0.4216196	0.0001596	0.3806725	-	0.4747693
d	0.0095560	0.0423055	0.0000053	0.3960555	-	0.4003278
	83	**84**	**85**	**86**	**87**	**88**
a	0.9891058	0.1760196	0.3157357	0.1088928	0.0571954	0.6900800
b	0.0050810	0.2359100	0.5576479	0.5819874	0.8261137	0.1031549
c	0.0000070	0.4058997	0.0827977	0.1436212	0.0781582	0.1229494
d	0.0058062	0.1823707	0.0438188	0.1654986	0.0385326	0.0838157
	89	**90**	**91**	**92**	**93**	**94**
a	0.0934022	0.1800999	0.0326864	0.0179278	0.1332934	0.1188172
b	0.8610838	0.6539740	0.4834023	0.9075247	0.4235893	0.7517930
c	0.0383097	0.0553496	0.4480451	0.0455933	0.0622594	0.0853497
d	0.0072043	0.1105766	0.0358662	0.0289542	0.3808580	0.0440401

3.3.3.2 Electron Affinity of Bichromophoric Dyes

The electron affinity is defined in this case as the difference in energy between the neutral and monoanionic species. Thus as electron affinity increases (becomes more positive), it becomes more thermodynamically favorable for the molecule to accept an electron to form an anion. If photoreduction is initiated by a one-electron transfer process, as the electron affinity of the dye increases, the photostability should decrease, as it becomes easier for the dye to accept an electron.

AM1 was used to calculate the electron affinity of PM3-optimized conformers of dyes **77**-**94**. The AM1 method was used as it is reportedly superior to PM3 for predicting orbital energies. The calculated electron affinity value for each conformer was weighted by multiplying by the normalized population (Table 18) and then totaled for each dye.

The population weighted average electron affinity is plotted against experimental lightfastness in Figure 3.24. Figure 3.25 shows the highest electron affinity value calculated for single conformers of each dye. If electron affinity were a good indicator of dye lightfastness, one would expect a correlation with a negative slope. Although there appears to be a negative trend, the scatter of the points is appreciable, and obfuscates the general trend. Electron affinity values calculated by this method do not appear to be good indicators of lightfastness.

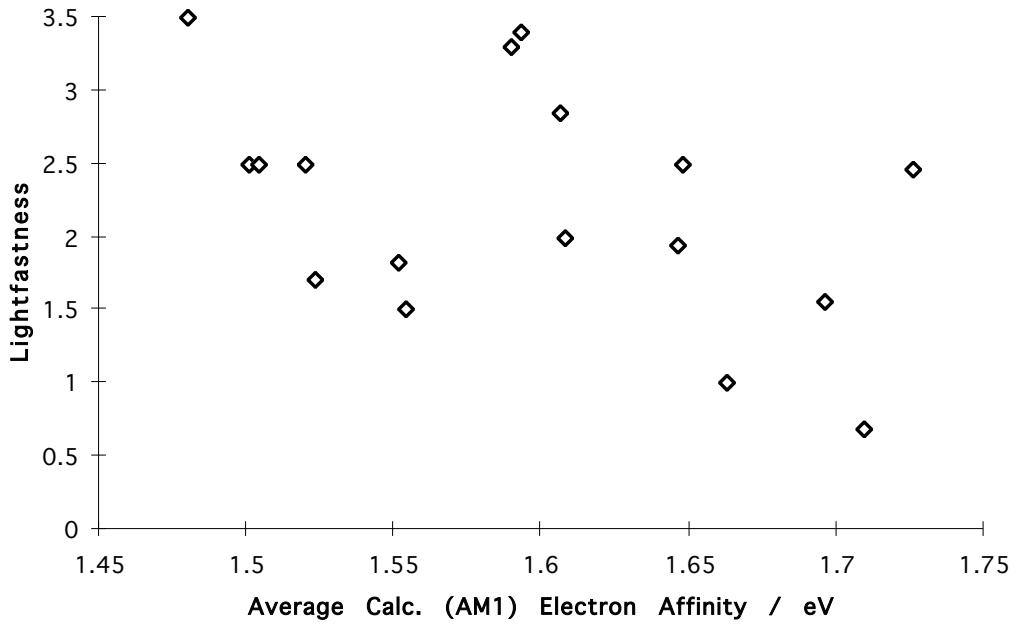

Figure 3.24 *Weighted average calculated (AM1) electron affinity of dyes **77-94** vs. experimental lightfastness.*

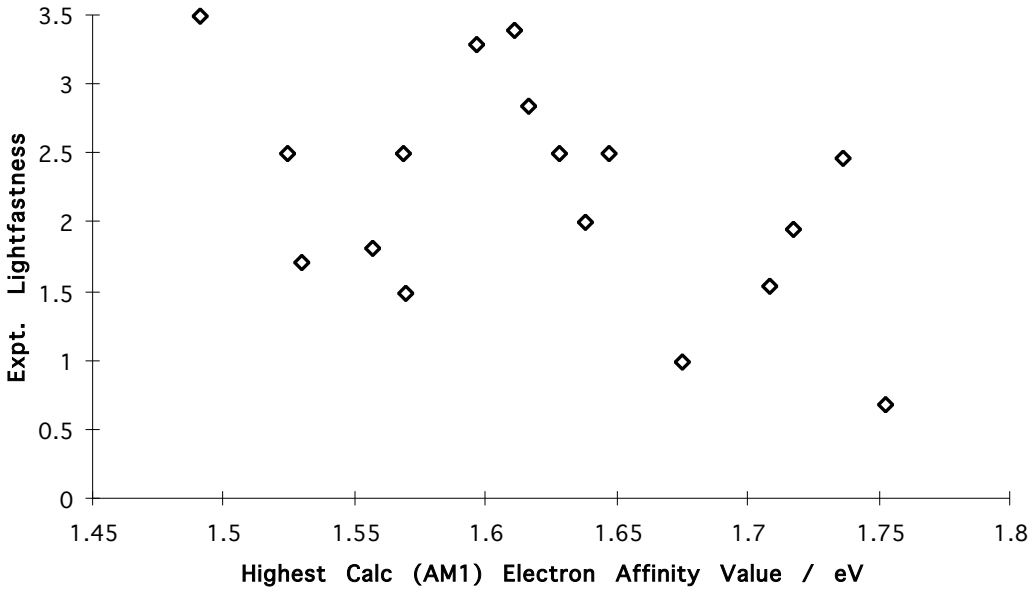

Figure 3.25 *Highest conformation value for calculated (AM1) electron affinity vs. lightfastness for dyes **77-94**.*

3.3.4 MODELING OF EXCITATION ENERGY TRANSFER

A theoretical model of energy transfer described in the Experimental section was used to assess the possibility of excitation energy flow between chromophores in bichromophoric dyes. The model assumes that excitation energy may be conducted from one chromophore to another via the tails of the MOs involved in light absorption found on atoms linking the two chromophores (Figure 3.26). The CI calculation level was chosen such that further increases in CI level did not significantly affect the energy or position of the predicted electronic transitions of interest. As shown in Table 19, ZINDO CI levels above 14 did not significantly alter the position nor energies of the excited states of interest for bichromophoric dyes containing hydroxybenzotriazoles (**77-83**). A similar set of calculations showed that CI level 15 was required to achieve stability of predicted spectra in dyes containing hydroxybenzophenone stabilizers (**84-94**).

Table 19 *Selection of CI level for ZINDO calculations of bichromophoric dyes containing a hydroxybenzotriazole moiety, using dye **83** as an example.*

		Changes if CI level is increased by 1	
CI Level	Calculation Time	State Energy	State re-ordering.
11	27 mins	Yes	No
12	26 mins	Yes	No
13	26 mins	Yes	Yes
14	1 hr 24 min	No	No
15	2 hr 43 min	No	No
16	4 hr 12 min	(CI 17 not tested)	(CI 17 not tested)

The unoccupied orbitals involved in UV and visible light absorption were identified and the MO eigenvectors of these orbitals on the linking atoms were obtained, as illustrated in Figure 3.26. It was assumed that energy would be transferred more easily if unoccupied orbital eigenvectors associated with UV and visible light absorption had large eigenvectors on atoms connecting the two chromophores. Table 20 shows representative data collected for conformer **a** of dye **82**. A representative calculation is shown in Table 21. The predicted excitation energy transfer rate values are reported along with experimental lightfastness data in Table 22. The logarithm of the modeled energy transfer estimation is plotted against lightfastness for each dye in Figure 3.27. If the energy transfer rate estimated by this method was a good indicator of lightfastness of dyes **77-94**, we should see a negative slope. The graph in Figure 3.27 shows considerable scatter, suggesting that this estimation of excitation energy transfer is not useful for predicting lightfastness.

Table 20 *Example of MO, geometric, and Boltzmann distribution data collected for each conformer of each dye structure for the estimation of excitation energy transfer.*

82 a	Eigenvectors		Eigenvector	Normalized	
Atom	LUMO	LUMO+1	Products	Boltzmann	Pop. of
1	-0.023004	-0.005740	1.320 E -4	conf. a =	**0.105421**
2	-0.001861	-0.003063	5.700 E -6		
3	0.013030	0.003720	4.850 E -5	R =	**3.988 Å**
4	-0.004896	-0.000553	2.707 E -6		
5	-0.015794	-0.007353	1.161 E -4	No. Atoms =	**7**
6	0.033222	0.070339	2.337 E -3		
7	-0.023004	-0.005740	1.320 E -4	**MO Overlap**	
		SUM:	**0.0022678**	**Per Atom =**	**0.000383**

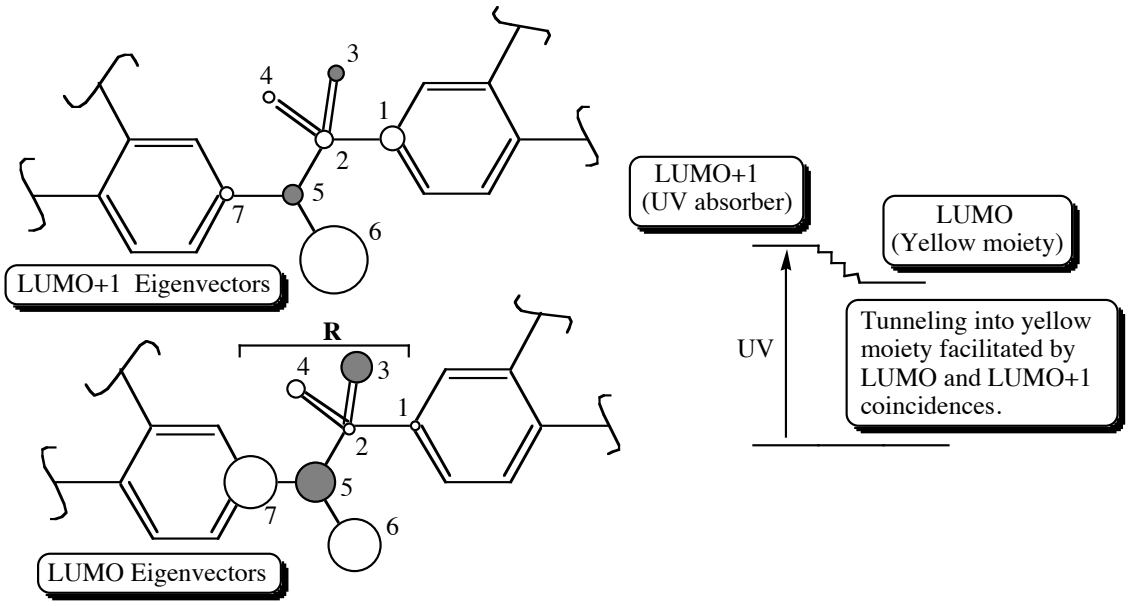

Figure 3.26 *Illustration of the data collected for estimating excitation energy transfer.*

Table 21 *Example calculation from an attempted estimation of excitation energy transfer rates in dye **82**.*

	Normalized. Population	Av. MO Overlap	**R** / Å	Av. MO Amplitudes	$e^{[-2R/50L]}$	Estimated Rate
82 a	0.10542	0.000383	3.998	0.002948	3.16 E -24	9.81 E -28
82 b	0.01948	-0.000076	4.037	0.000324	7.1 E -217	4.5 E -222
82 c	0.40033	-0.000332	4.012	0.009803	7.77 E -8	3.05 E -10
82 d	0.47477	0.0000111	4.057	0.006276	5.88 E -12	1.75 E -14
					SUM:	**3.05 E -10**

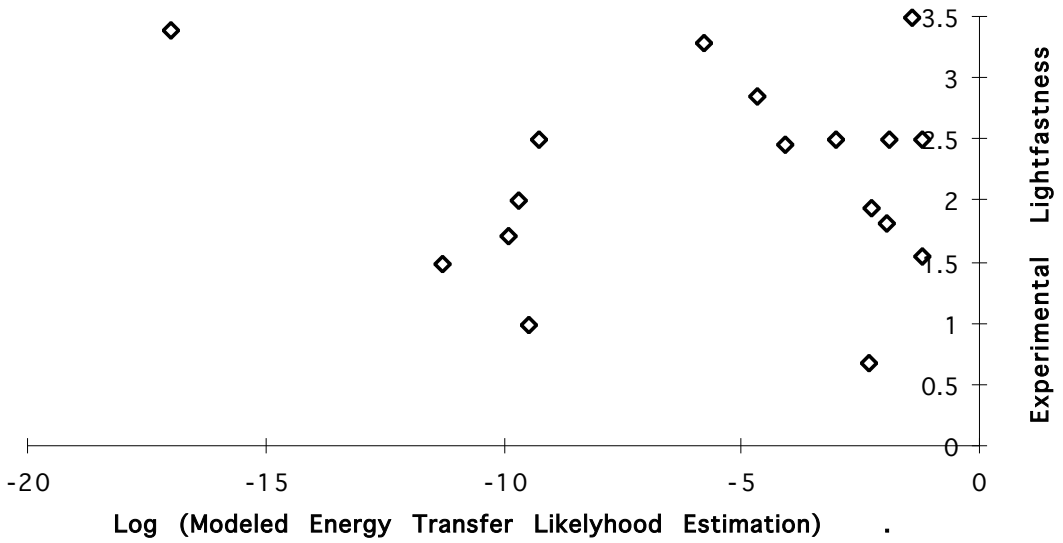

Figure 3.27 *Graph showing the relationship between the estimated energy transfer rate and experimental lightfastness of bichromophoric dyes **77-94**.*

There are a number of possible reasons why this molecular descriptor did not prove useful for predicting lightfastness. First, it was assumed that the lightfastness of dyes **77**-**94** was directly related to the rate of excitation energy transfer from the UV stabilizer moiety to the nitrodiphenylamine chromogen. No experimental energy transfer data were available for these compounds, and so the energy transfer model could not be tested. Secondly, the MOs used in the estimation were obtained using the INDO/S method, which has been shown to be a poor tool for calculating electronic spectra. A third reason pertains to the model itself, as there is no proof that excitation energy transfer is a factor which contributes towards the photostability of dyes **77-94**.

A possibility for future work would involve obtaining experimental excitation energy transfer data for a series of compounds and testing the transfer model developed in this thesis. If available, a more rigorous level of theory should be used to test the excitation energy transfer model.

Table 22 *Predicted (INDO/2) excitation energy transfer rate and experimental lightfastness (1-5) data for **77-94**.*

Structure	Calc. Log EET Rate	Experimental Lightfastness	Structure	Calc. Log EET Rate	Experimental Lightfastness
77	-4.69	2.85	**86**	-2.00	1.82
78	-4.10	2.47	**87**	-1.72	(not tested)
79	-2.27	1.95	**88**	-9.90	1.71
80	-2.37	0.69	**89**	-3.02	2.5
81	-1.25	1.55	**90**	-11.30	1.5
82	-9.52	1	**91**	-9.69	2
83	-9.26	2.5	**92**	-1.20	2.5
84	-17.02	3.4	**93**	-1.91	2.5
85	-5.83	3.3	**94**	-1.42	3.5

3.3.5 Design of Hydroxybenzotriazole-containing Bichromophoric Dyes with Enhanced Internal Conversion

3.3.5.1 Hydrogen Bond Lengths

Reducing the distance that the proton must travel during ESIPT should increase the speed of internal conversion, thus making other photochemical reactions less competitive. Compounds **95a-l** were optimized using AM1 and PM3. The AM1 method tended to return non-planar structures, which had very long hydrogen bonds. This is not a new result, as Enchev encountered the same problem when attempting to optimize the structure of a hydroxybenzotriazole [xciii]. The PM3 method returned planar structures, consistent with x-ray data, as previously discussed (Section 3.2.4). The results of the optimizations are given in Table 23. (For clarity, previously mentioned structures have been renumbered.)

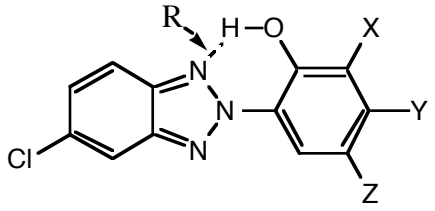

95

Table 23 *Predicted effects of substituents on hydrogen bond distance in **95**.*

	X	Y	Z	Dist. R / Å
95 a	H	H	H	1.840
95 b	H	H	Me	1.841
95 c	iPr	H	H	1.825
95 d	tBu	H	H	1.817
95 e	tBu	H	Me	1.817
95 f	H	H	SO_2NH_2	1.836
95 g	SO_2NH_2	H	H	1.818
95 h	iPr	H	SO_2NH_2	1.819
95 i	H	NH_2	H	1.839
95 j	H	H	$NHSO_2Me$	1.841
95 k	H	$NHSO_2Me$	H	1.835
95 l	iPr	H	$NHSO_2Me$	1.828

Clearly, increasing the bulk of substituent X, decreases the hydrogen bonding distance, as can be seen in the progression **95 a** - **c** - **d**. This appears to be predominantly a steric effect, as substitution of groups *meta* and *para* to the phenolic group has a minor effect on the hydrogen bond length (cf. **95 f**, **j** and **k**). Interestingly, the presence of a sulfonamide group *ortho* to the phenolic group has a large effect on hydrogen bond length, comparable to that of an *tert*-butyl group (cf. **95 d**, **e**, and **g**).

3.3.5.2 Prediction of Excited State Proton Lability

Increasing the excited state lability of hydroxybenzotriazole phenolic protons may also improve the efficiency of ESIPT. The enthalpy of

deprotonation of the phenol group in the first excited state was assessed for a series of structures, using the following techniques. Structures **95 a-l** were optimized using MOPAC PM3. PM3 excited state (OPEN(2,2)) SCF energy calculations using the COSMO screening model were used to calculate the heat of formation of **95 a-l** in an ester environment. The dielectric constant (relative permittivity) used to model the ester environment was that of ethyl acetate, taken as 6.0814 [ccvi]. Structures **95 a-l** were then carefully edited to remove the phenolic proton, leaving the molecule with a negative charge. The excited state PM3 SCF energy calculations were repeated on the phenolate ions, using the COSMO method to simulate the effect of an ester environment. The SCF energy of a proton in ethyl acetate was calculated to equal 234.3 kcal.mol.$^{-1}$ using PM3 COSMO. Without COSMO, PM3 SCF calculations returned the heat of formation for a naked proton as 353.6 kcal.mol.$^{-1}$, which compared favorably with the experimental value of 365.6897 kcal.mol.$^{-1}$ [ccvi].

The energy required to remove the solvated proton from the solvated, photoexcited hydroxybenzotriazoles **95a-l** to infinity was then calculated by considering an isodesmic reaction (Figure 3.28). The entropic contribution was neglected in these calculations of deprotonation energy. Therefore, the enthalpy associated with the removal of the phenolic proton in the first excited state must equal:

$$\Delta H_{deprotonation}\,(\text{Phenol}) = \Delta H_f\,(\text{Phenolate}) + \Delta H_f\,(\text{Proton}) - \Delta H_f\,(\text{Phenol})$$

Calculation results for the excited state deprotonation enthalpies of **95 a-l** in an ester environment, using PM3 COSMO SCF calculations in MOPAC, are given in Table 24. The positive enthalpy change in each case suggests that removal of the phenolic proton to infinity is endothermic (assuming that the entropic contribution is negligible). However, it appears that hydroxybenzotriazoles containing electron-withdrawing groups *ortho* or *para* to the phenolic group

contain protons that are more labile than structures containing electron donating groups. Also, from these results, it appears that the increase in

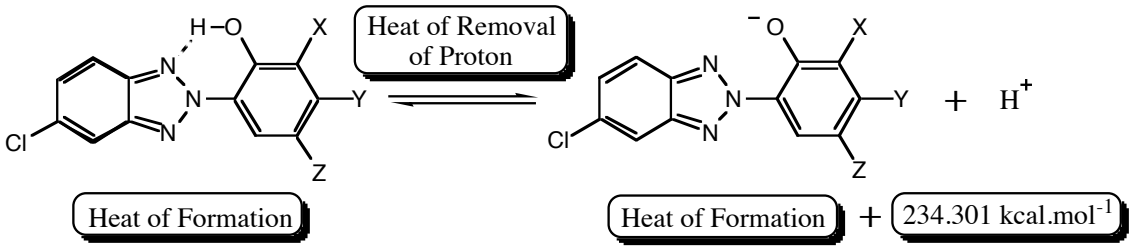

Figure 3.28 *Isodesmic reaction employed to calculate the energy required to remove a proton from hydroxybenzotriazole derivatives to infinity, modeled in a continuous dielectric medium of relative permittivity 6.0814.*

Table 24 *Enthalpy of deprotonation of **95 a-l** in the first excited state. COSMO PM3 SCF results reflect the energy values for structures solvated in an ester environment with a relative permittivity of 6.0814. Heat of formation of the proton in this environment was 234.3 kcal.mol^{-1}.*

Structure	ΔH_f (Phenol) (kcal.mol^{-1})	ΔH_f (Phenolate) (kcal.mol^{-1})	$\Delta H_{deprotonation}$ (kcal.mol^{-1})
95 a	152.3	62.8	+144.9
95 b	142.2	53.0	+145.1
95 c	136.8	47.4	+144.9
95 d	136.0	47.3	+145.6
95 e	125.9	37.5	+145.9
95 f	74.5	-19.0	+140.8
95 g	75.6	-19.8	+138.9
95 h	54.8	-38.1	+141.4
95 i	142.9	56.9	+148.4
95 j	58.9	-31.8	+143.6
95 k	56.2	-31.0	+147.1
95 l	43.7	-47.0	+143.6

lability of the proton is purely an electronic effect. Placement of a sulfonamide group *ortho* to the phenolic group (**95 g**) causes a significant decrease in the

enthalpy of excited state deprotonation, whereas incorporation of an isopropyl group in the same position (**95 c**) caused an increase in the enthalpy of deprotonation due to the ring activating character of this group. Interestingly, incorporation of a mesylamide group *meta* to the phenolic group (**95 j**) had a small effect on the enthalpy of deprotonation, suggesting that conjugation is an important factor.

If we assume that increasing the lability of the phenolic proton in the first excited state will lead to more facile ESIPT, these results suggest that placing electron-withdrawing groups *ortho* and *para* to phenolic group will increase ESIPT efficiency. Considering the results given in Table 23, it is possible to suggest certain features to incorporate into hydroxybenzotriazole-based bichromophoric dyes to enhance internal conversion. For improved internal conversion, the hydroxybenzotriazole moiety should contain a bulky, preferably electron-withdrawing group, *ortho* to the phenolic group, or an electron-withdrawing group *para* to the phenolic group. Two examples of hypothetical structures which incorporate these features are **96** and **97**.

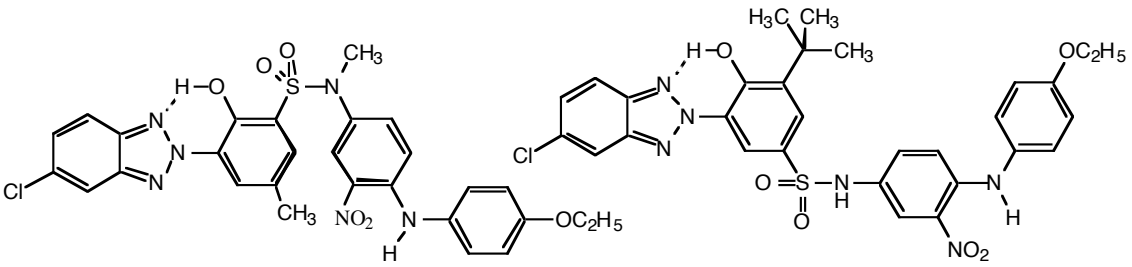

96 **97**

Hypothetical dye **96** contains an electron withdrawing group *ortho* to the phenolic group, which happens to be bulky. The bulk of this group is expected to i) reduce the OH…triazole-nitrogen hydrogen bonding distance, and ii) interfere with incoming electrophiles that might otherwise hydrogen bond with the OH group. The electron-withdrawing character of the sulfonamide group is expected to increase the lability of the phenolic proton in the first excited state. The presence of the methyl group *para* to the OH group is necessary in order to block this position during synthesis, for instance, during azo coupling with 4-

chloro-2-nitrophenyldiazonium sulfate. It is also anticipated that the presence of the methyl group will prevent the two chromophores from lying in the same plane, and hence impede chromophore interactions.

PM3 optimizations (without COSMO) suggested that hydrogen bonding between the sulfonamide linkage and the phenolic group was possible (**98b**), though energetically unfavorable (cf. **98a** and **98b**). A possible method of preventing hydrogen bonding between the sulfonamide N-H and the hydroxybenzotriazole-OH is to methylate the sulfonamide nitrogen, as in **96**. However, even after methylation of this group, PM3 calculations suggested that hydrogen bonding to the sulfonamide oxygens would be likely. Structures **96a** and **96b** show two low-energy conformers of **96**. The lowest energy conformer found (**96b**) contains a broken hydroxybenzotriazole hydrogen bond, which would have a deleterious effect on internal conversion. Despite this, it would still be interesting to synthesize this structure, as conformer **96b** might not be as energetically favorable in a polyester fiber environment.

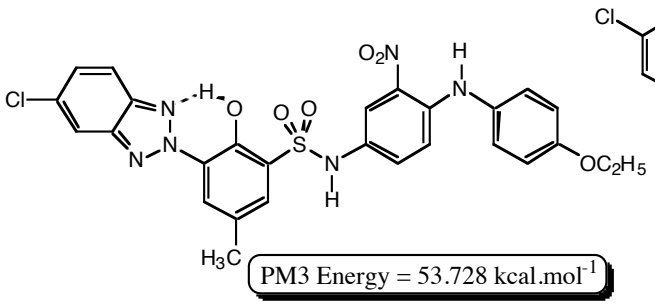

98a

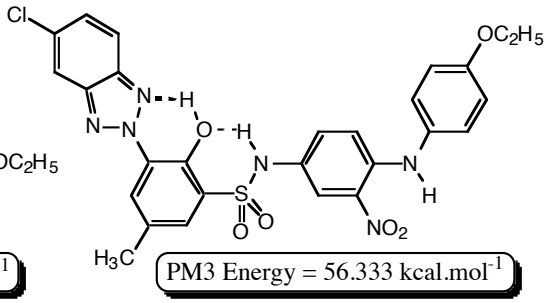

98b

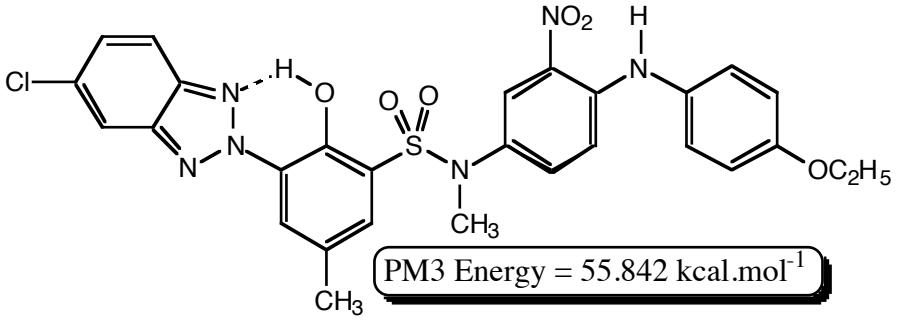

96a

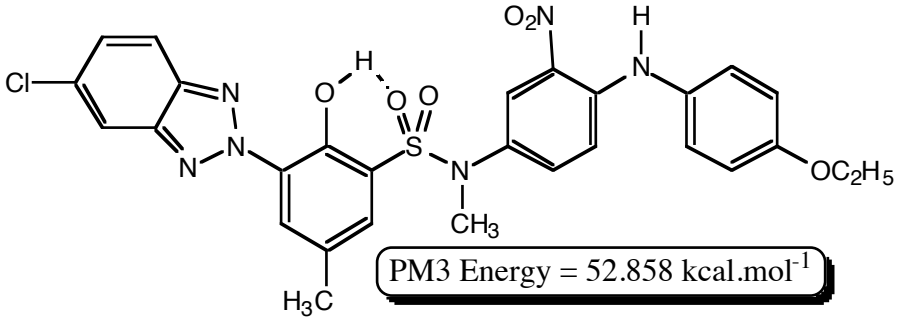

96b

Structure **97** contains a bulky group *ortho,* and an electron withdrawing sulfonamide group *para* to the phenolic group. Unlike **96**, undesirable intramolecular hydrogen bonding is not predicted in structure **97**. The anticipated features of the two hypothetical dyes are summarized in Figure 3.29.

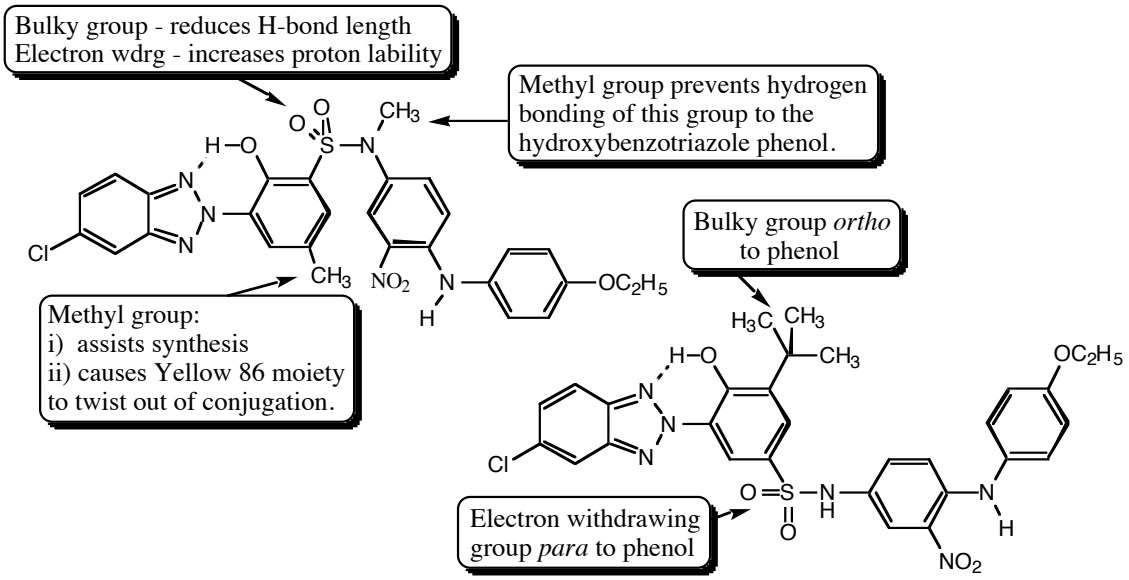

Figure 3.29 *Hypothetical dyes **96** and **97**, showing design features aimed at improving internal conversion of UV light, and hence photostability.*

3.4 IRON VS. CHROMIUM IN METAL COMPLEX DYES

3.4.1 METAL COMPLEX AZO DYES

Dyes **99**-**101** were selected for modeling studies on the basis of an earlier study [209] which showed that the lightfastness and washfastness of these dyes were significantly improved following post-metallization with Fe (III). Although an improvement in fastness was observed, Fe (III) treatment did not afford dyeings that were always as fast as those obtained by metallizing with Cr (VI).

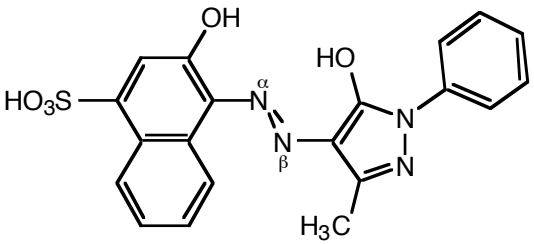

99

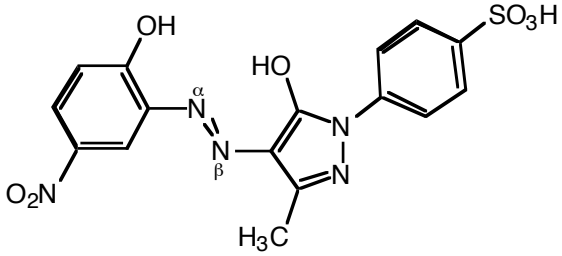

100

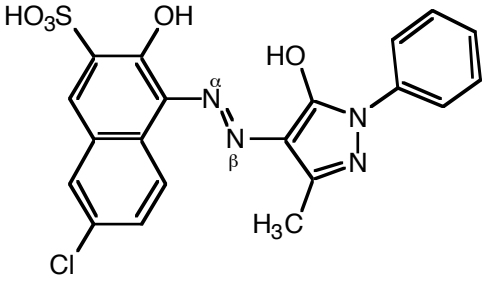

101

CI Mordant Red 7 (**99**), CI Mordant Orange 3 (**100**) and CI Mordant Red 19 (**101**) were optimized as quartet multiplicity Nα, Nα‘ naked anionic 1:2 Cr (III) complexes using INDO/2 parameters and an UHF SCF procedure in ZINDO. Geometry optimizations of the corresponding 1:2 Fe (III) complexes of **99**-**101** were performed concurrently using identical starting structures, except for the central metal atom, which was replaced immediately prior to starting the ZINDO optimization. As there are two possible electronic configurations for Fe (III), two separate optimizations of 1:2 Fe (III) complexes of **99**-**101** were performed from

identical starting structures -- one as doublet (low-spin) multiplicity and one as a sextet multiplicity (high-spin).

The results of the ZINDO Mulliken population analysis of the electrons residing in the atomic orbital overlap regions were interpreted by the CAChe graphical interface. This gave a measure of the nature and strengths of bonding interactions between the CMA and ligand atoms. Figure 3.30 shows an example of results from the optimization of chromium and iron complexes of CI Mordant Red 7 (**99**). In this rendition, strong covalent bonds are represented by solid cylinders, weak bonds are indicated by a dotted line, and essentially ionic interactions are represented by the absence of a directional bond. The high and low spin Fe (III) structures were similar.

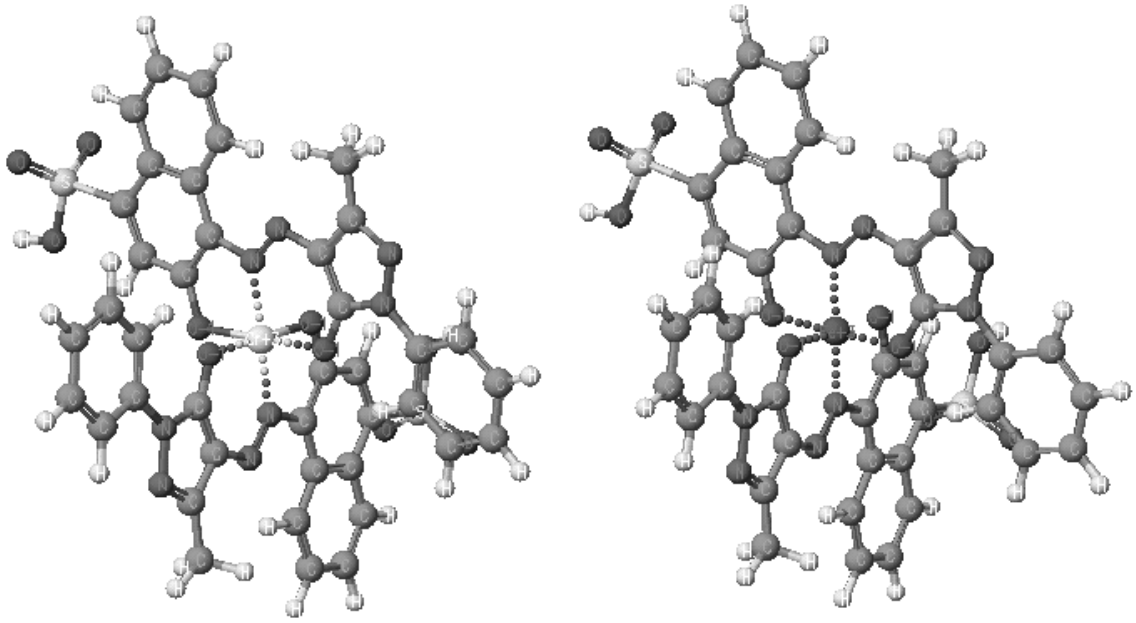

Figure 3.30 *Representative geometry optimization results for Cr (III) (left) and Fe (III) (right) complexes of **99**, including Mulliken population analysis. Covalent interactions between the central metal atom and the ligands are represented by solid cylinders; weak interactions are denoted by dotted lines, and ionic interactions are indicated by a lack of a directional bond.*

Geometry optimization results are summarized in Table 25 along with experimental fastness data [209]. Calculation times varied from 33 to 330 hours, and averaged 92 hours for each optimization. In the case of dyes **99**-

101, ZINDO predicted that CMA - ligand bonding was always stronger in the case of Cr. Furthermore, the optimized high spin and low spin Fe (III) structures were predicted to be similar in most cases. The results given in Table 25 suggest a relationship between bonding to the central metal atom and fastness properties. Dyes predicted to have weaker bonds to the central metal atom tended to have lower washfastness and lightfastness.

Table 25 *Predicted (INDO/2) metal-ligand bonding interactions and experimental fastness data [209] for metal complex dyes **99**-**101**.*

Structure		Expt. Fastness		Calc. Ligand - CMA Interactions	
ID	CMA	LF*	WF**	Low Spin	High Spin
99	Cr (III)	3	4-5	2 strong, 4 weak	N/A
99	Fe (III)	2	3-4	5 weak, 1 ionic	5 weak, 1 ionic
100	Cr (III)	3-4	4-5	2 strong, 4 weak	N/A
100	Fe (III)	2-3	2-3	1 strong, 5 weak	5 weak, 1 ionic
101	Cr (III)	3-4	4-5	2 strong, 4 weak	N/A
101	Fe (III)	3-4	3-4	1 strong, 5 weak	5 weak, 1 ionic

* Light fastness ratings (ACS Grayscale, 1-5 on wool at 170 kJ.m^{-2})

** Wash fastness ratings (ACS grayscale rating of color change (1-5) on wool : AATCC 61-1989/2A)

3.4.2 FORMAZAN DYES

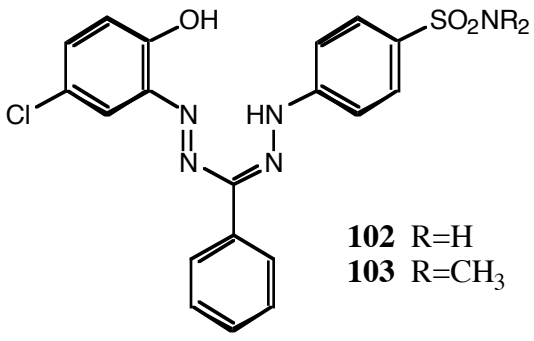

102 R=H
103 R=CH_3

Formazan dyes such as **102** and **103** form stable red to blue, 1:2 complexes with iron (III) (lxi, lxii). The 1:2 Fe complex of **102** has a deep violet color in methanol-water. ZINDO was used to investigate the bonding to the central metal atom in these compounds, in an attempt to explain why the iron complex formazan dyes possess brighter

colors and were faster to washing and light than iron complex azo dyes. The 1:2 Fe complex of **103** was optimized in ZINDO using a ROHF SCF procedure for iterative calculation of energy. The structure was optimized both as the high-spin (sextet) and low-spin (doublet) electronic configurations. As the number of atoms in this compound was large, calculation times were lengthy. Time in the dedicated coprocessor reached 27 days in the case of the low-spin calculation, and 22 days for the high spin optimization. Table 26 contains results pertaining to the optimizations, and Figure 3.31 shows the 1:2 Fe (III) complex of **103**, optimized as the low-spin (left hand structure) and the high spin (right hand structure). Clearly, bonding to the central iron atom was stronger in the case of the low-spin complex.

Table 26 *Calculated final structure energy and predicted metal ligand bonding interactions for 1:2 iron (III) complexes of **103** using high and low spin configurations.*

Multiplicity	Energy / Hartrees mol^{-1*}	CPU time	Fe (III) - Ligand Interactions
Doublet	-615.368327	644 Hours	3 strong, 3 weak
Sextet	-615.378496	533 Hours	5 weak, 1 ionic

* 1 Hartree = 627.51 kcal.

The calculated energy differences between the converged high and low spin structures was small (0.002%) compared to the total energy of the structures. As results reported in this thesis have shown that bond length errors average 1.7% and may be as high as 4.6% [210] from INDO/2 optimizations, it is unreasonable to expect ZINDO to be able to predict the spin multiplicity of a complex based upon a ZINDO-optimized geometry. It has been suggested that such a prediction may be feasible with the use of high level *ab initio* calculations [211].

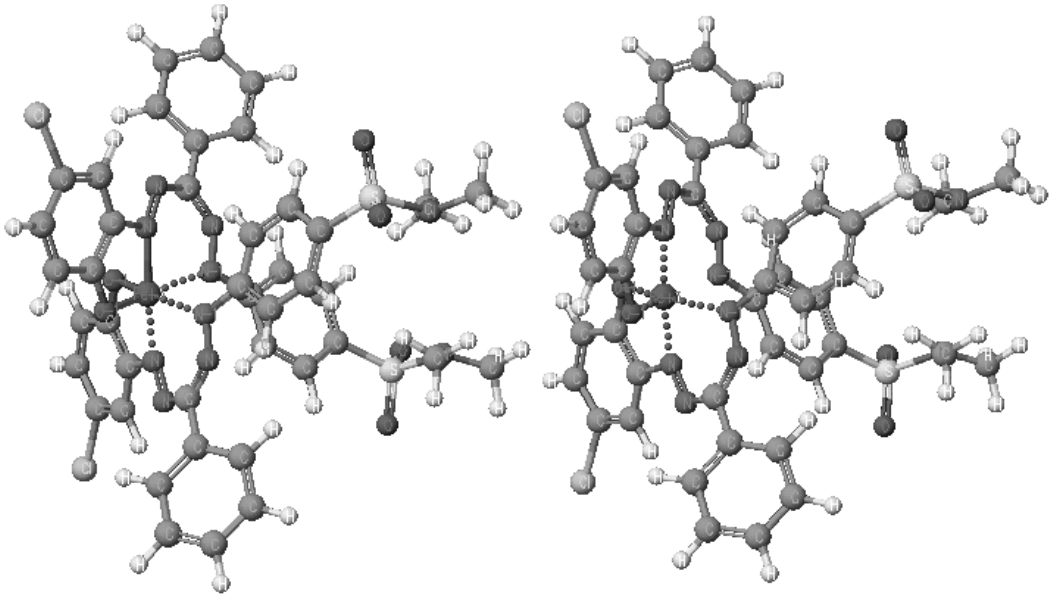

Figure 3.31 *Low-spin (left) and high-spin (right) optimized structures of the 1:2 complex of **103**. Strong covalent interactions are denoted by solid cylinders, weak interactions by dotted lines, and ionic interactions by the absence of a directional bond.*

3.4.3 MAGNETOCHEMISTRY

Samples of three iron complex azo dyes (**104-106**) and two iron complex formazan dyes (**102** and **107**) were obtained [212] as sodium salts and tested for magnetic susceptibility. Dye **104** is the 1:2 Fe (III) complex of CI Mordant Black 11, and **105** is structurally related to CI Mordant Orange 3 (**100**).

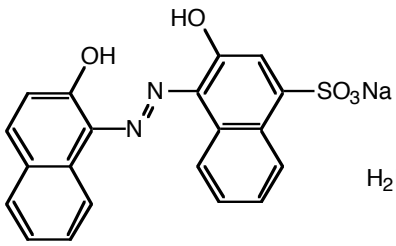

104

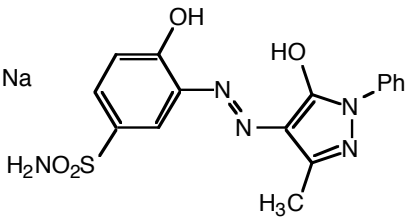

105

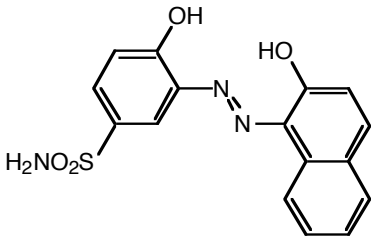

106

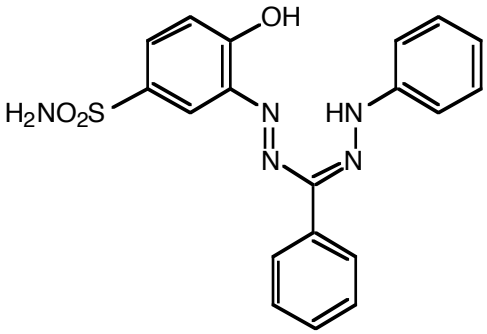

107

Iron forms mixed oxides containing both Fe (III) atoms of quartet and sextet multiplicity, and Fe (II) atoms of triplet multiplicity in an inverse spinel arrangement [213]. Thus, contamination of dye samples by solid inorganic iron oxides or hydroxides could give rise to higher than expected experimental multiplicities. Dyes **102**, **104-107** were found to be soluble in either ethyl acetate, or various mixtures of alcohol and water containing a trace of ammonia, and so were considered essentially uncontaminated by hydrated iron oxides.

$Hg[Co(NCS)_4]$ was used to characterize the magnetic field parameter ($H.\partial H/\partial y$) and standardize magnetic susceptibility measurements. The diamagnetic contribution of constituent ions and atoms were estimated using Pascale's constant tables, and subtracted from the measured total molar magnetic susceptibility, the difference being the paramagnetic susceptibility. Table 27 gives the experimental magnetic moments obtained from the paramagnetic susceptibilities of **102**, **104-107** and compares them to the

theoretical spin-only magnetic moments calculated using equation 2 from the estimated number of unpaired electrons in the complex, n, or from the estimated spin multiplicity of the complex, S. Due to the low symmetry of the complexes, it was assumed that the contribution of the orbital angular momentum and associated magnetic moment to the total magnetic moment was negligible for the calculation of $\mu^{(theory)}$ (hence, spin-only).

$$\text{Theoretical} \quad \mu_{spin\text{-}only} = 2\sqrt{(S(S+1))} = \sqrt{(n(n+2))} \qquad (2)$$

Table 27 *Experimental magnetic moments and multiplicities of dyes **102, 104-107**.*

Structure 1:2 Fe (III) of:	$\mu^{expt.}$ Bohr Magnetons	No. Unpaired Electrons	$\mu_{spin\text{-}only}$ (theoret.) Bohr Magnetons	Experimental Multiplicity
102	2.141	1	1.732	Doublet
104	5.929	5	5.916	Sextet
105	5.951	5	5.916	Sextet
106	6.326	5	5.916	Sextet
107*	4.061	3	3.873	Quartet

* Crude dye used

Clearly, the results given in Table 27 show that the Fe (III) azo dyes tested were high-spin complexes. Formazan Fe (III) complex dye **102** is definitely low-spin, and **107** is a low-spin compound, possibly contaminated with a high-spin impurity. The contribution of the orbital angular momentum of the atomic d-orbitals to the experimental magnetic moment will be somewhat greater for low spin Fe complexes than high spin, due to orbital triple-degeneracy of arrangements of one unpaired electron in three 3d (t_{2g}) orbitals in low-spin complexes, compared to the single possible arrangement of five unpaired electrons into five d-orbitals in the case of high-spin complexes. Thus,

we can expect larger errors for experimental magnetic moments of low-spin Fe (III) complexes.

Metal ligand bonds in high-spin Fe (III) complexes will be longer and weaker than those in low-spin complexes, due to the partial occupancy of the $2e_g$ antibonding orbitals. Molecular modeling showed that the metal-ligand bonding in Fe (III) formazan dye **102** (low-spin) was much stronger than the metal-ligand bonding in Fe (III) azo dyes (high-spin). As weaker bonds implies lower complex stability, we might expect Fe (III) formazan dyes to be faster to light and washing than Fe (III) azo dyes.

Due to high absorption intensity and substituent effects [214], it is generally accepted the color of metal complex dyes is due to π-π^* transitions associated with the dye ligands. The metal atom acts as a perturbation on the ligand π system, giving rise to a shift in color after complexation.

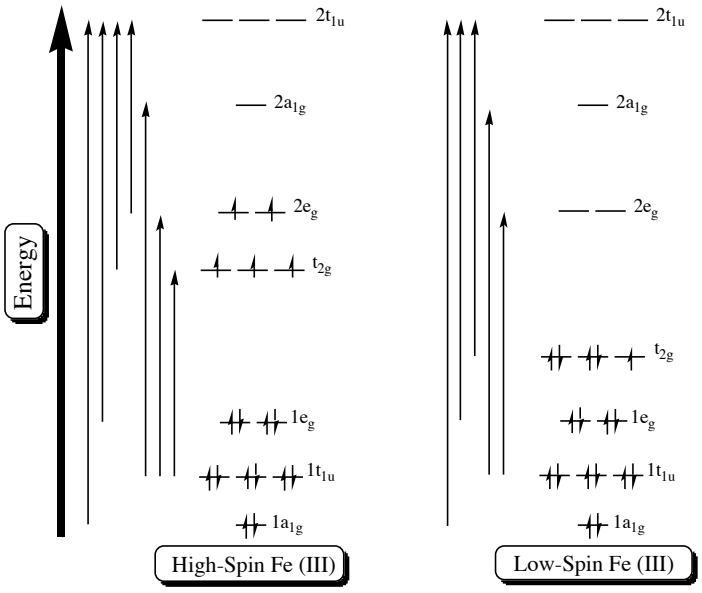

Figure 3.32 *Qualitative explanation for the dull color of high-spin Fe (III) complexes compared to low-spin based upon the range of transition energies in each.*

Nevertheless, electron and orbital distribution at the central metal atom may be related to the observed dullness of Fe (III) azo dyes, compared to the Fe (III) formazan dyes. A qualitative explanation is illustrated in Figure 3.32, which shows simplified MO diagrams for high and low spin configurations of Fe (III). The ligand π-MOs are not shown in this diagram, however, it should be considered that these orbitals will interact with the orbitals that are shown. Vertical arrows in Figure 3.32 represent allowed electronic transitions. The

length of the arrow is proportional to the energy associated with the transition, which in turn is related to the frequency of light absorbed. Although the MO diagram is not to scale, it is clear to see that the range of possible electronic transitions is greater in the case of the high-spin configuration than for the low-spin configuration. A large range of transition energies would necessarily lead to a broadening of the absorption envelope, and a dull color, as observed in high-spin Fe (III) dyes.

3.4.4 THEORETICAL CHARACTERIZATION OF DYE LIGANDS

The results presented thus far draw us toward the conclusion that in order to make bright, fast, 1:2 Fe (III) complex dyes, it is essential to employ ligands that give rise to a low-spin configuration. The nature of the ligand for Cr (III) is less crucial, as Cr (III) only has three electrons to fill the three t_{2g} orbitals, and usually no electrons are left over to occupy the e_g level. Figure 1.13 illustrates that low-spin configurations are likely in cases where acceptor ligand π-bonds interact with the d-orbitals of the central metal atom. All of the dyes considered so far use a mixture of donor and acceptor type ligand groups. In the case of the 1:2 metal complex of **106** (cf. **108**), although a resonance form may be written in which all three atoms connected to the iron atom are doubly bonded (**108b**), this is of high energy, as aromaticity is lost in two aromatic rings. Thus, this azo dye is best described as **108a**, in which the central metal atom is bonded via four donor and only two acceptor atoms.

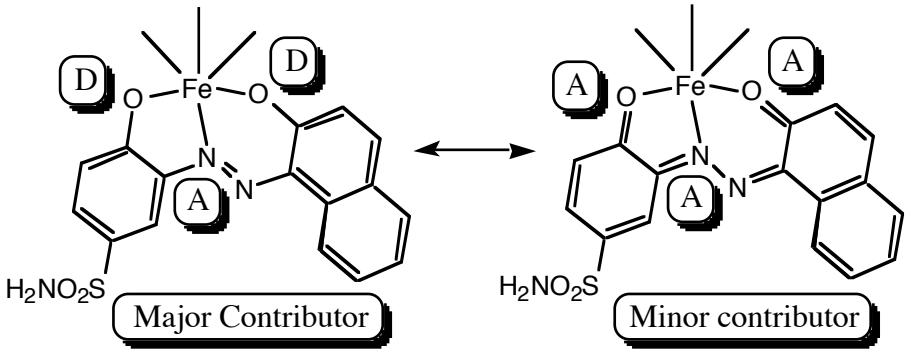

108a **108b**

Azo-pyrazolone dyes, such as the 1:2 Fe (III) complex of **100** (cf. **109**) may be considered in a similar fashion. Although it is possible to delocalize electrons without losing aromaticity, as shown in resonance form **109b**, the structure still contains two donor ligands and only one acceptor ligand. Compounds **109a** and **109b** are not equivalent in energy because of the lack of electronic symmetry. Thus, the ligand will still show significant bond alternation. However, as two acceptor groups can be obtained without losing aromaticity, it is perhaps not surprising that Bardole [209] found that metalization of *ortho*-hydroxyphenylazopyrazolone dyes with Fe (III) salts caused significant improvements in lightfastness.

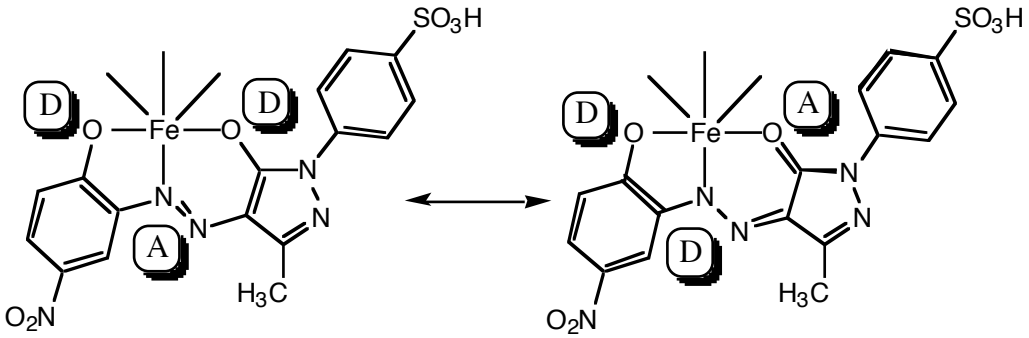

109a **109b**

Formazan dyes bond to the central iron atom using four acceptor atom centers and two donor atom centers. This is due to bond equivalence in the complexed state -- the formazan chromophore is effectively a symmetrical cyanine type structure when complexed with a metal, as **110a** and **110b** are degenerate.

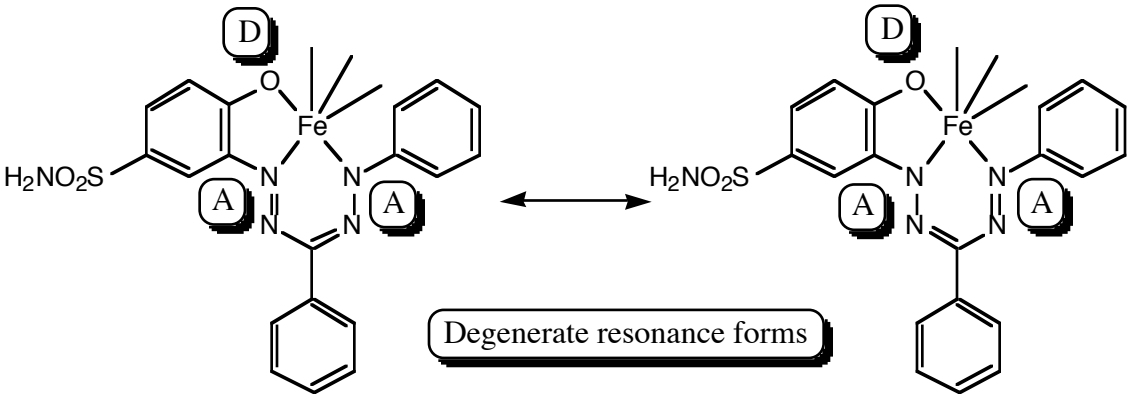

110a **110b**

Results from INDO/2 optimizations showed that the formazan chromophore in **103** was polyene in character before complexation, and cyanine in character as the Fe complexed dye. Figure 3.33 shows the bond numbering schemes for a formazan dye and an *ortho*-hydroxyphenylazopyrazolone dye. Figure 3.34 Figure 3.35 and show the calculated bond orders of the two dyes before and after complexation with Fe.

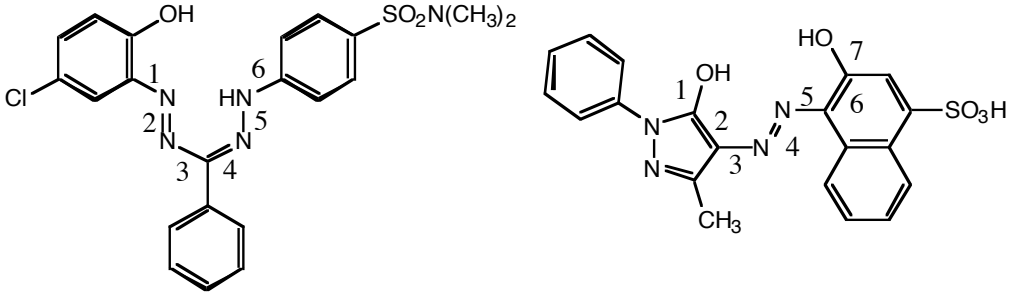

103 **99**

Figure 3.33 *Bond numbering scheme for **103** and **99**.*

A calculated bond order of 1 denotes an pure single bond, while a bond order of 2 is indicative of a pure double bond. As the bond order of the azo group (bond 4, Figure 3.35) in the complexed azo pyrazolone dye was high, suggesting that the azo form predominated in the complexed state, the azo form of the uncomplexed dye was used to assess the effect of complex formation.

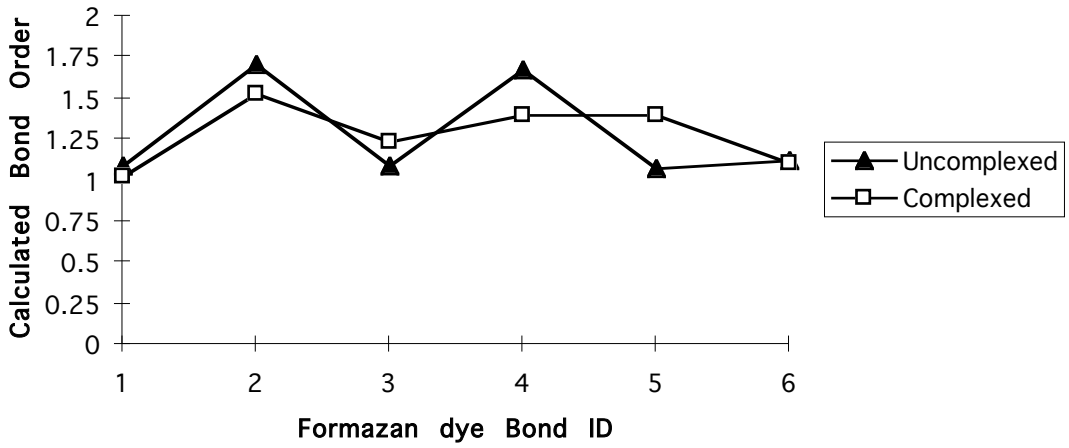

Figure 3.34 *Calculated (INDO/2) bond orders for formazan dye **103**.*

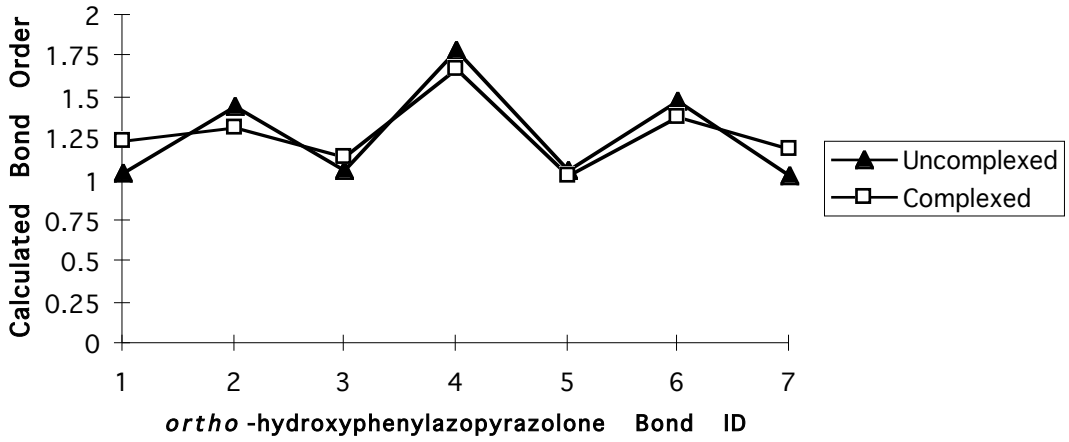

Figure 3.35 *Calculated (INDO/2) bond orders of azo dye **99**.*

Clearly, bond equalization after complexation is more pronounced in the case of the formazan dye than in the case of the azo dye. A possible cause for the azopyrazolone moiety of **99** not forming a cyanine type ligand after complex formation may be the lack of electronic symmetry in the azo-pyrazolone system.

4. CONCLUSIONS

4.1 GEOMETRY OPTIMIZATION

Protocols have been established that allow a wide range of dye structures to be optimized with reliability and repeatability, using sequences of manual adjustments, mechanical, and semi-empirical optimizations. Use of the protocols to obtain minimum energy structures goes part way to overcoming the starting structure sensitivity inherent in modern geometry optimization methods. In addition, the protocols developed improve the probability of locating global minima rather than local minima, and are applicable to structures containing azo groups, intramolecular hydrogen bonds, aminoazobenzene groups, and to metal complex dyes.

Semi-empirical methods were unable to optimize anthraquinone structures with reliability. The use of MOPAC or ZINDO semi-empirical methods on anthraquinone derivatives tended to generate non-planar structures. The reason for this shortcoming of semi-empirical methods is not clear.

Semi-empirical molecular modeling was able to predict the x-ray crystal structure of CI Disperse Yellow 86 and of CI Disperse Red 167, and shows promise as a predictive tool in dye chemistry. Of the various methods in use today, PM3 and AM1 appear to be best suited to modeling these types of compounds. In all cases, the largest errors that occurred in bond length prediction were associated with non-carbon atom bonds. This suggests that the data employed to generate the parameter sets used by the methods could have been slightly deficient for sulfur, oxygen and nitrogen.

Both AM1 and PM3 have shortcomings, especially their inability to handle non-carbon atoms in conjugated structures. For instance both PM3 and AM1 have a tendency to pyramidalize conjugated arylamino nitrogen atoms,

although pyramidalization is less apparent in the case of AM1. PM3 appears to be superior to AM1 in its ability to predict hydrogen bonding interactions. However, AM1 and PM3 showed comparable bond length prediction. Another shortcoming of the AM1 method was its inability to correctly predict the configuration of azobenzenes. AM1 geometry optimizations predicted the *cis* configuration of azobenzene to be more stable than the *trans* configuration. PM3 did not appear to possess the same flaw. Several of the problems associated with AM1 and PM3 are consistent with the hypothesis of Redington and Bock [xciv] that these two methods underestimate the contribution of π orbital overlap to the SCF energy of dye molecules.

As anticipated, MNDO and MINDO were not useful for predicting hydrogen bonding interactions. Both methods also gave low correlation coefficients for covalent bond length prediction. The INDO and CNDO methods were also useful for predicting hydrogen bonding. However, since CNDO and INDO methods give consideration to d-orbital interactions they are more useful than MOPAC methods for studying metal complex dyes.

The INDO/2 method is a useful tool for predicting dye-metal bonding. INDO/2 results are applicable to the design of useful ligands for Fe (III) metal complex dyes. Results of computations using INDO/2 in ZINDO suggested that dye-metal bonding in metal complex azo dyes is generally weaker in Fe (III) compounds than in Cr (III) analogs. Modeling results also suggested that bonding to the central iron atom was stronger in the case of low-spin complexes than high spin complexes, as would be expected based upon MO theory.

4.2 Prediction of Physical Properties

The ZINDO INDO/S method was inferior to PPP-based PISYSTEM for the prediction of the color and strength of azo dyes. Both methods effectively predicted the large Stoke's shift associated with ESIPT in hydroxybenzotriazoles. Clearly, the AM1 COSMO method used in conjunction

with CAChe LogP is useful for estimating the water solubility and octanol-water coefficient for disperse dyes.

Investigations using series of disperse dyes that had previously been characterized failed to identify a single molecular descriptor that could be used to predict the lightfastness of hypothetical structures. In the case of the azo dyes **44a-f**, the size of the study group was too small to draw firm conclusions. Relationships between predicted properties and experimental lightfastness of bichromophoric dyes **82-94** were obfuscated by random error. For instance, the ability to predict excitation energy transfer from one chromophore to another was not established.

Magnetic susceptibility measurements on metal complex dyes showed that azo dyes form high-spin complexes with Fe (III) whereas formazan dyes give low-spin Fe (III) complexes. It would seem that in order to be brightly colored and have good fastness properties Fe (III) complex dyes should be of doublet multiplicity.

The INDO/2 method can be used to predict which ligands would produce low-spin Fe (III) complexes versus high-spin Fe (III) complexes. At least two of the three chelating atoms of the dye ligand should be acceptor type groups, connected to the rest of the ligand via essential double bonds for the resultant Fe (III) complex to be low-spin. If the calculated bond order of pertinent bonds in the ligand tends to equalize after complexation with the metal atom, the chelating atoms in that section of the ligand may be viewed as acceptor ligands. It would appear that the INDO/2 method can be used to customize ligands for Fe (III) that give low-spin, bright, stable dyeings.

Clearly, it has been demonstrated that semi-empirical methods are useful for investigations in dye chemistry, provided that the limitations of each method are respected and that calculations are set up with care. The inherent reliance on empirical parameters probably accounts for the end-use specificity of semi-empirical methods. For instance, methods developed for spectroscopic predictions are not useful for predicting the occurrence of hydrogen bonds, or

solubility. For the same reason, semi-empirical methods may excel at the specific task for which they were developed, for instance the PPP method for color prediction. A drawback of current semi-empirical methods is that they are not useful for predicting long-range intermolecular interactions, such as dye-polymer interactions, as the parameters implemented are not valid for distances significantly larger normal atomic bond lengths.

The development of a “universal” semi-empirical method capable of predicting a wide range of physical properties would be challenging, due to the complexity of the Hamiltonian required and the necessary implementation of separate parameterizations for each property requested. Advances in computer engineering will shortly facilitate routine PC-based *ab initio* calculations on dye structures. It is possible that this family of methods, which are not reliant on empirical terms for calculations, will be applicable to a wider range of calculations than contemporary semi-empirical methods.

5. REFERENCES

1 J. Griffiths in N. S. Allen (Ed.), Developments in Polymer Photochemistry - 1, Vol. 1, Chpt. 6, Applied Science Publishing Ltd., London, (1980).

2 H. E. A. Kramer, The Lightfastness or Non-Photochemistry of Dyes, *Chimia*, **40**, 160-69, (1986).

3 C. H. Giles and R. B. McKay, The Lightfastness of Dyes: A Review, *Textile Res. J.*, **33** (7), 527-77, (1963).

4 G. S. Egerton and A. G. Morgan, The Photochemistry of Dyes II. -Some Aspects of the Fading Process, *J. Soc. Dyers Colour.* **86**, 242-48, (1970).

5 N. S. Allen, Photofading Mechanisms of Dyes in Solution and Polymer Media, *Rev. Prog. Colo.*, **17**, 61-71, (1987).

6 E. Bancroft, in Experimental Researched Concerning the Phylosophy of Permanent Colours, Cadell and Davies, Eds., 2nd ed., London, (1813).

7 D. Brownlie, The Chemical Action of Light on Dyed Colours, *J. Soc. Dyers Colour*, **18**, 288-98, (1902).

8 J. J. Hedges, Fading of Dyestuffs on Textile Fabrics. II. Influence of Regain, *J. Soc. Dyers Colour*, **44**, 341-50, (1928).

9 I. Bridgeman and A. T. Peters, Photochemical Degradation of Aminoazobenzene Disperse Dyes in Ethanolic Solution. Part I: Effect of Concentration, Water and Temperature, *Textile Res. J.*, **44**, 639-45, (1974).

10 R. Eichler, P. Richter, P. Vonhöne, Dispersionfarbstoffe und UV-Absorber für Auto-Textilien aus Polyesterfasern, *Textileveredlung*, **20** (4), 126-129, (1985).

11 C. H. Giles, J. DeBarnat, The Nature of Azo Dye Light Fading in Polyester and the Physical State of the Dye, *Textile. Res. J.,* **46**, 673-75, (1976).

12 S. Kitamura, K. Imada, and M. Katuda, Improving the Lightfastness of Disperse Dyes on Polyester Fiber, *Oral Presentation and Book of Papers, AATCC Intnl. Conf. and Exhibition, Nashville, TN,* Sept 15-18 (1996), pp. 202-211.

13 J. G. Pacifici and G. Irick Jr., Photochemistry of Azo Compounds. II.

Effect of Ketonic Sensitizers on Photoreduction of 4-Diethylamino-4'-nitroazobenzene, *Tetrahedron Lett.*, No. 27, 2207-10, (1969).

14 A. Albini, E. Fasini and S. Pietra, The Photochemistry of Azo Dyes. The Wavelength Dependent Photoreduction of 4-Diethylamino-4'-nitroazobenzene, *J. Chem. Soc. Perkin Trans. II.*, 1393-95, (1982).

15 I. Y. Chang and I. K. Miller, Photostability of Anthraquinone and Azo Dyes in N-Ethylacetamide (Nylon Model), *J. Soc. Dyers Colo.*, **102**, 46-53, (1986).

16 C. H. Giles, D. G. Duff and R. S. Sinclair, The Relationship Between Dye Structure and Fastness Properties, *Rev. Prog. Colo.*, **12**, 58-65, (1982).

17 R. H. Kienle, E. I. Stearns and P. A. van der Meulen, A Correlation of the Structure with Fastness to Light of Monoazo Dyes, *J. Phys. Chem.,* **50**, 363-73, (1946).

18 H. R. Chipalkatti, N. F. Desai, C. H. Giles and N. Macaulay, The Influence of the Substrate upon the Light Fading of Azo Dyes, *J. Soc. Dyers Colo.*, **70** (11), 487-501, (1954).

19 J. W. Cumming, C. H. Giles and A. E. McEachran, A Study of the Photochemistry of Dyes on Protein and other Substrates, *J. Soc. Dyers and Colo.*, **72** (8), 373-81, (1956).

20 J. H. Bowie, G. E. Lewis and R. G. Cooks, Electron Impact Studies. Part VIII. Mass Spectra of Substituted Azobenzenes; Aryl Migration on Electron Impact, *J. Chem. Soc. (B),* 621-28, (1967).

21 C. H. Giles, C. D. Shah, W. E. Watts and R. S. Sinclair, Oxidation and Reduction in Light Fading of Dyes, *J. Soc. Dyers Colo.*, **88**, 433-35, (1972).

22 M. F. Sartori, Spectral and Fastness Properties of Benzothiazolylazo Dyes*, J. Soc. Dyers Colo.*, **83**, 144-46, (1967).

23 A. Arcoria, M. L. Longo, and G Parisi, Photofading of Some Azo Disperse Dyes on Nylon Film, *J. Soc. Dyers Colour.,* **100**, 339-41, (1984).

24 A. Arcoria, M. L. Longo, E. Maccarone, G. Parisi and G. Perrini, Photofading Kinetics and Thermodynamics of some Azo Disperse Dyes in Amide Solvents under the Influence of UV Radiation, *J. Soc. Dyers Colo.*, **100**, 13-16, (1984).

25 I. Bridgeman and A. T. Peters, Photochemical Degredation of Aminoazobenzene Disperse Dyes in Ethanolic Solution Part II: Effect of pH and Dye Structure, *Textile Res. J.*, **44**, 645-49, (1974).

26 T. Kitao, Y. Watada, M. Matsuoka and K. Konishi, Contribution of Nitro Group on the Anomolous Photofading of some Azo Disperse Dyes, *Nippon Kagaku Kaishi (formally N. K. Zasshi)*, **95** (4), 757-61, (1974).

27 T. Shibusawa, T. Saito, T. Hamayose, The Basicity of Disperse Dyes, *Nippon Kagaku Kaishi (formaly N. K. Zasshi)*, **98** (2), Eng. 271, (1977).

28 H. P. Mehta and A. T. Peters, Substituent Effects on the Colour, Dyeing and Fastness Properties of 4-N-β-cyanoethyl-N-β-hydroxyethylamino-azobenzenes. Part I. Monosubstituted Derivatives, *Dyes Pigm.*, **2**, 259-69, (1981).

29 H. P. Mehta and A. T. Peters, Electron Impact-Induced Fragmentation of 4-Aminoazobenzene Dyes and Relationship with Photochemical Stability, *Applied Spectroscopy*, **28**, 241-43, (1974).

30 H. E. Schroeder and S. N. Boyd, Dyes for Hydrophobic Fibers, *Textile Res. J.,* **27** (4), 275-85, (1957).

31 C. Muller, Recent Developments in the Chemistry of Disperse Dyes and their Intermediates, *Am. Dyestuff Reporter*, **59** (3), 37-44, (1970).

32 G. Hallas, W. L. Ho and R. Todd, Synthesis and Electronic Spectra of some Disperse Dyes Derived from 8-Phenylazolilolidine, *J. Soc. Dyers. Colour*, **90**, 121-24, (1974).

33 G. Hallas and K. L. Ng., Synthesis and Electronic Spectra of some Disperse Dyes derived from 9-Phenylazo-1-ketojulolidine, *J. Soc. Dyers Colour*, **93**, 284-87, (1977).

34 H. P. Mehta and A. T. Peters, Substituent Effects on the Colour, Dyeing and Fastness Properties of 4-N-β-cyanoethyl-N-β-hydroxyethylaminoazo-benzenes. Part II. Disubstituted Derivatives, *Dyes and Pigm.*, **3**, 71-78, (1982).

35 H. S. Freeman and S. A. McIntosh, Irradiation of C.I. Disperse Yellow 23 and Disperse Orange 29 in an Ester Environment, *Textile Res. J.,* **64** (6), 309-15, (1994).

36 S. V. Sunthanker and V. Thanumoorthy, Chemical Structure and Lightfastness of Disperse Dyes, *Indian Journal of Chemistry,* **8**, 598-601, (1970).

37 F. M. Tera, L. A. Abdou, M. N. Micheal, and A. Hebeish, Fading Characteristics of some Monoazo Dyes on Cellulose Diacetate and Polyamide Films: Part II., *Polymer Photochemistry*, **6**, 375-83, (1985).

38 F. M. Tera, L. A. Abdou, M. N. Micheal and A. Hebeish, Fading Characteristics of some Monoazo Dyes on Cellulose Diacetate and Polyamide Films: Part I., *Polymer Photochemistry*, **6**, 361-74, (1985).

39 S. A. McIntosh, H. S. Freeman and P. Singh, X-ray Crystal Structure of Dyes 2-Nitro-4'-[N,N-bis(β-hydroxyethyl)amino] azobenzene and 2-Cyano-4'-[N,N-Bis-(β-hydroxyethyl)amino]-azobenzene, *Textile Res. J.*, **59** (7), 389-95, (1989).

40 S. A. McIntosh, H. S. Freeman and P. Singh, X-ray Crystal Structure of the Dye 4- (N,N-bis- (β-hydroxyethyl) amino) azobenzene, *Dyes Pigm.*, **17**, 1-10, (1991).

41 N. J. Bunce, G. Ferguson, C. L. Forber and G. J. Stachnyk, Sterically Hindered Azobenzenes: Isolation of Cis Isomers and Kinetics of Thermal Cis/Trans Isomerization, *J. Org. Chem.*, **52** (3), 393-98, (1987).

42 H. S. Freeman and W. N. Hsu, Photolytic Behavior of some Popular Disperse Dyes on Polyester and Nylon Substrates, *Textile Res. J.*, **57** (4), 223-34, (1987).

43 B. L. Richardson, Characterization of the Photodegredation Products of State of the Art Disperse Dyes on PET Fabric., *MS Thesis, College of Textiles, North Carolina State University, Raleigh, NC 27695-8301, USA*, (1992).

44 H. S. Freeman and S. A. McIntosh, Irradiation of C.I. Disperse Yellow 23 and Disperse Orange 29 in an Ester Environment, *Textile Res. J.,* **64** (6), 309-15, (1994).

45 S. J. Formosinho, Photochemical Hydrogen Abstractions as Radiationless Transitions*, J. Chem. Soc. Faraday Trans. II.*, **72**, 1332-39, (1976).

46 J. N. Pitts, L. D. Hess, E. J. Baum, E. A. Schuck, J. K. S. Wan, P. A. Leermakers and G. Vesley, The Transfer and Conversion of Electronic Energy in some Model Photochemical Systems, *J. Photochem. Photobiol.*, **4**, 305-21, (1965).

47 B. E. Blaisdell, The Photochemistry of Aromatic Azo Compounds in Organic Solvents, *J. Soc. Dyers Colour*, **65**, 618-28, (1949).

48 S. Hashimoto and K. Kano, The Photochemical Reduction of Nitrobenzene and its Reduction Intermediates. XI. The Photochemical Reduction of Azobenzene in Isopropyl Alcohol, *Bull. Chem. Soc. Jpn.*, **45**, 852-55, (1972).

49 J. G. Pacifici, G. Irick Jr., and C. G. Anderson, Photochemistry of Azo Compounds. III. Evidence for an Electron Transfer Process in Amine Solvents, *J Am. Chem. Soc.*, **91**, 5654-55 (1969).

50 G. Irick Jr. and J. G. Pacifici, Photochemistry of Azo Compounds. I. Photoreduction of 4-Diethylamino-4'-nitroazobenzene, *Tetrahedron Lett.*, No.17, 1303-06, (1969).

51 K. J. Sirbiladze, I. Rusznak, A. Vig, G. E. Krichevskiy, O. M. Anysimova and V. M. Anysimova, The Role of Free Radical Transformation in the Photodegredation of reactive Dyed Cellulosic Textiles, *Dyes and Pigm.*, **19**, 235-47, (1992).

52 G. Heijkoop and H. C. A. VanBeek, ESR Investigation of the Radical Intermediates Formed in the Photoreduction of Azo Dyes, *Rec. Trav. Chim. Pays-Bas.*, **96**, 83-85, (1977).

53 A. Arcoria, M. L. Longo, and G. Parisi, Photofading of some Azodisperse Dyes on Nylon Film, *J. Soc. Dyers Colour*, **100**, 339-41, (1984).

54 P. Y. Wang and I. J. Wang, Photolytic Behaviour of some Azo Pyridone Disperse Dyes on Polyester Substrates, *Textile Res. J.*, **62**, 15-20, (1992).

55 H. S. Freeman and S. A. McIntosh, Photolytic Properties of Ortho-Substituted 4-[N,N-Bis(β-hydroxyethyl)aminoazobenzenes in Polymer Substrates, *Textile Res. J.*, **59** (6), 343-49, (1989).

lvi D. M. Lewis, *personal communication, Dept. Colour Chemistry, Leeds University, Leeds, LS2 9JT*, (March 1998).

lvii P. E. Levi and E. Hodgson, A Textbook of Modern Toxicology, (2nd Ed.), Publ. Appleton and Lange, Stamford, CT., (**1997**).

lviii K. Parton, The Dyeing of Wool: Past, Present and Future, *J. Soc. Dyers. Colo.* **114**, 8-10 (1998).

lix J. Sokolowska-Gajda, H. S. Freeman, and A. Reife, Synthetic Dyes Based on Environmental Considerations. Part I. Iron Complexes for Protein and Polyamide Fibers, *Textile Res. J.* **64** (7), 388-396 (1994).

lx H. S. Freeman, J. Sokolowska-Gadja, and A. Reife, Synthesizing Premetallized Acid Dyes Based on Environmental Considerations, *Text. Chem. Color.*, **27** (2), 13-16 (1995).

lxi J. Sokolowska-Gajda, H. S. Freeman, and A. Reife, Synthetic Dyes Based on Environmental Considerations. Part 2. Iron Complexed Formazan Dyes, *Dyes and Pigm.*, **30** (1), 1-20 (1996).

lxii H. S. Freeman, J. Sokolowska-Gajda, and A. Reife, Iron-Complexed Formazan Dyes for Polyamide and Protein Substrates, *US Patent 5,677,434* (1997).

lxiii J. Griffiths, Colour and Constitution of Organic Molecules, Academic Press, NY, (1976).

lxiv Y. Yagi, Studies of the Absorption Spectra of Azo Dyes and their Metal-Complexes. III. The Electronic Absorption Spectra of Metal-Complexes Derived From Phenolazoacetoacetanilides, *Bull. Chem. Soc. Japan,* **36** (5), 487-92, (1963).

lxv T. A. Albright, J. K. Burdett, and M. Whangbo, Orbital Interactions in Chemistry, *Wiley (NY, Chichester, Brisbane, Toronto, Singapore)*, (**1985**).

lxvi H. M. Graves, L. G. Johnston and A. Reiser, The Effect of Mettallization on Singlet Oxygen Formation by Azo Dyes, *J. Photochem. Photobiol. A: Chem.*, **42**, 183-92, (1988).

lxvii J. Sokolowska-Gajda, Photodegredation of some 1:2 Metal-Complexed Formazan Dyes in an Amide Environment, *J. Soc. Dyers Colour*, **112**, 341-84, (1996).

lxviii H. S. Freeman and J. Sokolowska-Gajda, Photodegredation of CI Acid Orange 60 and CI Acid Green 25 in an Amide Environment, *Textile Res. J.*, **60** (4), 221-27, (1990).

lxix K. R. Mann, A. M. Blough, J. L. Schrenk, R. Scott Koefed, D. A. Freedman and J. R. Matachek, Mechanistic Aspects of the Photochemistry of [CpM (η^6-

arene)]$^{+}$ Complexes of Fe, Ru and Os, *Pure and Appl. Chem.*, **67** (1), 95-101, (1995).

lxx U. Lehmann and G. Rihs, Nα Nβ Isomerism of Azo Metal Complex Dyes: First Proof by x-ray Structure Analysis, in Z. Yoshida and T. Kitao (Eds.) Chemistry of Functional Dyes, *Book of Papers, The First International Symposium on Chemistry on Functional Dyes, Osaka, Japan*, (June 5-9th, 1989), pp.215-18.

lxxi J. F. Dawson, The Structure and Properties of Disperse Dyes in Polyester Coloration, *J. Soc. Dyers Colour*, **99** (7), 183-191, (1983).

lxxii J. Szadowski and C. Pryzybylski, Relationships between the Structure of Nitrodiphenylamine Derives Monoazo Acid Dyes and their Spectroscopic and Fastness Properties, *Dyes Pigm.,* **5**, 49-64, (1984).

lxxiii A. T. Peters, Derivatives of 4-Amino-2-Nitrophenylamine as Dyes for Synthetic Polymer Fibres, *J. Appl. Chem. Biotechnol.*, **26**, 131-34, (1976).

lxxiv A. T. Peters, Derivatives of 2,6-Dinitrodiphenylamine as Dyes for Synthetic fibres*, J. Appl. Chem. Biotechnol.,* **23**, 751-57, (1973).

lxxv N. A. Evans in N. S. Allen and J. F. McKellar (Eds.), Photochemistry of Dyed and Pigmented Polymers, Applied Science, London, (1980), pp. 130-32.

lxxvi R. S. Asquith, A. T. Peters and F. Wallace, The Fading of Nitrodiphenylamine Dyes in Relation to their Structure and Ultraviolet Absorption Spectra, *J. Soc. Dyers Colour,* **84** (10), 507-10, (1968)

lxxvii A. T. Peters, Electron-Impact-Induced Fragmentation of Nitrodiarylamine Disperse Dyes, *J. Soc. Dyers Colour*, **89**, 385-88, (1973).

lxxviii E. Fasani, S. Pietra and A. Albini, The Photocyclization of N-acyl-2-nitrodiphenylamines to Phenazine N-oxides: Scope and Mechanism, *Heterocycles*, **33** (2), 573-84, (1992).

lxxix T. P. Smith, K. A. Zaklika, K. Thakur, G. C. Walker, K. Tominaga and P. F. Barbara, Ultrafast Studies on Proton Transfer in Photostabilizers*, J. Photochem. Photobiol. A: Chem.*, **65**, 165-75, (1992).

lxxx W. N. Hsu, Design of Photofade Resistant Synthetic Dyes, Ph.D. Thesis, College of Textiles, North Carolina State University, Raleigh, NC 27695-8301, USA, (1991).

lxxxi G. M. Gantz and W. G. Sumner, Stable Ultraviolet Light Absorbers, *Textile Res. J.*, **27**, 244-51, (1957).

lxxxii R. A. Coleman and W. H. Peacock, Ultraviolet Absorbers, *Textile Res. J.*, **28**, 784-91, (1985).

lxxxiii H. E. A. Kramer, in H. Durr and J. Bovaslaurent (Eds.), Studies in Organic Chemistry. 40; Photochromism, Molecules and Systems, Elsevier, Amsterdam, (1990).

lxxxiv C. Merritt, G. W. Scott, A. Gupta and A. Yavrovian, Transient Absorption Spectra of 2-Hydroxybenzophenone Photostabilizers, *Chem. Phys. Lett.*, **69**, 169-73, (1980).

lxxxv M. E. Mason, J. C. Posey and H. S. Freeman, Design and Synthesis of Lightfast Disperse Dyes, *Book of Papers, American Association of Textile Chemists and Colorists International Conference and Exhibition, Chorlotte, NC.*, **Oct. 8-11, 1991**, pp 114-21.

lxxxvi G. Woessner, G. Goeller, P. Kollat, J. J. Stezowski, M. Hauser, U. K. A. Klein and H. E. A. Kramer, Photophysical and Photochemical Deactivation Processes of Ultraviolet Stabilizers of the (2-Hydroxypheny)benzotriazole Class, *J. Phys. Chem.*, **88**, 5544-50, (1984).

lxxxvii R. J. Greenwood, M. F. Mackay and J. F. K. Wilshire, Structure of an Ultraviolet Absorber: 2-(3'-t-Butyl-2'-hydroxy-5'-methylphenyl)-benzotriazole, *Aust. J. Chem.*, **45**, 965-68, (1992).

lxxxviii M. Wiechmann, H. Port, W. Frey, L. Lärmer and T. Elsässer, Time-Resolved Spectroscopy of Ultrafast Proton Transfer in 2-(2'-Hydroxy-5'-methylphenyl)benzotriazole in Liquid and Polymer Environments, *J. Phys. Chem.*, **95**, 1918-23, (1991).

lxxxix J. Catalan, P. Perez, F. Fabero, J. F. K. Wilshire, R. M. Claramunt and J. Elguero, Photophysical Properties of some 2-(2'-Hydroxyaryl)benzotriazoles: Dramatic Effect of an Ortho-Located Bulky tert-Butyl Group, *J. Am. Chem. Soc.*, **114**, 964-66,. (1992).

xc J. Catalan, J. C. DelValle, F. Fabero and N. A. Garcia, The Infulence of Molecular Conformation on the Stability of Ultraviolet Stabilizers Toward Direct and Dye-Sensitized Photoirradiation: The case of 2-(2'Hydroxy-5'-

methylphenyl)benzotriazole (TIN P), *J. Photochem. Photobiol.*, **61** (2), 118-23, (1995).

xci J. Catalan, F. Fabero, M. S. Guijarro, R. M. Claramunt, D. S. Maria, C. Foces-Foces, F. H. Cano, J. Elguero and R. Sastre, Photoinduced Intramolecular Proton Transfer as the Mechanism of Ultraviolet Stabilizers: A Reappraisal, *J. Am. Chem. Soc.*, **112**, 747-59, (1990).

xcii M. Allan, K. Asmis, C. Bulliard, E. Haselbach and P. Suppan, Triplet State Energy of the Photostabilizer Tinuvin P, *Helvetica Chimica Acta*, **76** (2), 993-94, (1993).

xciii V. Enchev, AM1 Study of Ground State Intramolecular Proton Transfer Reaction in 2-(2'-Hydroxy-5'-methylphenyl)benzotriazole and 2-(2'-Hydroxyphenyl)benzotriazole, *J. Mol. Struct. (Theochem.)*, **288**, 63-66, (1993).

xciv R. L. Redington and C. W. Bock, MO Study of Singlets, Triplets and Tunneling in Tropolone. I. Geometries, Tunneling and Vibrations in the Ground Electronic State, *J. Phys. Chem.*, **95**, 10284-94, (1991).

xcv E. lewars, A. Holder, L. A. Burke, M. Sopek, S. Cabaniss, K. Gundertofte, E. Garcia, J. Gano, P. Seliger, G. Csonka, W. Huang, J. Rodriguez, L. Olsen, Y. J. Zheng, *Electronic Discussion via Computational Chemistry List, Oct-Nov, 1995* Archive URL: **http://ccl..osc.edu/chemistry.html**

xcvi J. J. P. Stewart, Optimization of Parameters for Semiempirical Methods. II. Applications*, J. Comp. Chem.*, **10** (2), 221-64, (1989)

xcvii S. Morigana, Anti-Sublimation Type UV Absorbers, *Poster Presentation and Personal Communication, AATCC International Conference and Exhibition, Nashville, TN,* Sept. 15-18, (1996).

xcviii H. S. Freeman, Method for Producing Lightfast Disperse Dyestuffs Containing a Built in Photostabilizer [Molecule] Compound, US Patent **4,902,787**, (1990).

xcix H. S. Freeman, *Personal Communication*, (1994).

c H. S. Freeman, The Design and Synthesis of Novel Lightfast Dyes, *(Unpublished), Semiannual Report No: 13 to the Textile Dye Lightfastness Consortium*, (1992).

ci H. S. Freeman and J. C. Posey Jr., Analogs of Disperse Red 167 Containing a Built in Photostabilizer Moiety, *Dyes Pigm.*, **20**, 147-69, (1992).

cii H. S. Freeman and J. C. Posey Jr., An Approach to the Design of Lightfast Disperse Dyes-Analogs of Disperse Yellow 42, *Dyes Pigm.*, **20**, 171-95, (1992).

ciii J. Michl and V. Bonà´ci´c - Kouteck´y, Electronic Aspects of Organic Photochemistry, John Wiley + Sons inc., NY, (1990).

civ A. I. Kiprianov and L. A. Lazukina, Cyanine Dyes with Two Conjugated Chromophores. VII, *Zh. Org. Khim.*, **4**, 1480-86 (Eng. 1423-27), (1968).

cv J. Fabian and H. Hartman, Light Absorption of Organic Colorants, Springer-Verlag, (NY), (1980).

cvi G. G. Dyadyusha, A. M. Kolesnikov and A. D. Kachkovski, Ultraviolet and Visible Absorption Spectra of Biscarbocyanine Dyes, *Dyes Pigm.*, **10** (2), 111-21, (1989).

cvii M. Kasha, H. R. Rawls and M. Ashraf El-Bayoumi, The Exciton Model in Molecular Spectroscopy, *Pure Appl. Chem.*, **11**, 371-92, (1965).

cviii M. Kaschke, N. P. Ernsting, B. Valeur and J. Bourson, Subpicosecond Time-Resolved Intramolecular Electronic Energy Transfer in Flexible Bichromophoric Courmarin Molecules, *J. Phys. Chem.*, **94**, 5757-61, (1990).

cix D. L. Dexter, A Theory of Sensitized Luminescence in Solids, *J. Chem. Phys.,* **21** (5), 836-50, (1953).

cx S. Levy, M. B. Rubin and S. Speiser, Orientational Effects in Intramolecular Electronic Energy Transfer in Bichromophoric Molecules, *J. Photochem. Photobiol. A: Chem.*, **66**, 159-69, (1992).

cxi S. Levy, M. B. Rubin and S. Speiser, Orientational Effects in Intramolecular Electronic Energy Transfer in Bichromophoric Molecules. II. Triplet-Triplet Transfer, *J. Photochem. Photobiol. A: Chem.*, **69**, 287-94, (1993).

cxii Y. Ren, Z. Wang, H. Zhu, S. J. Weininger and W. G. McGimpsey, Intramolecular Energy Transfer from Upper Triplet States in Rigidly Linked Bichromophoric Molecules, *J. Am. Chem. Soc.*, **117**, 4367-73, (1995).

cxiii J. Grabowska, A. Hajzner, A. Choynowski and K. Sienicki, Electron Transfer and Back Transfer in Bichromophoric Donor-Acceptor Systems, *J. Chem. Phys.*, **99** (2), 1172-77, (1993).

cxiv S. Depaemelaere, L. Viaene, M. Van der Auweraer, F. C. DeSchryver, R. M. Hermant and J. W. Verhoeven, Non-radiative Decay Processes on the Intramolecular Charge Transfer State in a Rigid Bichromophoric System, *Chem. Phys. Lett.*, **215** (6), 649-55, (1993).

cxv M. Matsuoka, Molecular Orbital Design, Synthesis and Characteristics of Functional Dyes for Electrooptical Applications, in A. T. Peters and H. S. Freeman, (Eds.), Colour Chemistry. The Design and Synthesis of Organic Dyes and Pigments, Chpt. 3, Elsevier Appl. Science, (1991), pp. 61-84

cxvi G. J. Ashwell, I. Sage and C. Trundle, Molecular Electronic Materials, in G. J. Ashwell (Ed.), Molecular Electronics, Wiley, NY, (1992), pp. 2-64

cxvii A. Hinchliffe, Modelling Molecular Structures, Wiley, (1994).

cxviii J. Rival, Molecular Modeling. Semi-Empirical and Empirical Methods of Theoretical Chemistry in C. Ögretir and I. G. Csizmadia (eds.) Computational Advances in Organic Chemistry: Molecular Structure and Reactivity, Kluwer Acad. Publ., Netherlands, (1991), pp. 229-59.

cxix N. L. Allinger, Conformational Analysis. 130. MM2. A Hydrocarbon Force Field Utilizing V_1 and V_2 Torsional Terms, *J. Am. Chem. Soc.*, **99** (25), 8127-34, (1977).

cxx M. Wolfsberg and L. Helmholtz, The Spectra and Electronic Structure of the Tetrahedron Ions MnO_4^-, CrO_4^{-2} and ClO_4^-, *J. Chem. Phys.*, **20**, 837-43, (1952).

cxxi R. Hoffman, An Extended Hückel Theory. I. Hydrocarbons, *J. Chem. Phys.*, **39** (6), 1397-1412, (1963)

cxxii R. Pariser and R. G. Parr, A Semi-Empirical Theory of the Electronic Spectra and Electronic Structure of Complex Unsaturated Molecules. I., *J. Chem Phys.*, **21**, 466-71, (1953).

cxxiii R. Pariser and R. G. Parr, A Semi-Empirical Theory of the Electronic Spectra and Electronic Structure of Complex Unsaturated Molecules. II., *J. Chem Phys.*, **21**, 767-76, (1953).

cxxiv J. A. Pople, Electron Interaction in Unsaturated Hydrocarbons, *Trans. Faraday. Soc.*, **49**, 1375-85, (1953).

cxxv K. Nishimoto and N. Mataga, Electronic Structure and Spectra of some Nitrogen Heterocycles, *Z. Physik. Chem. (Frankfurt),* **12**, 335-38, (1957).

cxxvi H. A. Hammond, The Calculation of Excited State and Ground State Properties of Conjugated Heteroatomic Molecules Using a Single SCF-LCAO-CI Method Including σ-Polarization, *Theoret. Chim. Acta (Berl.),* **18**, 239-49, (1970).

cxxvii K. Nishimoto and L. S. Forster, SCFMO Calculations of Heteroatomic Systems with the Variable β-Approximation. I. Heteroatomic Molecules Containing Nitrogen or Oxygen Atoms, *Theoret. Chim. Acta (Berl.)*, **4**, 155-65, (1966).

cxxviii R. L. Flurry Jr., E. W. Stout and J. J. Bell, The Inclusion of Non-Nearest Neighbor β Terms in Pariser-Parr-Pople Type SC MO Calculations, *Theoret. Chim. Acta (Berl.),* **8**, 203-11, (1967).

cxxix J. A. Pople, D. P. Santry and G. A. Segal, Approximate Self-Consistent Molecular Orbital Theory. I. Invariant Proceedures, *J. Chem. Phys.*, **43** (10), s129-35 (supplemental), (1965).

cxxx J. A. Pople and G. A. Segal, Approximate Self-Consistent Molecular Orbital Theory. II. Calculations with Complete Neglect of Differential Overlap, *J. Chem. Phys.*, **43** (10), s136-51 (supplemental), (1965).

cxxxi J. A. Pople and G. A. Segal, Approximate Self-Consistent Molecular Orbital Theory. III. CNDO Results for AB_2 and AB_3 Systems, J. Chem. Phys. 44 (9), 3289-96, (1966).

cxxxii J. DelBene and H. H. Jaffé, Use of the CNDO Method in Spectroscopy. I. Benzene, Pyridine and the Diazines, *J. Chem. Phys.*, **48** (4), 1807-13, (1968).

cxxxiii J.DelBene and H. H. Jaffé, Use of the CNDO Method in Spectroscopy. II. Five-Membered Rings, *J. Chem. Phys.*, **48** (9), 4050-55, (1968).

cxxxiv J. DelBene and H. H. Jaffé, Use of the CNDO Method in Spectroscopy. III. Monosubstituted Benzenes and Pyridines, *J. Chem. Phys.*, **49** (3), 1221-29, (1968).

cxxxv J. A. Pople, D. L. Beveridge and P. A. Dobosh, Approximate Self-Consistent Molecular Orbital Theory. V. Intermediate Neglect of Differential Overlap, *J. Chem. Phys.*, **47** (6), 2026-33, (1967).

cxxxvi R. N. Dixon, Approximate Self-Consistent Field Molecular Orbital Calculations for Valence Shell Electronic States, *J. Mol. Phys.,* **12** (1), 83-90, (1967).

cxxxvii J. Ridley and M. Zerner, An Intermediate Neglect of Differential Overlap Technique for Spectroscopy: Pyrrole and the Azines, *Theoret. Chim. Acta (Berl.),* **32**, 111-34, (1973).

cxxxviii A. D. Bacon and M. C. Zerner, An Intermediate Neglect of Differential Overlap Theory for Transition Metal Complexes: Fe, Co and Cu Chlorides, *Theoret. Chim. Acta. (Berl.),* **53**, 21-54, (1979).

cxxxix W. P. Anderson, W. D. Edwards, M. C. Zerner, Calculated Spectra of Hydrated Ions of the First Transition-Metal Series, *Inorg. Chem.*, **25**, 2728-32, (1986).

cxl N. C. Baird and M. J. S. Dewar, Ground States of σ-Bonded Molecules. III. The MINDO Method and its Application to Hydrocarbons, *J. Chem. Phys.*, **50** (3), 1262-80, (1969).

cxli M. J. S. Dewar and E. Haselbach, Ground States of σ-Bonded Molecules. IX. The MINDO/2 Method, *J. Am. Chem. Soc.*, **92** (3), 590-98, (1970).

cxlii R. C. Bingham, M. J. S. Dewar and D. H. Lo, Ground States of Molecules. XXV. MINDO/3. An Improved Version of the MINDO Semiempirical SCF-MO Method, *J. Am. Chem. Soc.*, **97**, 1285-93, (1975).

cxliii M. J. S. Dewar and W. Thiel, Ground States of Molecules. 39. MNDO Results for Molecules Containing Hydrogen, Carbon, Nitrogen and Oxygen, *J. Am. Chem. Soc.*, **99**, 4907-17, (1977).

cxliv M. J. S. Dewar, E. G. Zoebisch, E. F. Healey and J. J. P. Stewart, AM1: A New General Purpose Quantum Mechanical Molecular Model, *J. Am. Chem. Soc.*, **107**, 3902-09, (1985).

cxlv E. Lewars, A. Holder, L. A. Burke, M. Sopek, S. Cabaniss, K. Gundertofte, E. Garcia, J. Gano, P. Seliger, G. Csonka, W. Huang, J. Rodriguez, L. Olsen, Y. J. Zheng, *Electronic Discussion via Computational Chemistry List, Oct-Nov, 1995.*

cxlvi J. J. P. Stewart, Optimization of Parameters for Semiempirical Methods. I. Method*, J. Comp. Chem.*, **10** (2), 209-20, (1989).

cxlvii J. J. P. Stewart, Optimization of Parameters for Semiempirical Methods. II. Applications, *J. Comp. Chem.*, **10** (2), 221-64, (1989).

cxlviii Y.-J. Zheng, K. M. Merz Jr., G. K. Farber, Theoretical Examination of the Mechanism of Aldose-Ketose Isomerization, *Protein Engineering*, **6**, 479-84, (1993).

cxlix M. A. Rios and J. Rodriguez, Semiempirical Study of Compounds with OH-O Intramolecular Hydrogen Bond, *J. Comput. Chem.*, **13**, 860-66, (1992).

cl J. J. P. Stewart, MOPAC: A Semiempirical Molecular Orbital Program, *J. Comp.-Aided Mol. Design*, **4**, 1-105, (1990).

cli R. Naef, PISYSTEM V3.1 (1994), Im Budler 6, CH-4419, Lupsingen, Switzerland.

clii J. J. P. Stewart, *Personal Communication*, Oct 30th, 1995.

cliii W. J. Hehre, Practical Strategies for Electronic Structure Calculations, Wavefunction, CA, (1995)

cliv J. Griffiths, The Historical Developments of Modern Colour and Constitution Theory*, Rev. Prog. Colour*, **14**, 21-32, (1984).

clv J. Griffiths, Modern Dye Chemistry, *Chemistry in Britain*, **Nov. 1986**, 997-1000.

clvi J. Griffiths, Recent Developments in the Colour and Constitution of Organic Dyes, *Rev. Prog. Colour*, **11**, 37-57, (1981).

clvii M. Adachi and S. Nakamura, Comparison of the INDO/S and the CNDO/S Method for the Absorption Wavelength Calculation of Organic Dyes, *Dyes Pigm.,* **17** (4), 287-96, (1991).

clviii G. F. Castellani and J. C. J. Bart, Colour Prediction of Organic Dye Molecules on a Microcomputer - a Readily Available form of the PPP-MO Method for Teaching and Research, *Dyes Pigm.*, **5**, 165-70, (1984).

clix G. Hallas and R. Marsden, Colour and Constitution of some N-Phenylpyrrolidinylazo Dyes: Application of the PPP Molecular Orbital Method, *Dyes Pigm.*, **6**, 463-75, (1985)

clx Y. Yogo, H. Kikuchi, M. Matsuoka and T. Kitao, Colour and Constitution of Anthraquinonoid Dyes. Part I - Modified PPP Calculations and Substitution Effects, *J. Soc. Dyers Colour*, **96** (9), 475-80, (1980).

clxi M. Matsuoka, K. Takagi, H. Obayashi, K. Wakasugi and T. Kitao, Colour and Constitution of 1,4-Naphthoquinonoid Dyes - Modified PPP-MO Calculations and Substitution Effects, *J. Soc.Dyers Colour*, **99** (26), 257-60, (1983).

clxii J. Griffiths, Practical Aspects of Colour Prediction in Organic Dye Molecules, *Dyes Pigm.*, **3**, 211-33, (1982).

clxiii C. Schumacher, K. Bredereck and F. Reidle, New Approaches in the Design of Reactive Dyes, *Book of Papers, 17th IEVTCC Congress*, Vienna, June 5-7th, (1996).

clxiv M. Zerner, *Electronic Communication via the Computational Chemistry List*, Oct. 1995,
Archive URL: **http://ccl.osc.edu/chemistry.html**

clxv U. Dinur, B. Honig and K. Schulten, On the Nature of Excited Electronic States in Cyanine Dyes. Implications for Visual Pigment Spectra, *Chem. Phys. Lett.*, **72** (3), 493-97, (1980).

clxvi F. Momicchioli, I. Baraldi, G. Ponterini and G. Berthier, Electronic Spectra and Trans-Cis Isomerism of Streptopolymethine Cyanines. A CS INDO CI Study, *Spectrochimica Acta*, **46A** (5), 775-91, (1990).

clxvii D. Hinks, J. Lye and H. S. Freeman, Computer-Aided Dyestuff Design, *Book of Papers, American Association of Textile Chemists and Colorists International Conference and Exhibition, Atlanta, GA.*, (**Oct. 8-11, 1995**), pp. 74-85

clxviii D. Hinks, *Unpublished observations*.

clxix G. L. Estiu, A. H. Jubert, J. Molina, J. Costamagna, J. Canales and J. Vargas, A Theoretical Investigation of the Structure and Electronic Spectra of Porphyrin Homolog Macrocycles. Hexaazacyclophane and its Nickle and Copper Complexes, *Inorg. Chem.*, **34**, 1212-20, (1995).

clxx G. L. Estiú, A. H. Jubert, J. Costamagna, J. Vargas, Quantum Chemical Calculations of the Structures and Electronic Properties of N, N'-Bis(3,5-dibromosalicylidene) -1,2-diaminobenzene and its Cobalt (II) Complex. The Origin of the Redox Activity of the Cobalt Complex, *Inorg. Chem.*, **35**, 263-66, (1996).

clxxi E. Chamot, P. Cahill, M. Mitchell, J. Golab, *Electronic Discussion via the Computational Chemistry List, Jan. 1996,*
Archive URL: **http://ccl.osc.edu/chemistry.html**

clxxii Hyperchem V3 (1993), Autodesk Inc, 2320 Marinshipway, Sausalito, CA 94965, USA.

clxxiii M. M. Awad, P. K. McCarthy and G. J. Blanchard, Photoisomerization of Cyanines. A Comparative Study of Oxygen and Sulphur-Containing Species, *J. Phys. Chem.*, **98**, 1454-58, (1994).

clxxiv M. S. Topaler, V. M. Mamaev, Ye. B. Gluz, V. I. Minkin, and B. Ya. Simkin, Tunnelling Effects in the Double Transfer Reaction of 2,5-Dihydroxy-1,4-benzoquinone, *J. Mol. Struct.,* **236**, 393-401, (1991).

clxxv J. Elguero, P. Goya, A. Martinez, and I. Rozas, On the Tautomerism of 2-Phenylacyl-4-pyrimidones and Related Compounds, *Chem Ber.,* **122**, 919-24, (1989).

clxxvi V. Enchev, AM1 Srudy of Ground State Intramolecular Proton-Transfer Reaction, *Comptes Rendus de l'Academie Bulgare des Sciences*, **46** (1), 67-69, (1993).

clxxvii J. M. Bofill, J. Castells, S. Olivella and A. Sole, Kinetic Interprettation of Aromaticity: A Theoretical Study, *J. Org. Chem*, **53**, 5148-9, (1988).

178 CAChe Worksystem 3.6, (1993) (CAChe Scientific) Oxford Molecular Group, Box 4003,Beaverton, OR 97076.

179 H. S. Freeman, J. C. Posey Jr. and P. Singh, X-ray Crystal Structure of Disperse Red 167, *Dyes Pigm.,* **36** (5), 487-92 (1963).

180 H. S. Freeman and P. Singh, *Unpublished Work*.

181 M. G. Hutchings, Software Review: PISYSTEM for Windows Version 3.1. A Program for the Calculation of Excited State Properties Including Colour of pi-Electron Based Molecules, *Dyes and Pigm.* **29**, 95-101 (1995).

182 J. Griffiths, Practical Aspects of Colour Prediction of Organic Dye Molecules, *Dyes and Pigm*. **3**, 211-33.

183 N. Bodor, Z Gabanyi, and C. Wong, A New Method for the Estimation of Partition Coefficient, *J. Am. Chem. Soc* ., **111**, 3783-6 (1989).

184 N. Bodor and M. J. Huang, A New Method for the Estimation of Aqueous Solubility of Organic Compounds, *J. Pharmaceutical Sciences*, **81** (9), 954-60 (1992).

185 A. Klamt and G. Schuurmann, COSMO: A New Approach to Dielectric Screening with Explicit Expressions for the Screening Energy and its Gradient*, J. Chem. Soc. Perkin Trans. II*, 799-805 (1993).

186 Varian Associates, Paolo Alto, CA., USA.

187 Ventron Instruments Corp., Paramount, CA., USA.

188 H. S. Freeman, J. C. Posey Jr., and P. Singh, X-ray Crystal Structure of Disperse Red 167, *Dyes and Pigm.*, **20**, 279-89.

189 H. S. Freeman, M. E. Mason and P. Singh, *Unpublished Data*, (1991)

190 C. M. Nunn, L. Van Meervelt, S. Zhang, M. H. Moore, O. Kennard, DNA-Drug Interactions. The Crystal Structures of d(TGTACA) and d(TGATCA) Complexed with Daunomycin., *J. Mol. Biol.,* **222,** 167-77, (1991).

191 M. H. Moore, W. N. Hunter, B. d'Estaintot, O. Kennard, DNA-Drug Interactions. The Crystal Structure of d(CGATCG) Complexed with Daunomycin., *J. Mol. Biol.,* **206**, 693-707, (1989).

192. J. Griffiths, Colour and Constitution of Organic Molecules, Academic Press, NY, (1976).

193. G. S. Hartly, The Cis Form of Azobenzene, *Nature*, **140**, 281-81, (1937).

194. E. Lewars, A. Holder, L. A. Burke, M. Sopek, S. Cabaniss, K. Gundertofte, E. Garcia, J. Gano, P. Seliger, G. Csonka, W. Huang, J. Rodriguez, L. Olsen, Y. J. Zheng, *Electronic Discussion via Computational Chemistry List, Oct-Nov, 1995.*
Archive URL: **http://ccl/osc/edu/chemistry.html**

195. R. L. Redington and C. W. Bock, MO Study of Singlets, Triplets and Tunneling in Tropolone. I. Geometries, Tunneling and Vibrations in the Ground Electronic State*, J. Phys. Chem.*, **95**, 10284-94, (1991).

196. J. A. Bikker, D. F. Weaver, Theoretical Studies Applicable to the Design of Novel Anticonvulsants. Part 2. A Comparison of AM1, MNDO, and PM3 Semiempirical Molecular Orbital Conformational Analysis of Dihydropyridine Calcium Channel Blockers, *J. Mol. Struct.,* **281**, 173-184, (1993).

197. C. B. Aakeröy, Enthalpies of Formation of Carboxylic Acids and Proton Affinities of Carboxylate Anions: A Comparison of MNDO, AM1 and PM3, *J. Mol. Struct.,* **281**, 259-267, (1993).

198. R. Karaman, J. L. Huang, J. L. Fry, Correlation of the Acidity of Substituted Phenols, Anilines and Benzoic Acids Calculated by MNDO, AM1, and PM3 with Hammett-Type Substituent Constriants, *J. Comp. Chem.,* **11** (9), 1009-1016, (1990).

199. P. C. Yates, B. Patel, Semiempirical Molecular Orbital Calculations on Dye Molecules, *J. Mol. Struct.,* **315**, 117-22, (1994).

200 G. L. Baughman and E. J. Weber, Estimation of Water Solubility and Octanol/Water Partition Coefficient of Hydrophobic Dyes. Part I: Relationship between Solubility and Partition Coefficient, *Dyes and Pigm.*, **16**, 261-71 (1991).

201 S. A. Siddiqui, Studies of Solvent Dyeing. Part I: Preparation of Disperse Dyes and Determination of their Solubility Parameters, *Text. Res. J.*, **51**, 527-33 (1981).

202 E. Sawicki, Physical Properties of Aminoazobenzene Dyes. VII. Absorption Spectra of 4-Aminoazobenzene Dyes in Ethanol, *J. Org. Chem.* **22**, 915-19, (1957).

203 M. Martynoff, Absorption Spectra and Structure of Aminoazo Derivatives. I. The Three Isomeric Aminoazobenzenes and their Monoacid Salts, *Compt. Rend* ., **235**, 54-57, (1952).

204 J. Griffiths and B. Roozpeikar, Synthesis and Electronic Absorption Spectra of Dicyano Derivatives of 4-Diethylaminoazobenzene, *J. Chem. Soc. Perkin Trans. I* ., **1976** (1), 42-48.

205 D. Hinks,*Personal Communication*, (1995).

ccvi D. R. Lide (Ed.), CRC Handbook of Chemistry and Physics, (76th Edition), Publ. Chemical Rubber Company Publishing Co., FL. (1996).

ccvii H. S. Freeman and S. A. McIntosh, Photolytic Properties of ortho-substituted 4-[N, N,-Bis(β-hydroxyethyl)aminoazobenzenes in polymer substrates, *Textile Res. J.*, **59** (6), 343, (1989).

ccviii G. Reinert and F. Fuso, Stabilization of Textile Fibres Against Ageing, *Rev. Prog. Coloration*, **27**, 32-41 (1997).

209 H. A. Bardole, Iron (II) and Iron (III) as alternatives to chromium in the metallization of mordant dyes, *Masters Thesis, College of Textiles, Norht Carolina State University, Raleigh, NC 27695 - 8301*, (1996).

210 J. Lye, H. S. Freeman, P. Singh, M. E. Mason, and D. Hinks, Molecular Modeling in Dye Chemistry. Part I: Studies Involving two Disperse Dyes, *submitted to Text. Res. J.,* (1998).

211 R. Boca, *Personal communication, Dept. Inorganic Chemistry, Slovak Technical University, SK-812 37 Bratislava, Slovakia*, (Oct. 1997).

212 J. Sokolowska-Gadja, *Personal communication, North Carolina State University, College of Textiles, Box 8301, Raleigh, NC 27695-8301,* (Oct 1997).

213 J. E. Huheey, Inorganic Chemistry: Principles of Structure and Reactivity, Harper and Row, NY, Evanstow, San Franscico, London, (1972).

214 J. Griffiths, A. N. Manning and D. Rhodes, The Prediction of Colour Change in Dye Equillibria. II - Metal Complexes of *Ortho*-Hydroxybenzenes, *J. Soc. Dyers Colo.*, **88**, 400-3 (1972).